UNIVERSITY OF COPENHAGEN
FACULTY OF SCIENCE

Master Thesis

Maren Berglioth Malling

The Balmer Decrement of Low Redshift Active Galactic Nuclei

Comparing two methods of calculation for a large sample.

Supervisor: Marianne Vestergaard
Dark Cosmology Centre, Niels Bohr Institute, University of Copenhagen
Date of Submission: August 15th, 2016

Abstract

Observations indicate that emission from the Narrow Line Region (NLR) of Active Galactic Nuclei (AGN) is reddened by dust. This dust is generally assumed to be located in the NLR itself. The Broad Line Region (BLR) is assumed to be dust-free, as the temperatures and photon fluxes in the region are too extreme for dust to survive. The electron density in the NLR is $\sim 10^3\,\mathrm{cm}^{-3}$. The electron density of the BLR is not well known, but is believed to be higher than that of the NLR to within an order of magnitude of $10^8 - 10^{10}$.

I have investigated the Balmer decrement (the ratio of Hα/Hβ emission line fluxes) for a sample of 873 AGN selected from the Sloan Digital Sky Survey, Data Release 7. Using two different methods to determine the narrow and broad components of the Hα and Hβ emission lines, I calculated the NLR Balmer decrement and the BLR Balmer decrement before any correction for dust extinction. I then used the NLR Balmer decrement to determine the color excess, E(B-V), and the total extinction, A(V). These results indicate an average of $1.5 - 2.5$ magnitudes of dust in the NLR of my sample objects.

I corrected the spectra for extinction due to dust, after which I calculated the Balmer decrements of the corrected spectra. By correcting the AGN spectra for the internal reddening caused by dust in the NLR, I assumed to have accounted for any internal reddening of the AGN. Based on this assumption, I used The BLR Balmer decrements to examine the gas density in the BLR. For this sample, I find a mean BLR Balmer decrement of $1.7 - 1.8$ after correction for the effects of dust. This result indicates an electron density in the BLR of $\sim 10^{13}\ \mathrm{cm}^{-3}$.

Contents

1 Introduction

Active Galactic Nuclei (AGN) are compact regions at the center of galaxies which emit radiation strongly at all wavelengths, from radio to gamma rays (Peterson, 1997). Accretion of matter onto a supermassive black hole at the center of the AGN is powering this emitted radiation. The central black hole is surrounded by an accretion disk, and the disk is surrounded by a structure of dust and gas, which is often referred to as a torus. Two distinct regions of line-emitting gas are found in AGN. Closest to the central engine is the Broad Line Region (BLR), which produces strong, broad emission lines with linewidths of up to 10000 km s^{-1}. The width of these lines is belived to be caused by Doppler broadening due to the high velocity of the gas in the region. The Narrow Line Region (NLR) is located farther from the central black hole and accretion disk, at a distance of kpc. This region produces strong, narrow emission lines with a linewidth of $\sim$ 500 km s^{-1} (Peterson, 1997; Netzer & Laor, 1993). The BLR is believed to be located within the inner radius of the torus. Depending on the viewing angle, the torus-like structure of gas and dust blocks out optical and UV radiation, and this explains why not all AGN show broad emission lines (Urry & Padovani, 1995). The emission from the NLR is not obsured, as the region is located outside the perimeters of the torus.

The electron density in the NLR is $\sim 10^3\,\mathrm{cm}^{-3}$. This density has been established by measuring the ratio of intensity of certain pairs of narrow emission lines, such as [SII] λ6716/[SII] λ6731, as this ratio is density dependent at such densities as are found in the NLR. The density of the BLR, on the other hand, is not well known, as such density indicators are not available at high densities. It is believed to be higher than that of the NLR to within an order of magnitude of $10^8 - 10^{10}$ (Osterbrock & Ferland, 2006; Peterson, 1997).

The NLR is assumed to contain dust, which causes reddening of the emitted spectrum. It is, however, unlikely that the BLR contains any dust (Osterbrock & Ferland, 2006; Netzer & Laor, 1993). Netzer & Laor explain that the NLR and BLR are separated by a 'gap' which does not have any significant line emission. They present a model in which the distribution of dust in the AGN explains both the non-emitting gap and the different amounts and types of line emission from the two regions. According to their model, dust is embedded in the NLR gas, but cannot survive in the BLR because of the extreme temperatures in the region. They argue that the dust density rises towards the center of the AGN, and that the dust sublimates at a radius close to the center which coincides with the size of the BLR. Osterbrock & Ferland explain that refractory elements such as Al, Ca, Si, and Fe are detected in the BLR spectrum. If dust were present in the BLR, these elements would be strongly depleted because they become attached to the dust grains.

Determining the amount of dust in the ISM of the Milky Way Galaxy is fairly straightforward. Each stellar type has a very characteristic emitted spectrum, and by comparing an unreddened stellar spectrum with a reddened one, it is possible to determine the color excess, E(B-V), and the total extinction, A(V), of the stellar spectrum due to dust. The unreddened stellar spectrum is known from nearby stars, for which the amount of dust along the line of sight is minimal.

To measure the dust extinction for more complex systems, such as entire star-forming galaxies, the ratios of Hydrogen Balmer lines are often used. These ratios, which are generally referred to

as Balmer decrements, are well known from theoretical calculations. The hydrogen atom is very well understood, and the ratio of emission lines can be predicted by atomic theory. The Balmer decrements are only slightly influenced by gas temperature and electron density in a low-density gas, but they are strongly influenced by dust extinction. Therefore, the Balmer decrements are often used as reddening indicators. By measuring the observed ratio of the two lines and comparing to the expected theoretical ratio, the amount of extinction due to dust can be determined (Osterbrock & Ferland, 2006; Momcheva et al., 2013). In this work, the Balmer decrement refers only to the ratio of the line fluxes of the Hα and Hβ emission lines. In what follows, the ratio of Hα/Hβ measured for the narrow line region is referred to as the NLR Balmer decrement. Similarly, the ratio measured for the broad line region is referred to as the BLR Balmer decrement.

With Case B recombination at a temperature of 10^4 K and electron density of $10^4\,\mathrm{cm}^{-3}$, the intrinsic Balmer decrement for a typical low density HII region is 2.85. Case B describes a gas which is optically thick to the ionizing radiation of the Lyman series, except for Lα. The gas in the NLR is denser than that of a typical HII region, but the density is still low enough for the Balmer decrement to be a good indicator for extinction. For the NLR, the value quoted for the intrinsic Balmer decrement is 3.1 (Osterbrock & Ferland, 2006). This value is based of observations. After dereddening several observed NLR spectra, the intrinsic ratio of the Hα/Hβ lines is found to be 3.1 on average. This increase from the recombination value of 2.85 is explained by collisional excitation of Hα resulting from the higher density of the NLR compared to a typical HII region.

In the BLR, the gas density is higher than that of the NLR to within an order of magnitude of $10^8 - 10^{10}$, and high-density effects such as inelastic electron-atom collisions become dominant. This changes the ratio of the Balmer emission lines in ways which are not completely well understood. Therefore, it is generally considered that the Balmer decrement cannot be used as a reddening indicator for the BLR (Osterbrock & Ferland, 2006; Dong et al., 2008).

In my analysis, I assume that dust is present in the NLR, but that the high temperatures and photon energies of the BLR are too extreme for any substantial amount of dust to survive there (MacAlpine, 1985). By correcting the AGN spectra for the internal reddening caused by dust in the NLR, I therefore assume to have accounted for all internal reddening of the AGN. When measuring the Hα/Hβ ratio for the BLR after correcting the spectrum for the effects of dust, any deviation from the theoretical value of 3.1 (if that is indeed the applicable value for the BLR) must therefore be due to high density effects rather than dust.

2 Scientific Goal

In this study, I explore two different methods of calculating the BLR Balmer decrement for a large sample of AGN and compare the advantages and disadvantages of each method. My goal is to determine which method gives the most robust results. By assuming that no dust is located in the BLR, I use the NLR Balmer decrement to correct the AGN spectrum for internal dust reddening. After correction for the effects of dust, I use the BLR Balmer decrement is to investigate the density of the gas in the BLR.

3 Data and Sample of Objects

For this study, I have used a sample of 873 AGN selected from the Sloan Digital Sky Survey (SDSS) Data Release 7 (DR7) Quasar Catalog. The SDSS Quasar Catalog contains 105.783 spectroscopically confirmed AGN. The selection criteria for these objects are: Luminosities larger than $M_i = -22.0$ (the catalog calculations are based on a cosmology with $H_0 = 70$ km s^{-1} Mpc^{-1}, $\Omega_M = 0.3$, and $\Omega_\Lambda = 0.7$), at least one broad emission line with Full Width at Half Maximum (FWHM) larger than 1000 km s^{-1} or interesting/complex absorption featues, and highly reliable redshift measurements (Schneider et al., 2010). The spectral resolution of the 1D spectra is R $\sim$ 1850–2200. The spectra are constant in vacuum wavelength, with a pixel scale of 10^{-4} in log-wavelength, corresponding to 69 km s^{-1} (Shen et al., 2011). The spectra cover a wavelength region of 3800–9200 Å (Schneider et al., 2010)

3.1 Sample Selection

To be able to determine the narrow line Balmer decrements, I needed to select spectra with a high enough quality to be able to clearly distinguish the narrow line component from the broad line component of the Hα and Hβ emission lines. I therefore selected objects with a median spectral signal-to-noise ratio (S/N) of minimum 15 as listed in the SDSS catalog. I subsequently re-calculated the median S/N of those objects selected for my samples using the flux and error spectra obtained from the SDSS catalog. The values printed on the sample spectra shown in the text are those obtained from the re-calculation. The objects selected have a maximum redshift of 0.3. This is to ensure that the Hα line lies within the spectral coverage of the SDSS. With these limits on S/N and redshift, 1340 objects are available in the SDSS DR7 Quasar catalog.

The SDSS survey contains a large number of objects which are identified as AGN by the above-mentioned criteria, but which may not be 'bona fide' AGN on closer inspection. My aim was to examine the Balmer decrement of objects which are typical of their class, and I therefore excluded a number of objects from the original sample. First, I excluded objects for which part of the spectrum are masked in the processing phase, rendering this part of the spectrum unusable. In some cases, the entire Hα or Hβ emission line was missing from the spectrum, or the line was truncated. After excluding these objects from the sample I took the remaining candidate objects through the first steps of data analysis as described in §4. More specifically, I fitted a continuum model, as described in §4.5 and a emission line model, as described in §4.6. After this initial round of model fitting, I examined the validity of the models by several methods. I subtracted the line fit model from the continuum subtracted spectrum and integrated over the residual spectrum in a wavelength ranges covering the Hα and Hβ emission lines. These line ranges are described in detail in §4.7. I calculated a ratio of the residuals to the spectral flux in the wavelength range of both the Hα and Hβ lines and found that specifically for the Hβ emission lines, the residuals was at a very high level for some objects. I inspected those objects for which the residuals made up more than 20% of line flux. The spectra of the majority of these objects did not look like those of bona fide AGN, but more like star forming galaxies. Also, many of these spectra had a low S/N, which makes it harder to distinguish between

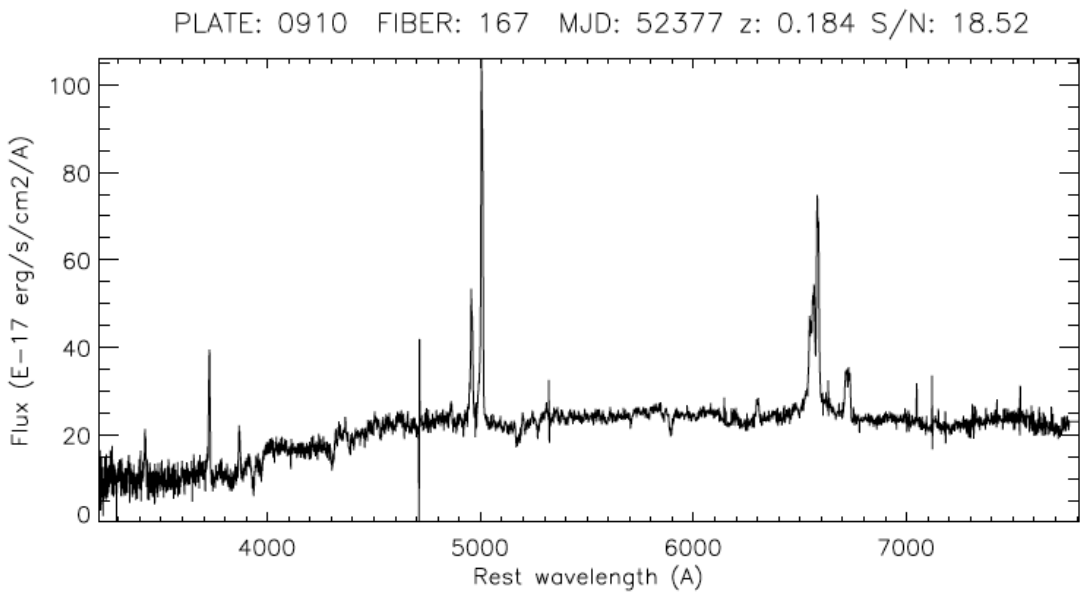

Figure 1: Example of an AGN spectrum which looks more like that of a star forming galaxy. I excluded this type of spectrum from the sample because it is not representative of the class of objects I want to examine.

an AGN spectrum and a galaxy spectrum. I therefore excluded a total of 139 objects with galaxy-like spectra, as these are not representative of the class of objects I wanted to examine. An example of such a spectrum is seen in figure 1.

There is a strong anti-correlation in AGN spectra: When Fe is strong, O is week (Boroson & Green, 1992). In my line fitting models, I used the width of the [OIII] doublet ([OIII] $\lambda\lambda 4959, 5007$) to dictate the velocity broadening of the NLR gas. By coupling the width of the narrow lines together (as they originate in the same NLR gas), I determined the narrow components of the Hα and Hβ lines. The [OIII] doublet is therefore crucial to getting a precise fit of the narrow component of the Balmer lines. The [OIII] doublet blends with Fe lines located at almost the same wavelengths, and Fe also blends with the narrow Hβ emission line, which is weaker than [OIII] yet. When the Fe emission is very dominant, it is complicated and often impossible to extract a realistic model of [OIII], and therefore to model the narrow Balmer line components, in particular Hβ. A large number of the available object spectra have very strong Fe emission. I tried to obtain good fits to the narrow Balmer lines for these spectra by adjusting the model parameters, which turned out to be both difficult and time consuming. The same problem arose with objects with very broad, irregular line profiles. I therefore selected to exclude a total of 297 objects from the sample which have either strong Fe emission and/or very broad, irregular line profiles, as it would be too time consuming to include them in the sample at this point. Figure 2 shows an example of an Fe-rich spectrum where the [OIII] lines are very weak. Figure 3 shows an example of a spectrum with broad, irregular line profiles.

After excluding these objects, I have a sample of 873 objects. For these objects, I initially attempted to do all the steps of model fitting described in §4, including correction of the spectra for

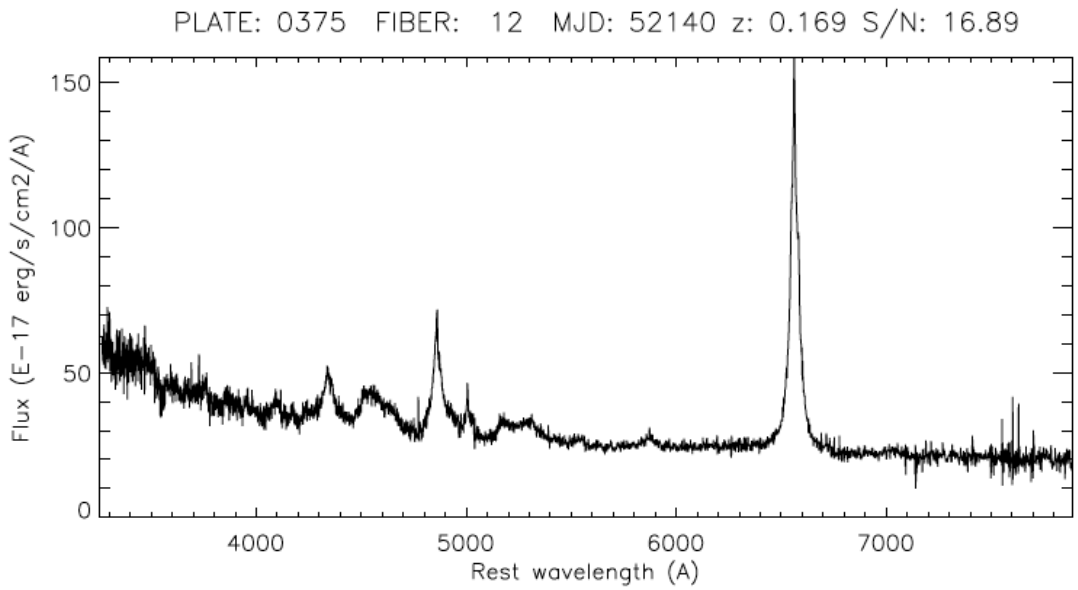

Figure 2: Example of an AGN spectrum with strong, dominant Fe emission. The [OIII] doublet ([OIII] $\lambda\lambda 4959, 5007$) is blended with the Fe lines and very weak, making it difficult to determine the width of the narrow emission lines. I excluded this type of spectrum from the sample because it is too time consuming at this point to include them.

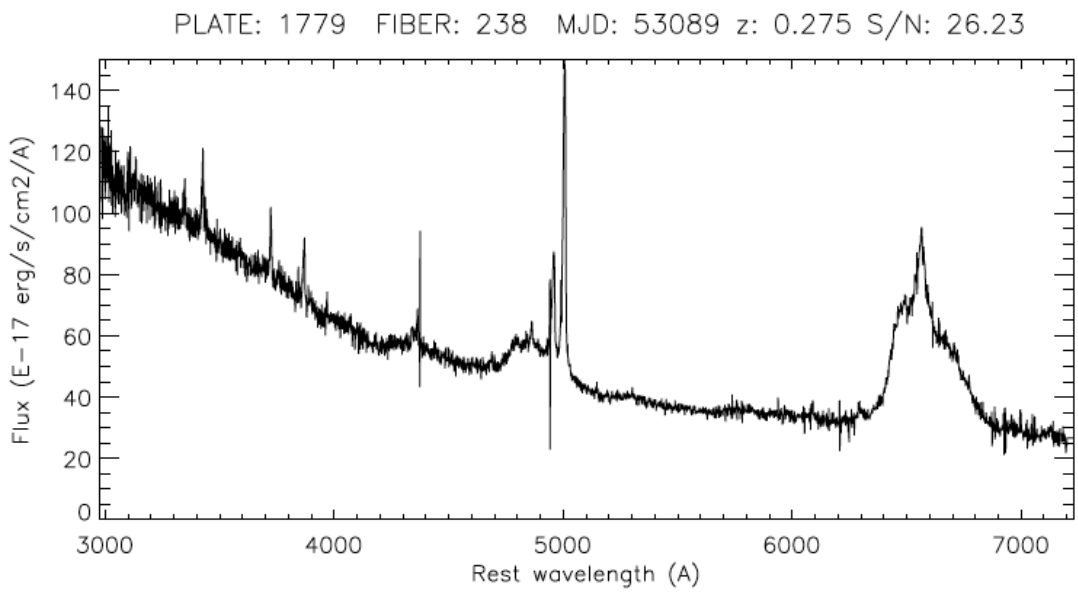

Figure 3: Example of a AGN spectrum with very broad, irregular Balmer line profiles. These profiles are complicated to model well, and often the narrow component is hard to separate from the broad component. I excluded this type of spectrum from the sample because it is too time consuming at this point to include them.

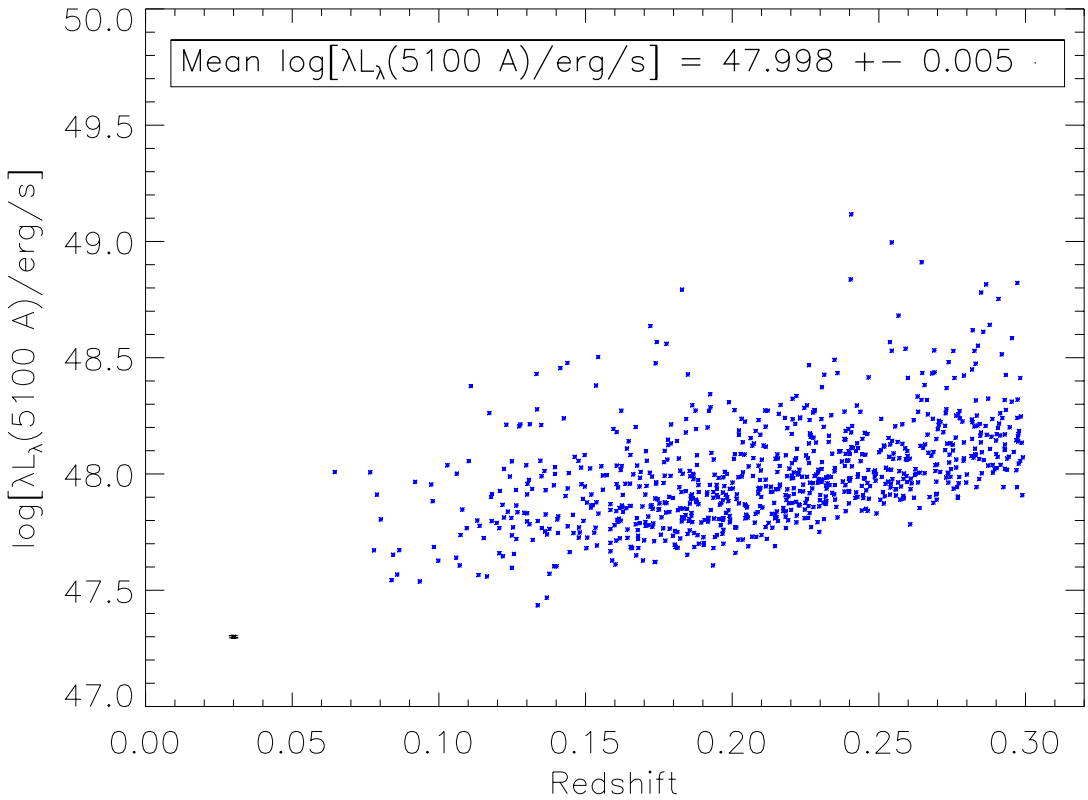

Figure 4: log[$\lambda L\lambda$(5100A)/erg/s] as a function of redshift for the 873 objects in the main sample, which includes the test sample. A typical error bar i shown in the lower left corner.

the effects of dust, as described in §4.8, and the subsequent refitting of the spectra as described in §4.9. However, I found that it was not possible to obtain reliable model fits to the corrected spectra for a large number of the objects in the sample. Therefore, I decided to select a small subsample of 93 objects for which I trust the model fit both before and after correction for dust effects. For the subsample, I aimed at selecting high S/N spectra which are representative of the general population of AGN. These spectra all contain broad Hα and Hβ emission lines, and have clear narrow line components. I will refer to the smaller sample as the **test sample** and the larger sample as the **main sample**. Note that the test sample is included in the main sample. Figure 4 shows log[λL_λ(5100 A)/erg/s] as a function of redshift for the 873 objects in the main sample, including the objects in the test sample. L_λ(5100 A) is the monochromatic luminosity at 5100 A.

4 Data Analysis

I used two alternative methods to determine the Balmer decrements. A brief overview of these methods is given in §4.1 and §4.2, and the steps are explained in detail in §4.4 - §4.9. I will refer to the first method as the **isolation method** and the second method as the **refit method**. To correct the spectra for the effects of dust, I used two different extinction curves, as explained in 4.3

With the test sample, I used both the isolation method and the refit method. My main goal was to investigate and compare these two methods of determining the Balmer decrements to see if one method gives more robust results. The objects in the test sample are selected based on their high S/N and clear narrow line components, and they are therefore suitable for testing both methods. For these objects, I trust the model fit to give sufficiently precise results, and I wanted to compare these to the results using the isolation method, which does not rely on fitting an emission line model to the line flux ratio in question (Hα/Hβ) but rather measures the line fluxes using the flux spectrum directly. With the main sample, I only used the isolation method, as it was not possible to determine the Hα and Hβ narrow line fluxes sufficiently precisely by modeling the lines for many of the objects in the sample, as is done in the refit method. Regardless of the method used, I used both extinction curves.

To do the data analysis, I have written a large number of scripts in Interactive Data Language (IDL). Some of these scripts are based on scripts made available to me by my advisor, Marianne Vestergaard. A couple of these I have used directly, e.g. a short script which implements the Fe template described in 4.5.2 as part of the continuum fitting process. However, the majority of the scripts made available to me, I have either used as inspiration, or adjusted and developed to suit this project. For example, the scripts developed specifically for the data analysis with the isolation method have all been written by me, as are the scripts used to calculate the extinction due to dust and correct the spectra. However, the majority of the contents of the scripts for the refit method are likewise written entirely by me. I have occasionally drawn on IDL scripts made publicly available, such as the MPFIT package.[1], which I used to fit my continuum and emission line models.

[1]Found on: http://cow.physics.wisc.edu/ craigm/idl/idl.html

4.1 Method 1: Isolating the Emission Lines

I determined the continuum level under the emission lines by doing a model fit as described in §4.5. After subtracting the continuum, I modeled the emission lines as described in §4.6. After this initial model fitting, I subtracted the modeled line profiles of the broad Hα and Hβ to obtain an isolated narrow line Hα and Hβ spectrum. This is not a model of the narrow emission lines, but rather the residual flux left over after subtracting the model of the broad lines, as is further described in §4.7 Likewise, I obtained a broad line Hα and Hβ spectrum by subtracting the narrow line Hα and Hβ spectrum as well as the [NII] λ6584, [NII] λ6548, [OIII] λ4959, [OIII] λ5007 modeled line profiles from the continuum subtracted spectrum. Then I integrated over these line spectra in the line ranges described in §4.7 to obtain the broad and narrow Hα and Hβ line fluxes respectively, and these I used to calculate the BLR and NLR balmer decrements respectively before correction for dust effects. I thereafter used the NLR Balmer decrement to correct both line spectra for the effects of dust, as described in §4.8. Integrating over these corrected spectra in the line ranges once more, I obtained the BLR and NLR balmer decrements corrected for the effects of dust.

4.2 Method 2: Refitting the Corrected Spectra

As in the isolation method, I started by determining the continuum level under the emission lines by doing a model fit as described in §4.5. After subtracting the continuum, I modeled the emission lines as described in §4.6. The Hα and Hβ narrow line fluxes determined from the line fit I then used to determine the NLR balmer decrement, and this I used to correct the original spectra for the reddening effects of dust, as described in §4.8. I then determined the continuum level of this corrected spectrum by doing another round of continuum fitting. I subtracted the continuum level from the corrected spectrum, after which I modeled the emission lines again. The Hα and Hβ broad line fluxes based on the modeled broad line components of the dust-corrected spectrum are those that I used to determine the BLR Balmer decrement corrected for dust effects.

4.3 Selection of Extinction Curve

The extinction curve describes the extinction (combined absorption and scattering of light) at different wavelengths due to dust. The choice of extinction curve therefore influences the amount of correction to the spectra at the location of the Hα and Hβ emission lines. Different extinction curves indicate different sizes and distribution of dust grains. Based on a study of 9566 AGN from the SDSS catalog, (Hopkins et al., 2004) conclude that the SMC extinction curve best describes the internal dust reddening of AGN. However, (Kauffmann et al., 2003) describe that many of the AGN in the SDSS catalog show some star formation. In this case, the Calzetti extinction curve could be more appropriate, as it is often used for star-forming galaxies. In figure 5, I show the two extinction curves in the wavelength range covered by the SDSS spectra. As seen in the figure, the two curves are very close to the same value at the wavelength position of the Hα and Hβ emission lines. In the short wavelength range below 5500 Å, which includes the wavelength position of the Hβ emission line at

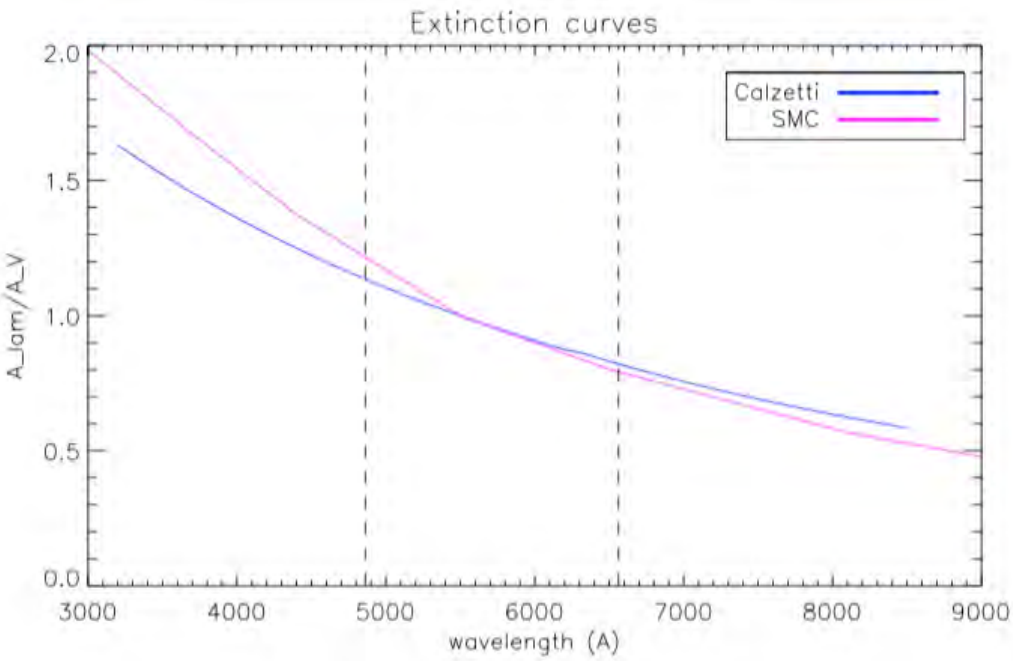

Figure 5: Comparing the extinction curves in the wavelength range covered by the SDSS spectra. The SMC extinction curve (magenta) is steeper than the Calzetti extinction curve (blue) throughout the range. At the wavelength position of the Hβ emission line (4681 Å, marked by vertical dashed line) the SMC curve indicates a slightly greater extinction than the Calzetti curve, while the reverse is the case at the wavelength position of the Hα emission line (6563 Å, marked by vertical dashed line).

4681 Å, the SMC curve indicates a greater extinction than the Calzetti curve. At wavelengths longer than 5500 Å, including the wavelength position of the Hα emission line at 6563 Å, the Calzetti curve indicates a greater extinction. I chose to use both of these curves and compare the results. I calculated the extinction using the SMC extinction curve of (Gordon et al., 2003) and the Calzetti extinction curve of (Calzetti et al., 1994), following the steps described in §4.8.

4.4 Initial Correction of the Spectra

SDSS wavelengths are vacuum wavelengths. I used the IDL procecure 'vactoair' to convert these to air wavelengths. I shifted the spectra to rest frame using: restwavelength = airwavelength/(1 + z), where z is the redshift. I used the improved redshift values of Hewett & Wild (Hewett & Wild, 2010). I corrected the spectra for foreground reddening in the Milky Way Galaxy using the Schlegel, Finkbeiner, & Davis (Schlegel et al., 1998) dust map and the O'Donnell extinction curve with $R(V) = 3.1$ (O'Donnell, 1994). This reddening is unrelated to the intrinsic AGN reddening which I want to determine using the NLR Balmer decrements.

4.5 Continuum Fitting

My fitting process is done in two steps. First I determined the contiuum level under the emission lines by fitting a model. My continum model contains several emission line models, which are only included as placeholders to better determine the continuum level. In particular, this prevents the wings of the

broad lines from pulling the fitted continuum level up too high. I again fitted these emission lines during the line fitting process described in §4.6, thereby determining the line fluxes. To be able to accurately measure the line fluxes of the Hα and Hβ emission lines, the continuum has to be carefully subtracted from the spectrum. AGN spectra contain a multitude of broad and narrow emission lines, including Fe II lines, and it is almost impossible to find regions in the optical part of the spectrum with no emission lines where the continuum can be measured (Dong et al., 2008). Also, the Fe II lines often blend with the broad Hβ line and the narrow oxygen lines, and the Fe II lines need to be subtracted before the Hβ line flux can be precisely measured. Therefore, I chose to simultaneously fit a model consisting of several components:

- A single power law describing the AGN contiuum emission
- An Fe II emission line template
- A Balmer continuum template
- An AGN host galaxy model
- A model of the broad Hα, Hβ and Hγ lines
- A model of several other emission lines

Each of these components is described in detail below. The fit routine was allowed to run for a maximum of 200 iterations per round and max two rounds of fitting. The second round used the final parameters of the first round as starting parameters.

4.5.1 Power Law

I fitted a single power law to the entire rest wavelength range. The power law is defined as: $a\lambda^{\alpha}$, where a is the amplitude, λ the wavelength, and α is the power law exponent, which is defined to be positive. The power law is normalized at 5500 Å, and the allowed range of the slope is $[-5, 2]$. The spectra of many AGN have a very steep slope in the UV, and other studies of this kind have used a broken power law to fit such spectra (Dong et al., 2008; Shen et al., 2011). It is an open question whether the intrinsic AGN continuum is in fact flat in the optical, or whether it is due to the contribution of the host galaxy that this part of the spectrum becomes flat (Selsing et al., 2016; Vanden Berk et al., 2001). The spectra of this sample do not contain enough of the UV spectrum to be able to determine whether a single or a broken power law would give the better fit. I therefore chose to use a single power law.

4.5.2 Fe Template

I used an Fe II emission line template based on the Fe emission of I ZW1 (Véron-Cetty et al., 2004). This template is based on a single AGN, which has very narrow lines with an intrinsic width of 900 s^{-1}. During the fitting process, the template is broadened using a Lorentzian kernel and scaled to match the observed spectrum.

4.5.3 Balmer Continuum Template

To create the Balmer continuum models, I followed the procedure of Dietrich et al (Dietrich et al., 2003). The Balmer continuum consists of the higher order Balmer lines (excluding Hα, Hβ and Hγ, which I fitted individually). Given a specific density and temperature, atomic theory predicts the intensity of these lines. I tested whether including a Paschen continuum model improved the fits and found no significant difference, so I left it out.

4.5.4 Host Galaxy Model

The AGN host galaxy model is a composite of three template spectra of galaxies aged $5 \cdot 10^8$ yrs, $1 \cdot 10^9$ yrs and $5 \cdot 10^9$ yrs. The individual galaxy spectra are shown in figure 6. Each of these three spectra is scaled by an amplitude which I fitted as a free parameter, and the spectra are added up to form one galaxy component.

After the first round of continuum fitting, I found that many of the models had a very large host galaxy component. I selected a sample of 20 objects which had been modeled with a very high galaxy contribution. For these objects, I tried to put a constraint on the amplitude of each of the three galaxy templates to see if it was possible to obtain a good fit with a smaller contribution. In most cases, the fitting routine reached the imposed upper limit without finding a solution. Only in a few cases was a solution reached which resulted in a smaller galaxy component.

There is too little of the UV spectrum available in these spectra to determine if the high galaxy contribution is realistic. Each individual fit would need a lot of fine adjustment to possibly find another solution, and this solution becomes very arbitrary. I chose not to make these additional adjustments, as this information is not important for the purpose of my study. Instead I measured the host galaxy contribution to the total flux in three separate wavelength ranges: 5500-5700 Å, 6000-6200 Å, 7250-7500 Å and flagged those objects with a galaxy contribution of more than 80% of the total flux in the wavelength ranges for future reference.

4.5.5 Broad Balmer Lines

I modeled each of the broad Hα, Hβ and Hγ lines using a single Lorentzian profile. These line fits are preliminary fits which are only included to better determine the continuum level, and the lines are refitted after subtraction of the continuum model. I used a mask to exclude any pixels which fall within 1500 s^{-1} of the line center from the fit. I assumed the lines to have the same redshift and profile and fitted them with a common Half Width at Half Maximum (HWHM).

4.5.6 Other Emission Lines

I included a model of each of the narrow lines [SII] λ6717, [SII] λ6731, OI λ6300, [OIII] λ4959, [OIII] λ5007, and one broad line: HeI λ5876 in the fit. By including these selected lines, I was able to better determine the continuum level between the lines. The lines were subsequently refitted during the line fitting process. I constrained the line center of each line to within 100 Å of the wavelength value listed

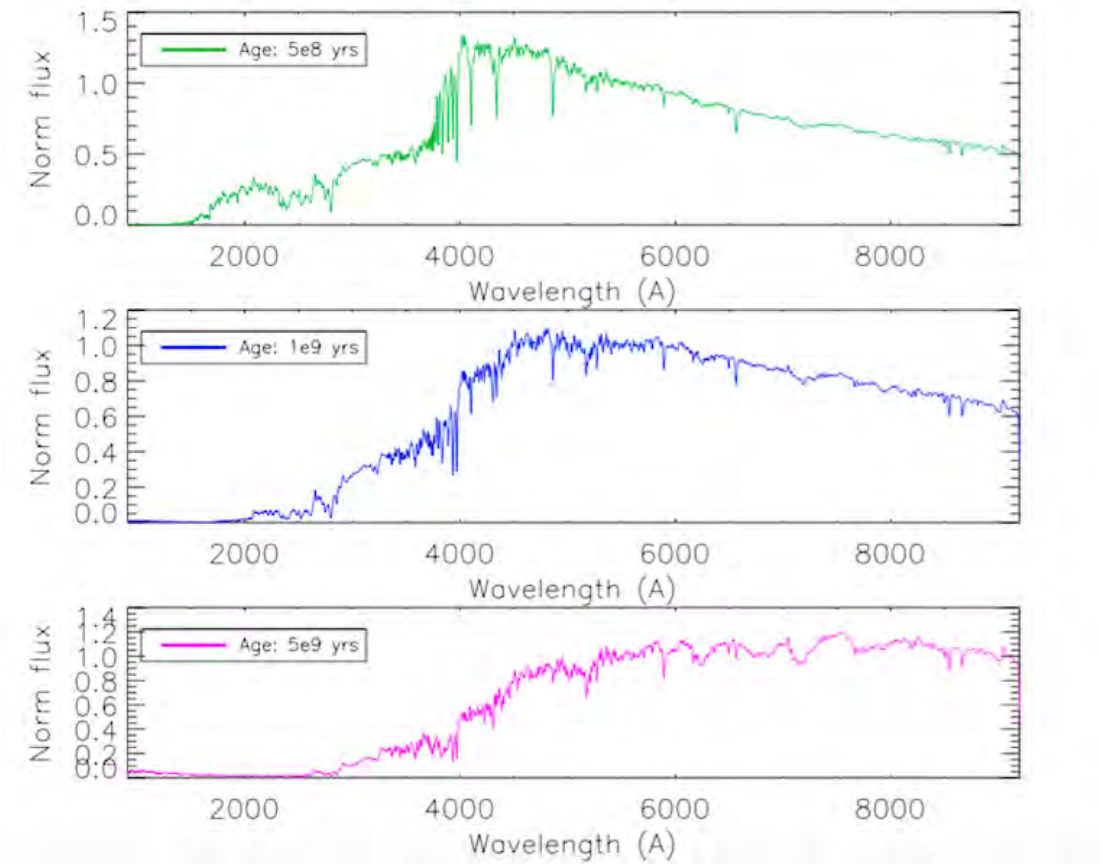

Figure 6: Template spectra of galaxies aged $5 \cdot 10^8$ yrs, $1 \cdot 10^9$ yrs and $5 \cdot 10^9$ yrs. The three spectra combined make up the AGN host galaxy component which is part of the continuum model. Each of the three spectra is scaled by an amplitude, which is fitted as a free parameter, and the spectra are added up to form one galaxy component.

in table 1 and fitted each line with a single Lorentzian profile. I constrained the narrow lines to the same HWHM, as these lines originate in the same NLR gas. The HWHM of HeI $\lambda5876$, I fitted as a free parameter independent of the other lines, as this is a broad line.

4.5.7 Comments on Continuum Fit

When including many components like a power law, Fe template, Balmer continuum template and host galaxy model in the continuum fit, the solutions are not unique. The fit does not determine the contribution of the individual components well, and there could be several other solutions which are equally good. I needed to determine and subtract the total amount of flux not associated with the line emission, and the contribution of the individual components was not important for my analysis, so I disregarded this degeneracy.

4.6 Emission Line Fitting

To create a continuum-free spectrum, I subtracted the best-fit models of the power law, Fe template, Balmer continuum template and host galaxy model from the restframe spectrum. Then I ran my line fitting routine. A complete list of emission lines included in the fit is found in table 1. I sorted the lines into groups with similar properties. These groups are indicated as $b1, b2$ and n. The $b1$ group contains the broad components of the Balmer lines. $b2$ is an intermediate group of broad Helium lines, and n is the group of narrow lines, including the narrow components of the Balmer lines. The broad Balmer lines in the $b1$ group are fitted with one to three Gaussians. The broad Helium lines in $b2$ are fitted with one or two Gaussians, and the narrow lines in the n group are fitted with a single Gaussian.

For a Gaussian profile, the Full Width at Half Maximum (FWHM) is $2\sqrt{2\ln 2}\sigma \approx 2.35\sigma$, where σ is the standard deviation of the Gaussian. For each Gaussian, the lines within a group are fitted with the same parameter value σ. The mean of each Gaussian function, μ, is defined in terms of a velocity offset from the line center of a given emission line as: $\mu = \lambda_0 \cdot \left(1 + \frac{v_{off}}{c}\right)$, where λ_0 is the restframe line center of a given emission line and c is the speed of light in vacuum.

Lines with less than 15 pixels near line center are excluded. This is to avoid fitting very narrow or weak lines, which may in fact be just noise in the spectrum. This is particularly important for the broad profiles with several Gaussian components.

I coupled the line fluxes of certain lines together at a specific ratio: The line flux of the narrow [NII] $\lambda6548$ is fixed at 1/3 of the narrow [NII] $\lambda6584$ line flux. The line flux of the narrow [OIII] $\lambda4959$ is fixed at 1/3 of the narrow [OIII] $\lambda5007$ line flux. The lines are all fitted simulaneously using the MPFIT package, again allowing up to two rounds of maximum 200 iterations.

Figure 7 shows a representative example of the results of continuum and line fitting for one of the objects in the test sample. The displayed spectrum is before correction for the effects of dust. The fitted line models are used to determine the NLR Balmer decrements to be used for correction for dust effects. In figure 8, I show an expanded view of the Hα and Hβ line fits for the same sample spectrum. The NLR and BLR Balmer decrements before correction for the effects of dust are displayed on these

Line	Line center (Å)	Type
[OII] λ3726	3726.032	n
[OII] λ3729	3728.815	n
[NeIII] λ3869	3869.060	n
Hδ	4102.892	b1
Hδ_n	4102.892	n
Hγ	4340.464	b1
Hγ_n	4340.464	n
[OIII] λ4363	4363.210	n
Hβ	4861.325	b1
Hβ_n	4861.325	n
HeII λ4686	4685.710	b2
HeII$_n$ λ4686	4685.710	n
HeI λ4471	4471.000	b2
[OIII] λ4959	4958.911	n
[OIII] λ5007	5006.843	n
HeI λ4713	4712.500	b2
HeI λ4921	4921.931	b2
HeI λ5016	5015.678	b2
HeI λ5876	5875.670	b2
HeI$_n$ λ5876	5875.670	n
[OI] λ6300	6300.304	n
[NII] λ6548	6548.040	n
Hα	6562.800	b1
Hα_n	6562.800	n
[NII] λ6584	6583.460	n
[SII] λ6717	6716.440	n
[SII] λ6731	6730.810	n

Table 1: List of emission lines. Line Centers in are in restframe air wavelengths. Forbidden transitions are marked with square brackets. Type n lines are narrow lines.. Type b1 are broad Balmer lines, and type b2 are semi-broad He lines. Source: 'The Atomic Line List v2.04' (http://www.pa.uky.edu/ peter/atomic/)

plots. These Balmer decrements are found using the modeled line fluxes. For further illustration, I show three more examples in the appendix. Figure 30, 31, and 32 show examples of continuum and line fitting, and expanded views of the line fits are seen in figure 33, 34 and 35.

4.7 Isolation of Broad and Narrow Balmer Lines

This step is part of the isolation method only and is performed after the initial continuum and line fitting described in §4.5 and §4.6. My aim was to isolate the narrow component of the Hα and Hβ lines respectively and create a narrow line specrum containing only these components - and to do the same with the broad component of the lines.

To obtain a spectrum containing only the narrow Hα and Hβ lines, I subtracted the best-fit model of the broad Hα and Hβ lines from the continuum subtracted spectra. Also, I subtracted the model of the narrow nitrogen lines ([NII] λ6584, [NII] λ6548) which blend with the broad Hα line, and the narrow oxygen lines ([OIII] λ4959, [OIII]λ5007) which blend with the broad Hβ line. The broad Balmer lines are easier to model than the narrow Balmer lines, and assuming that the model of these

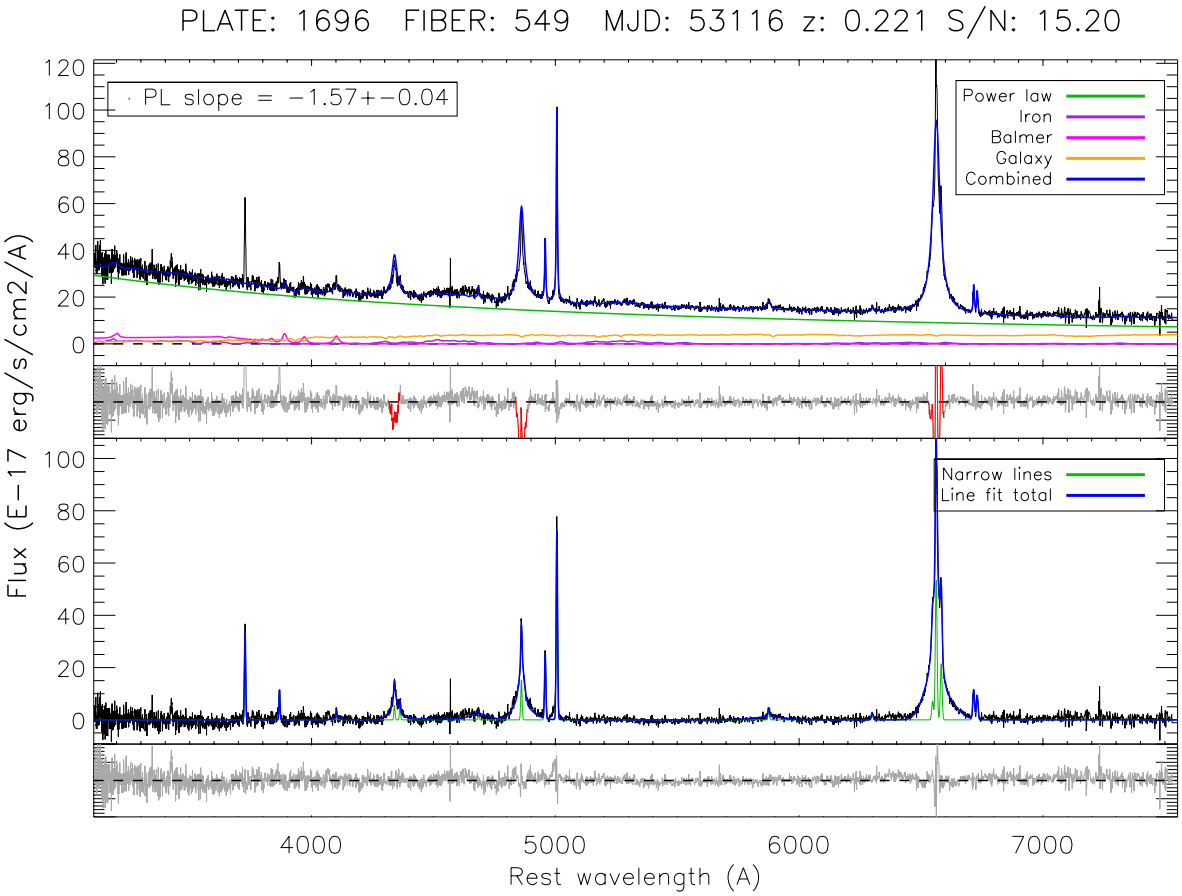

Figure 7: Representative example of the results of continuum and line fitting of a spectrum before correction for dust effects. Top panel: Continuum fit as described in §4.5. Observed spectrum in black. Fitted model components are: power law (green), FeII emission (purple), Balmer continuum (magenta), host galaxy (orange). Combined best-fit model in blue. This model includes preliminary line fits, which are only used to better determine the continuum level. Residuals of the continuum fit in second panel below, with masked out wavelengths marked in red. Third panel: Line fit as described in §4.6. Observed spectrum in black. Narrow lines in green and best-fit line model (including both broad and narrow line components), in blue. For clarity, only the narrow lines are shown. In figure 8, I show an expanded view of the line fit which includes the modeled broad line profile and the individual Gaussian components pertaining to that model. Residuals of the line fit in bottom panel below. Power law slope is displayed in upper left corner. SDSS plate, fiber and mjd are indicated above plot along with redshift (z) and S/N.

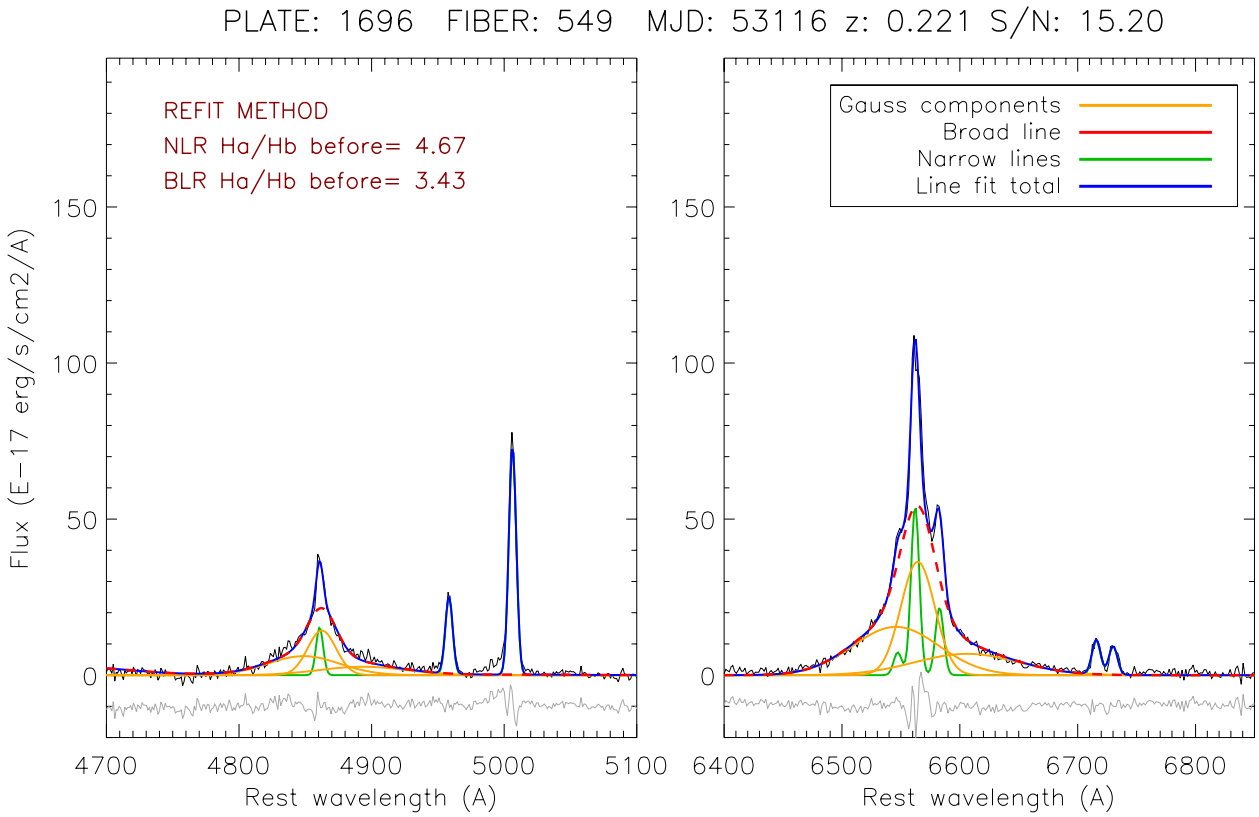

Figure 8: Expanded view of line fits for object shown in figure 7. Left panel: Hβ line fit. Right panel: Hα line fit. Observed spectrum in black. The modeled broad line profile is red dashed line. The individual Gaussian components pertaining to the model of the broad line profile are in orange. Narrow lines in green. Best-fit line model in blue. Residuals of the line fits are displayed below, offset for clarity. BLR and NLR Balmer decrements (before correction for the effects of dust) are displayed. These Balmer decrements are calculated using the Hα and Hβ broad and narrow line fluxes from the line fit shown in figure 7, and I have used the SMC extinction curve. In figure 13 I show the same line fits after correction for dust effects.

broad lines can be trusted, I took the remaining residuals in a narrow wavelength range around each of the line centers of Hα and Hβ respectively to represent the narrow line component of the line.

The narrow wavelength range I defined as follows: I used a velocity offset of ± 800 km s^{-1} to set an initial narrow wavelength range around each of the Hα and Hβ line centers. Within this wavelength range, I compared the residual flux at each pixel step with the corresponding error level (boxcar smoothed with a smoothing width of 5 pixels). At the wavelength where the error exceeded the residual flux, I set the final limits of the narrow wavelength range. Outside this range, I set the flux value to zero, in effect creating a spectrum of only the narrow components of the Hα and Hβ lines. I what follows, I refer to this spectrum as the isolated narrow line spectrum. I integrated over each of the lines in this isolated narrow line spectrum to obtain the Hα and Hβ narrow line fluxes. These fluxes I used to calculate the NLR Balmer decrement.

In a similar fashion, I created a broad line Balmer spectrum by subtracting all modeled lines from the continuum subtracted spectrum, except the models of the broad Hα and Hβ lines and the models of the narrow Hα and Hβ lines. Instead of subtracting the modeled narrow lines, I subtracted the isolated narrow line spectrum. I then defined a broad wavelength range by using a velocity offset of ± 8000 km s^{-1} to set an initial broad wavelength range around each of the Hα and Hβ line centers. Again I compared the residual flux at each pixel step within the range with the corresponding boxcar smoothed error level, and set the final limits of the broad wavelength range at the wavelength where the error exceeded the the flux. By setting the flux value to zero outside the range, I created a spectrum of only the broad components of the Hα and Hβ lines, which I in the following will refer to as the isolated broad line spectrum. I integrated over each of the lines in this isolated broad line spectrum to obtain the Hα and Hβ broad line fluxes, and I used these to determine the BLR Balmer decrement.

Finally, I corrected both the isolated narrow line spectrum and the isolated broad line spectrum for the effects of dust using the NLR Balmer decrement, as described in §4.8. Then I integrated over each spectrum using the exact same line ranges as before correction for dust effects to obtain the broad and narrow line fluxes after correction for dust effects. These line fluxes I used to calculate the NLR and BLR Balmer decrements after correction for dust effects.

Figure 9 shows an example of the isolated narrow line spectrum before and after correction for dust effects, giving an expanded with of the Hα and Hβ lines. Figure 10 shows an example of the isolated broad line spectrum before and after correction for the effects of dust. The object is the same as in 7 and 8, but here the results of using the isolation method are shown. I used both the SMC extinction curve and the Calzetti extinction curve to correct the spectra, but here I am displaying only the result of using the SMC curve for illustration purposes. I show three more examples of isolated line spectra in the appendix: Isolated narrow line spectra in figure 36, 37 and 38, and isolated broad line spectra in figure 39, 40 and 41.

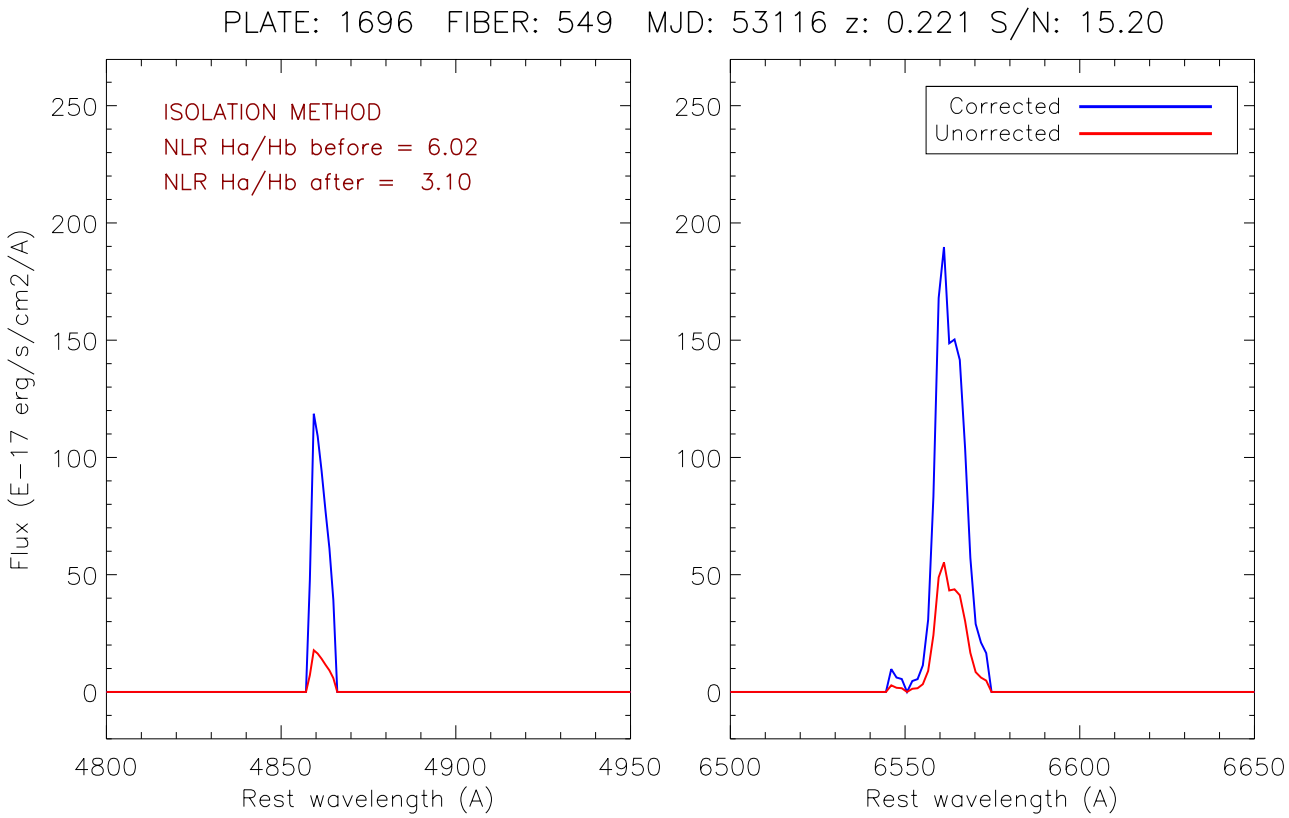

Figure 9: Representative example of the isolated narrow Hα and Hβ emission line spectrum before and after correction for dust effects. I used the SMC extinction curve. The narrow lines are isolated by subtracting the continuum and modeled broad Hα and Hβ lines. Same object as shown in figure 7 and figure 8. The isolated broad line spectrum for the same object is shown in figure 10. NLR Balmer decrements before and after correction for the effects of dust are displayed. These Balmer decrements are the result of direct integration over the isolated narrow line spectrum in the line ranges before and after correction for dust effects (see §4.7).

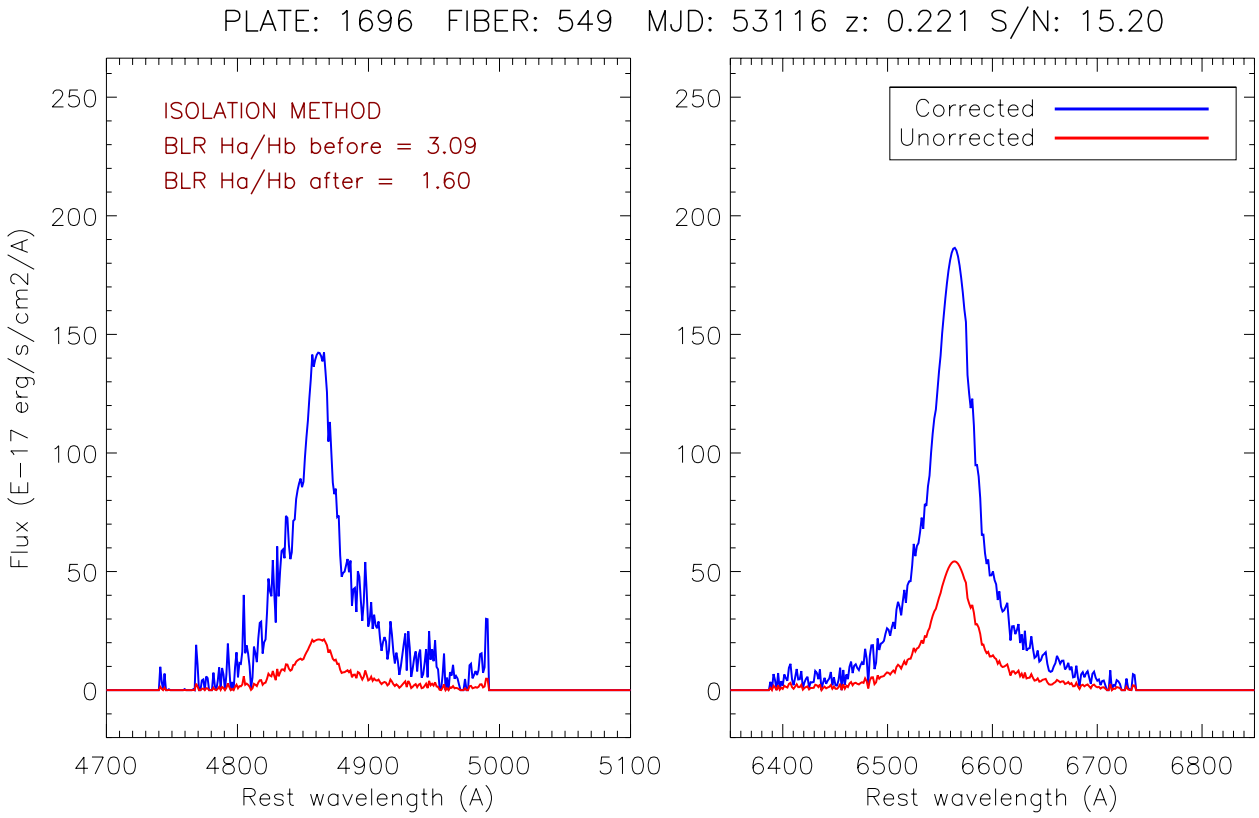

Figure 10: Representative example of the isolated broad Hα and Hβ emission line spectrum before and after correction for dust effects. I used the SMC extinction curve. The broad lines are isolated by subtracting the continuum, the modeled narrow [NII] and [OIII] lines, and the isolated narrow line spectrum seen in figure 9. Same object as shown in figure 7 and figure 8. The isolated narrow line spectrum for the same object is shown in figure 9. BLR Balmer decrements before and after correction for the effects of dust are displayed. These Balmer decrements are the result of direct integration over the isolated broad line spectrum in the line ranges before and after correction for dust effects (see §4.7).

4.8 Correcting The Spectra For Dust Extinction

To correct the spectra for the effects of dust up to and including dust in the NLR, I used the NLR Balmer decrement to determine the amount of dust:

The color excess due to dust extinction of the $H\alpha$ and $H\beta$ emission lines can be expressed as:

$$A(H\beta) - A(H\alpha) = E(H\beta - H\alpha) = -2.5 \times \log_{10}\left[\frac{(H\alpha/H\beta)_{int}}{(H\alpha/H\beta)_{obs}}\right] \tag{1}$$

Where $(H\alpha/H\beta)_{int}$ is the intrinsic NLR Balmer decrement, and $(H\alpha/H\beta)_{obs}$ is the observed one. This color excess can be related to the broadband color excess, E(B-V), via an extinction curve $\kappa(\lambda)$:

$$A(\lambda) = \kappa(\lambda)E(B - V) \tag{2}$$

Using this, the extinction at $H\alpha$ and $H\beta$ can be expressed as:

$$E(H\beta - H\alpha) = E(B - V)\left[\kappa(H\beta) - \kappa(H\alpha)\right] \tag{3}$$

Combining the equations gives an expression for E(B-V) as a function of the observed NLR Balmer decrement:

$$E(B - V) = \frac{E(H\beta - H\alpha)}{[\kappa(H\beta) - \kappa(H\alpha)]} \tag{4}$$

$$= \frac{-2.5}{[\kappa(H\beta) - \kappa(H\alpha)]} \times \log_{10}\left[\frac{(H\alpha/H\beta)_{int}}{(H\alpha/H\beta)_{obs}}\right] \tag{5}$$

The Calzetti extinction curve is given by:

$$\kappa(\lambda) = 2.659(-1.857 + 1.040x) + R(V) \text{ for } (0.63\,\mu m \leq \lambda \leq 2.20\,\mu m) \tag{6}$$

$$\kappa(\lambda) = 2.659(-2.156 + 1.509x - 0.198x^2 + 0.011x^3) + R(V) \text{ for } (0.12\,\mu m \leq \lambda \leq 0.63\,\mu m) \tag{7}$$

Where $x = 1/\lambda$ is the inverse of the wavelength in microns, and $R(V) = A(V)/E(B - V)$ is the total-to-selective extinction ratio. Using $R(V) = 4.05$ gives a value of the extinction curve at the wavelength of the two lines of $\kappa(H\alpha) = 3.33$ and $\kappa(H\beta) = 4.60$.
For the SMC extinction curve, I interpolated the extinction curve to the wavelength position of the Hα and Hβ emission lines and found $\kappa(H\alpha) = 2.17$ and $\kappa(H\beta) = 3.33$ using $R(V) = 2.74$. The value of the intrinsic NLR Balmer Decrement is 3.10 (Osterbrock & Ferland, 2006). These values I used to calculate the color excess using eqn (5). I then calculated the total extinction at the V-band as:

$$A(V) = R(V) \cdot E(B - V) \tag{8}$$

To find the absolute extinction at each wavelength, $A(\lambda)$, I used:

$$A(\lambda) = \kappa(\lambda) \cdot E(B-V) = \frac{A(\lambda)}{A(V)} \cdot R(V) \cdot E(B-V) \tag{9}$$

Where $\frac{A(\lambda)}{A(V)}$ is the value of the extinction curve at each wavelength step of the spectrum, which I calculated by interpolating the extinction curve to the rest wavelength array of each spectrum. The optical depth, $\tau(\lambda)$, is found as:

$$\tau(\lambda) = A(\lambda)/1.086 \tag{10}$$

This I used to correct the spectra using the expression:

$$F(\lambda) = F(\lambda, 0) \cdot \exp(-\tau(\lambda)) \leftrightarrow \tag{11}$$

$$F(\lambda, 0) = F(\lambda) \cdot \exp(\tau(\lambda)) \tag{12}$$

Where $F(\lambda, 0)$ is the unreddened (corrected) spectrum and $F(\lambda)$ is the observed spectrum, which has been reddened by the dust. In all my calculations, I assumed that this dust is located primarily in the NLR. In figure 11, I show an example of a spectrum before and after correction for the effects of dust using both the SMC and the Calzetti extinction curves. In the appendix, I show three more examples in figure 42, 43 and 44 .

4.9 Refitting of The Corrected Spectra

This step is part of the refit method and is only performed for spectra in the test sample. In order to determine the NLR and BLR Balmer decrements of the dust-free spectra, I once again fitted the continuum model described in §4.5. Many of these corrected spectra have very steep slopes at wavelengths shorter than ∼4000 Å. In order to be able to obtain a resonable fit and be able to determine the Hα and Hβ line fluxes, I opted to exclude the wavelength range blueward of 4600 Å. I still fitted a single power law, but I adjusted the limits of the power law slope to [-12, 2] to be able to fit the steeper spectra. After subtracting the continuum, I fitted the emission lines using the same model as described in §4.6. The broad and narrow Hα and Hβ emission line fluxes obtained from the line fit I then used to determine the BLR Balmer decrement and NLR Balmer decrement after correction for the effects of dust.

In figure 12 I show the results of the continuum and line fitting after correction for dust effects for the same object as shown in figure 7. The spectrum has been corrected for dust extinction using the NLR Balmer decrement displayed in figure 8, which has been determined using Hα and Hβ broad and narrow line fluxes from the line fit and the SMC extinction curve. In my analysis of each spectrum, I used both the SMC and the Calzetti extinction curves, but for illustration purposes, I show only the results of using the SMC extinction curve here. The difference in the corrected spectra using the two curves is small, as illustrated in figure 11.

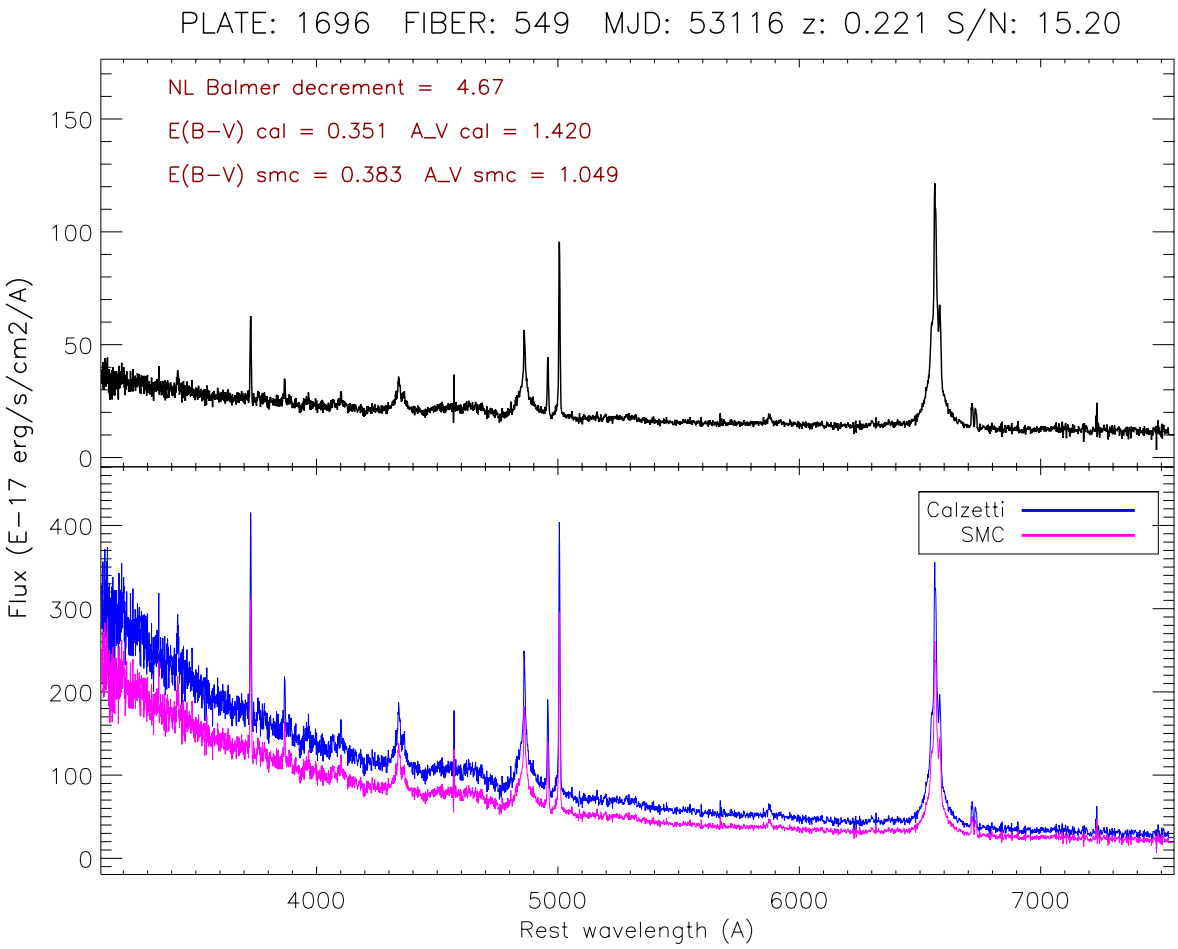

Figure 11: Top panel: Example of spectrum before correction for dust effects Bottom panel: same spectrum after correction for dust effects using the SMC and Calzetti extinction curves. Same object as shown in figure 7. The color excess, E(B-V), and the total extinction, A(V) are displayed for both extinction curves, along with the NLR Balmer decrement used for the correction. The Balmer decrement used, I have calculated using the narrow line fluxes from the line fits.

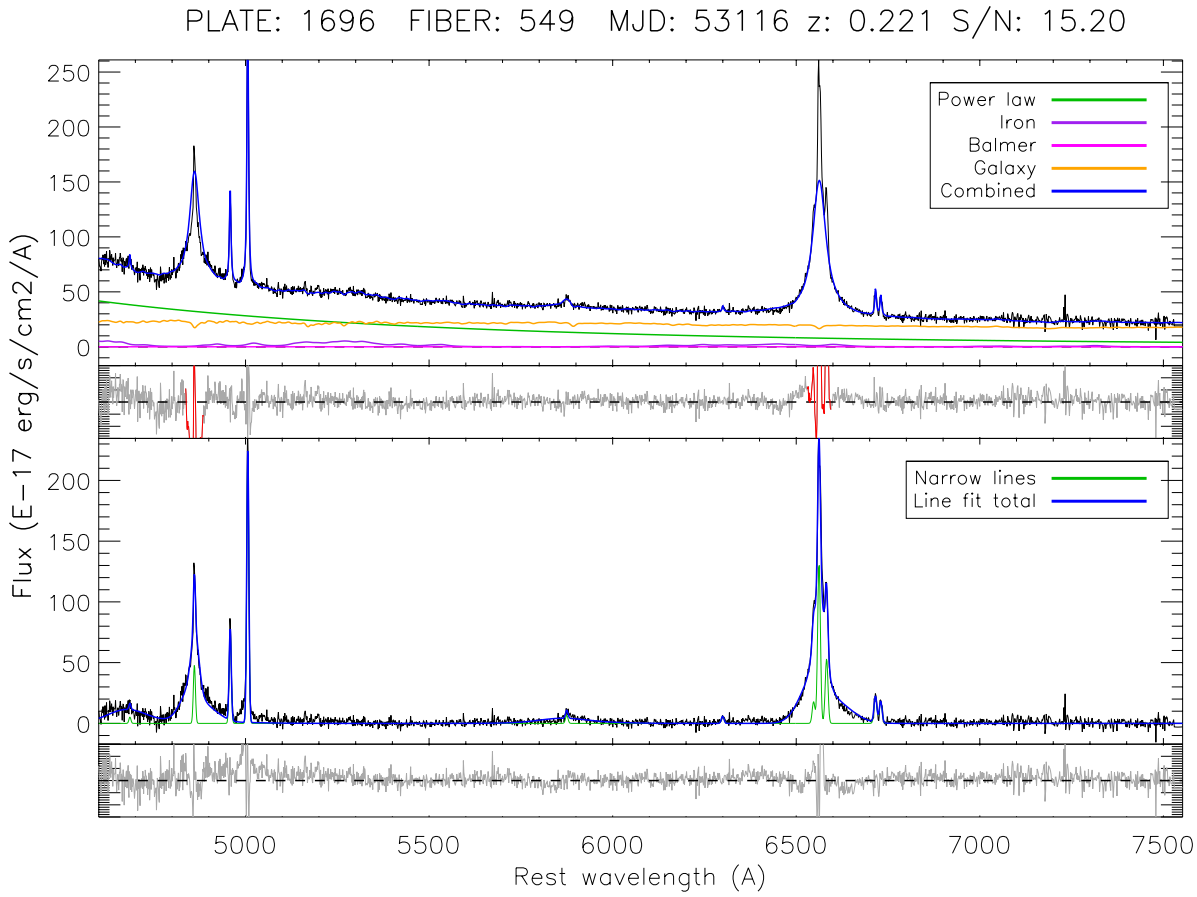

Figure 12: The results of fitting the spectrum after correction for the effects of dust for the same object as shown in figure 7. The spectrum has been cut off at 4600 Å to allow for easier fitting. Refer to figure 7 caption for further plot details. Expanded view of linefit after correction for the effects of dust is displayed in figure 13.

An expanded view of the Hα and Hβ line fits after correction for dust effects is found in figure 13. The NLR and BLR Balmer decrements after correction for dust effects are displayed on the plot. Compared with the line fit before correction for dust effects (seen in figure 8), the residuals are larger. This object is selected from the test sample, which generally is selected for having good line fits, but still the residuals grow larger after when using the refit method to correct for the effects of dust.

Three more examples of continuum and line fitting after correction for dust effecs are found in the appendix in figure 45, 46 and 47, and a close look at line fits are seen in figure 48, 49 and 50.

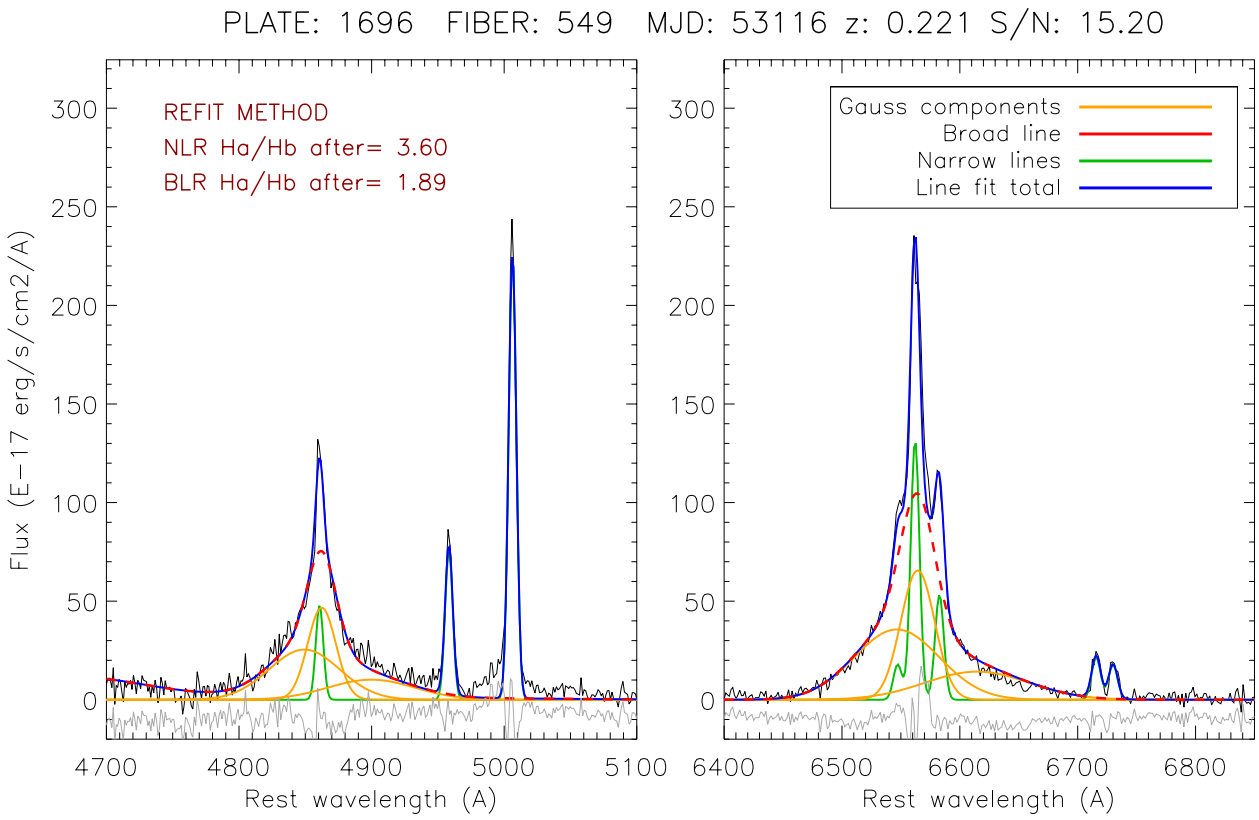

Figure 13: Expanded view of line fits for object shown in figure 12 after correcting the spectrum for dust. Left panel: Hβ line fit. Right panel: Hα line fit. Observed spectrum in black. The modeled broad line profile is red dashed line. The individual Gaussian components pertaining to the model of the broad line profile are in orange. Narrow lines in green. Best-fit line model in blue. Residuals of the line fits are displayed below, offset for clarity. BLR and NLR Balmer decrements (after correction for dust effects) are displayed. These Balmer decrements are calculated using the Hα and Hβ broad and narrow line fluxes from the line fit shown in figure 12, and I have used the SMC extinction curve. In figure 8 I show the same line fits before correction for dust effects. As is seen, the residuals after correction for dust effects are larger than before correction.

4.10 Estimation of Uncertainties on the Balmer Decrements

To estimate the uncertainties on the individual Balmer decrements, I used standard error propagation. For a function of several variables f, where each variable is measured with the (independent and random) uncertainties δx, δz etc, the uncertainty on f is given by:

$$\delta f = \sqrt{\left(\frac{\partial f}{\partial x}\delta x\right)^2 + \cdots + \left(\frac{\partial f}{\partial z}\delta z\right)^2} \tag{13}$$

For the Balmer decrements, the equation reduces to:

$$\delta\left(\frac{H\alpha}{H\beta}\right) = \left(\frac{H\alpha}{H\beta}\right) \cdot \sqrt{\left(\frac{\delta H\alpha}{H\alpha}\right)^2 + \left(\frac{\delta H\beta}{H\beta}\right)^2} \tag{14}$$

Where $H\alpha$ and $H\beta$ are the emission line fluxes and $\delta H\alpha$ and $\delta H\beta$ are the accumulated errors on these line fluxes. Each of the line fluxes have uncertainties from several sources, depending on the method used: A flux uncertainty (δ_{flux}) which is the statistical error inherent in the spectrum due to photon noise and processing. A continuum uncertainty (δ_{cont}), which is the uncertainty on determining the continuum level under the emission line, and A line model uncertainty (δ_{line}) which is the uncertainty on the line model. For the corrected spectra, the uncertainty on the NLR Balmer decrement used to calculate E(B-V) using eqn (5) propagates to the uncertainty on the line fluxes after correction for dust effects. This uncertainty I will refer to as the correction uncertainty (δ_{corr}).

I determined δ_{flux} by integrating over the SDSS variance spectrum in a wavelength range across each emission line and taking the square root of the integrated result. As described in §4.7, this wavelength range is found using a velocity offset of ± 8000 km s^{-1} from the rest frame line center for the broad lines and a velocity offset of ± 800 km s^{-1} from the rest frame line center of the narrow lines.

To estimate δ_{cont}, I selected 5 spectra with flat continua and representative noise levels and calculated the mean and the RMS around the mean of the flux level in two emission line free wavelength ranges. This RMS is an estimate of the poisson distribution of the flux, or the variation of the flux level. I chose to estimate the uncertainty on the continuum level under the emission lines in this manner rather than the more time consuming procedure of increasing and decreasing the continuum level by 1σ (1 standard deviation) and refitting the models.

I calculated δ_{line} using the residuals obtained by subtracting the continuum model from the spectrum. The residuals represent the difference between the model and the data. To get an estimate of how well the model has determined the emission line flux, I squared the residuals in the wavelength range of the line (to account for negative values), summed, and took the square root of the total. This is my estimate of the uncertainty on the line model.

δ_{corr} I found by propagating the error on the NLR Balmer decrement using standard error propagation, as per eqn (13). For a given extinction curve, eqn (5) depends on only one variable: $(H\alpha/H\beta)_{obs}$. The uncertainty on E(B-V) thus is: δE(B-V) = constant $\cdot \left(\frac{\delta(H\alpha/H\beta)_{obs}}{(H\alpha/H\beta)_{obs}}\right)$ (the relative error on the NLR Balmer decrement). Further propagating the error through eqn (9), eqn (10) and eqn (12), I

find $\delta\tau(\lambda) = \tau(\lambda) \cdot \left(\frac{\delta E(B-V)}{E(B-V)}\right)$, and $\delta F(\lambda, 0) = F(\lambda, 0) \cdot \delta\tau(\lambda)$. This means that the uncertainty on the corrected spectrum due to the uncertainty on the observed NLR Balmer decrement can be found by scaling the corrected spectrum by the uncertainty on $\tau(\lambda)$. The spectrum thus obtained I treated as an error spectrum. I squared this spectrum, integrated in the wavelength ranges of the lines, and taken the square root of the result:

$$\delta_{corr} = \sqrt{\sum (F(\lambda) \cdot \delta\tau(\lambda))^2 \cdot \delta\lambda} \tag{15}$$

Where $\delta\lambda$ is the wavelength step between each pixel of the spectrum in the line range.

4.10.1 Isolation Method Line Flux Uncertainties

When using the isolation method, the error on each of the line fluxes before correction for dust effects is found as (taking the $H\alpha$ flux as an example):

$$\delta H\alpha_{uncorr,iso} = \sqrt{\delta^2_{flux} + \delta^2_{cont}} \tag{16}$$

I do not include δ^2_{line}, as the line flux is found by integrating over the line spectrum itself, not from the model fit. Here, I implicitly trust the model of the Broad line, which is subtracted from the spectrum to create the isolated narrow line spectrum and assume that no significant uncertainty is derived from this step. Likewise, I trusted the model of the narrow [NII], S, and [OIII] lines subtracted to create the isolated broad line spectrum. The uncertainty on the corrected line flux is only δ_{corr} , as no further continuum or line fitting is involved, and δ^2_{flux} has already been acconted for in the first step.

$$\delta H\alpha_{corr,iso} = \delta_{corr} \tag{17}$$

4.10.2 Refit Method Line Flux Uncertainties

When using the refit method, the error on each of the line fluxes before correction for dust effects is found as:

$$\delta H\alpha_{uncorr,refit} = \sqrt{\delta^2_{flux} + \delta^2_{cont} + \delta^2_{line}} \tag{18}$$

Comparing to eqn (16), an extra term (δ^2_{line}) enters due to the unertainty on the line model. After correcting the spectra for dust extinction, a new round of continuum fitting and line fitting is performed. The uncertainty on the corrected line fluxes is therefore calculated as:

$$\delta H\alpha_{corr,refit} = \sqrt{\delta^2_{cont} + \delta^2_{line} + \delta^2_{corr}} \tag{19}$$

The flux uncertainty term (δ^2_{flux}) is included in δ^2_{corr}, as it has been propapaged through the uncertainty on the NLR Balmer decement used for correcting the spectra.

4.10.3 The Uncertainty on the Mean of the Balmer Decrements

The error on the mean of the Balmer decrements has been calculated using the error propagation rule. I squared the error on each Balmer decrement, summed these and divided by the number of Balmer decrements. For N Balmer decrements this is expressed as:

$$\delta\left(\frac{H\alpha}{H\beta}\right)_{mean} = \frac{\sqrt{\sum(\delta(\frac{H\alpha}{H\beta})_i^2 + \delta(\frac{H\alpha}{H\beta})_{i+1}^2 + \cdots + \delta(\frac{H\alpha}{H\beta})_N^2)}}{N} \tag{20}$$

5 Results

Here I present the distribution of Balmer decrements before and after correction for the effects of dust up to and including dust in the NLR. The NLR Balmer decrements are presented in §5.1 and the BLR Balmer decrements are presented in §5.3 for both samples. My results for the total extinction in the V-band, A(V), are presented In §5.2.

For the test sample, results using both the isolation method described in §4.2 and the refit method described in §4.1 are presented. For the main sample, I used only the isolation method. It was not possible to use the refit method for the main sample, as I was not able obtain a good model fit to the narrow Hα and Hβ line fluxes for many of the objects in the sample. For both the main sample and the test sample, I used the SMC as well as the Calzetti extinction curves to correct the spectra for dust extinction. I wanted to compare the results using the two extinction curves to see if the choice makes any significant difference in the resulting Balmer decrements. I summarize my findings regarding the extinction curves in §6.2.

5.1 NLR Balmer Decrements Before and After Correction

I calculated the NLR Balmer decrements both before and after correction for the effects of dust. The NLR Balmer decrements before correction for dust effects, I used to calculate E(B-V) and A(V) as described in §4.8 using both the SMC and the Calzetti extinction curves.

The NLR Balmer decrements after correction for dust effects can be used as a check of the validity of the correction. When calculating the color excess E(B-V) using eqn (5), the intrinsic NLR Balmer decrement is set to 3.1. If the spectra are corrected properly, the NLR Balmer decrement derived from the corrected line fluxes should therefore give 3.1, indicating a color excess of 0.

Table 2 summarizes the mean, median and standard deviation of the distribution NLR Balmer decrements before and after correction for the effects of dust for both samples and both extinction curves. Figure 14 shows the distribution of NLR Balmer decrements for the test sample before correction for dust effects using the isolation method, while figure 16 shows the distribution for the test sample before correction for dust effects using the refit method.

The mean of each distribution before correction for the effects of dust is quite high compared with the intrinsic value of 3.1, regardless of the method used. This indicates a high mean dust content in the sample objects, as I further describe in §5.2. Also, the standard deviation of the distributions of

	TEST ISO, SMC	**TEST ISO, CAL**	**TEST REFIT, SMC**	**TEST REFIT, CAL**	**MAIN ISO, SMC**	**MAIN ISO, CAL**
	BEFORE		**BEFORE**		**BEFORE**	
Mean	7.016±0.165		5.727±0.084		7.135±0.094	
Median	6.022		5.107		6.190	
Stddev	4.010		1.983		3.801	
	TEST ISO, SMC	**TEST ISO, CAL**	**TEST REFIT, SMC**	**TEST REFIT, CAL**	**MAIN ISO, SMC**	**MAIN ISO, CAL**
	AFTER		**AFTER**		**AFTER**	
Mean	3.100±0.088	3.100±0.113	3.159±0.908	3.457±1.630	3.100±0.059	3.100±0.075
Median	3.100	3.100	3.135	3.312	3.100	3.100
Stddev	0.001	0.001	0.488	0.641	0.002	0.002

Table 2: NLR Balmer Decrements for the test sample and the main sample, before and after correction for the effects of dust. Mean, median and standard deviation of each distribution is listed. ISO indicates the isolation method and REFIT the refit method. SMC indicates the SMC extinction curve and CAL the Calzetti extinction curve. Results are indicated with three decimal spaces to illustrate the very small differences when using the two different methods and the two different extinction curves.

	TEST ISO, SMC	**TEST ISO, CAL**	**TEST REFIT, SMC**	**TEST REFIT, CAL**	**MAIN ISO, SMC**	**MAIN ISO, CAL**
	BEFORE		**BEFORE**		**BEFORE**	
Mean	3.212±0.005		3.434±0.008		3.348±0.006	
Median	3.204		3.447		3.200	
Stddev	0.462		0.530		0.788	
	TEST ISO, SMC	**TEST ISO, CAL**	**TEST REFIT, SMC**	**TEST REFIT, CAL**	**MAIN ISO, SMC**	**MAIN ISO, CAL**
	AFTER		**AFTER**		**AFTER**	
Mean	1.655±0.010	1.654±0.012	1.876±0.047	1.887±0.061	1.785±0.005	1.784±0.007
Median	1.544	1.543	1.811	1.824	1.602	1.600
Stddev	0.619	0.619	0.652	0.684	0.973	0.973

Table 3: BLR Balmer Decrements for the test sample and the main sample, before and after correction for the effects of dust. Mean, median and standard deviation of each distribution is listed. ISO indicates the isolation method and REFIT the refit method. SMC indicates the SMC extinction curve and CAL the Calzetti extinction curve.

	TEST ISO, SMC	**TEST ISO, CAL**	**TEST REFIT, SMC**	**TEST REFIT, CAL**	**MAIN ISO, SMC**	**MAIN ISO, CAL**
Mean E(B-V)	0.683±0.020	0.625±0.018	0.532±0.024	0.487±0.022	0.686±0.012	0.629±0.011
Median E(B-V)	0.619	0.567	0.465	0.426	0.644	0.590
Stddev E(B-V)	0.341	0.313	0.258	0.236	0.389	0.356
Mean A(V)	1.870±0.055	2.533±0.074	1.457±0.067	1.973±0.091	1.881±0.032	2.547±0.044
Median A(V)	1.695	2.296	1.274	1.725	1.765	2.391
Stddev A(V)	0.935	1.266	0.707	0.958	1.065	1.443

Table 4: Color excess (E(B-V)) and absolute extinction (A(V)) for the test sample and the main sample, in units of magnitudes, calculated from the NLR Balmer decrements using eqn (5) and eqn (8). Mean, median and standard deviation of each distribution is listed. ISO indicates the isolation method and REFIT the refit method. SMC indicates the SMC extinction curve and CAL indicates the Calzetti extinction curve.

NLR Balmer decrements before correction for dust effects is quite large with both methods. These very broad distributions could in part be due to uncertainties on the measurements, but they do indicate a large spread of NLR Balmer decrements in the objects before correction for the effects of dust. If I assume that only the dust content of the objects varies, then these results show a great variation of the dust content in the NLR of my sample objects.

A few of the NLR Balmer decrements before correction for the effects of dust are exceptionally high, giving each distribution a long tail. A single object in the test sample (isolation method) has a NLR Balmer decrement of 36.46 before correction for dust effects. However, this object was flagged during the calculations for having a low narrow line Hβ flux. As a way to quickly assess the validity of the line fluxes when calculating the Balmer decrements, I used the flux uncertainty (δ_{flux}) described in §4.10. If the calculated line flux is below $3\delta_{flux}$, I set a flag. In the main sample, 10 objects are similarly flagged for having a narrow Hβ line flux below $3\delta_{flux}$ before correction for dust effects. The NLR Balmer decrements of these objects are: [47.90, 36.46, 23.55, 18.91, 16.62, 16.42, 12.31, 11.32, 7.50, 6.48]. These are all high values compared to the mean of the distribution. Since they are flagged, the linje fluxes are weak and have a relatively high uncertainty. Therefore, these are not valid results.

After correction for the effects of dust, the spread of the distibutions of NLR Balmer decrements are much smaller, in particular when using the isolation method. This clearly seen if figure 15, which shows the distribution after correction for the test sample using the isolation method, and in figure 17, which shows the distribution after correction for the test sample using the refit method.

For the test sample, the isolation method gives a distribution of NLR Balmer decrements after correction for dust effects with a mean of 3.100 ± 0.088 when using the SMC extinction curve, and with a mean of 3.100 ± 0.113 when using the Calzetti extinction curve. Both results are highly consistent with the expected value of 3.1 for the intrinsic NLR Balmer decrement. Using the refit method on the test sample likewise gives a distribution of NLR Balmer decrements after correction for dust effects consistent with 3.1 within 1σ, but with larger errors than the isolation method. Using the SMC extinction curve for the correction results in a mean NLR Balmer decrement of 3.159 ± 0.908 after correction. The Calzetti curve gives a mean of 3.457 ± 1.631 after correction. Both of these results are within 1σ of the expected value of 3.1, but with a large error. Overall, these results indicate that the isolation method gives more robust results than the refit method.

For the main sample, I only used the isolation method. The distributions of NLR Balmer decrements before and after correction for dust effects are very similar to those of the test sample using the isolation method, and I have placed the figures in the appendix. Figure 51 shows the distribution before correction for dust effects and figure 52 shows the distributions after correction for dust effects. Both extinction curves give a mean NLR Balmer decrement after correction for dust effects consistent within 1σ with the expected value of 3.1.

5.2 The Total Extinction, A(V)

Table 4 summarizes my results for A(V) and E(B-V) for both samples. A(V) is a measure of the amount of extinction in units of magnitudes. Regardless of the method used, my results indicate

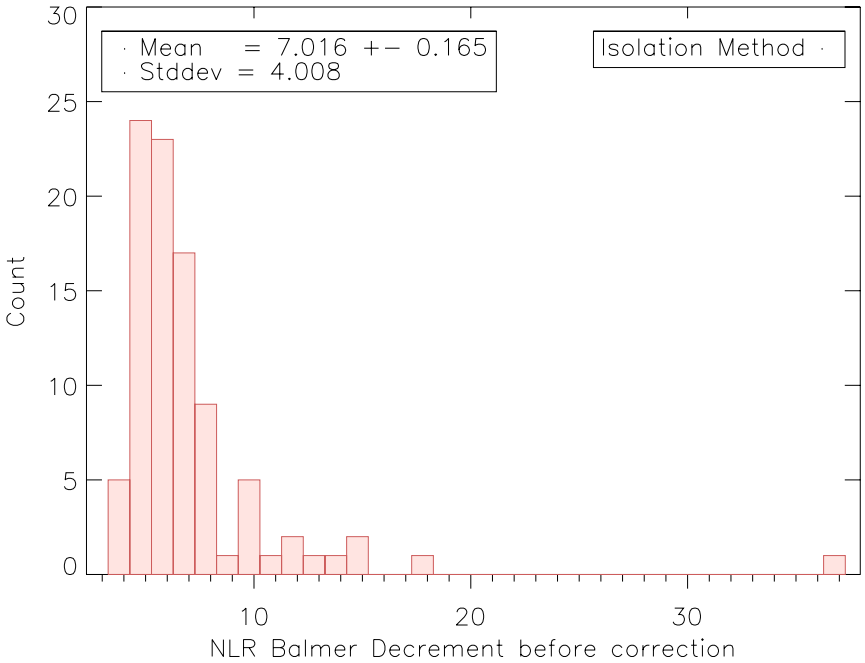

Figure 14: Distribution of NLR Balmer decrements before correction for the effects of dust for the test sample objects. The decrements are found using the isolation method (§4.1) and are are used to calculate E(B-V) and A(V) and correct the spectra for extinction due to dust.

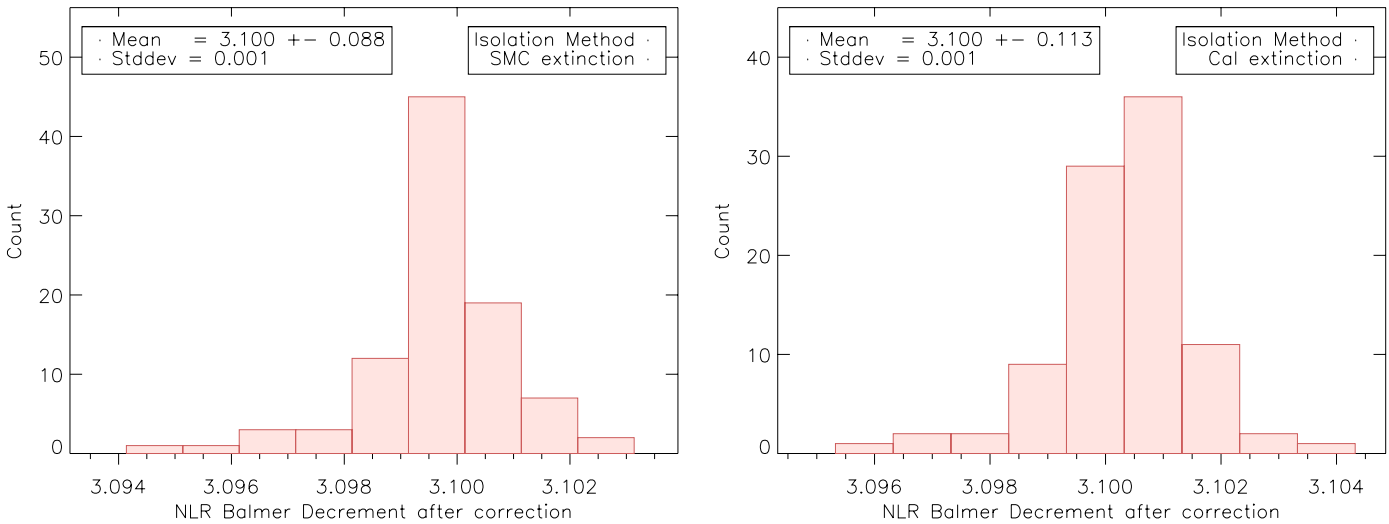

Figure 15: Distribution of NLR Balmer decrements for the test sample objects after correction for the effects of dust using the isolation method. Left panel: Using the SMC extinction curve. Right panel: Using the Calzetti extinction curve. The mean of each distribution is consistent within 1 σ of the expected value of 3.1 for the intrinsic NLR Balmer decrement

between 1.5 and 2.5 magnitudes of dust on average in the sample objects, which is surprisingly high. The distributions also have a large spread, which again indicates a large variation in the dust content of the objects.

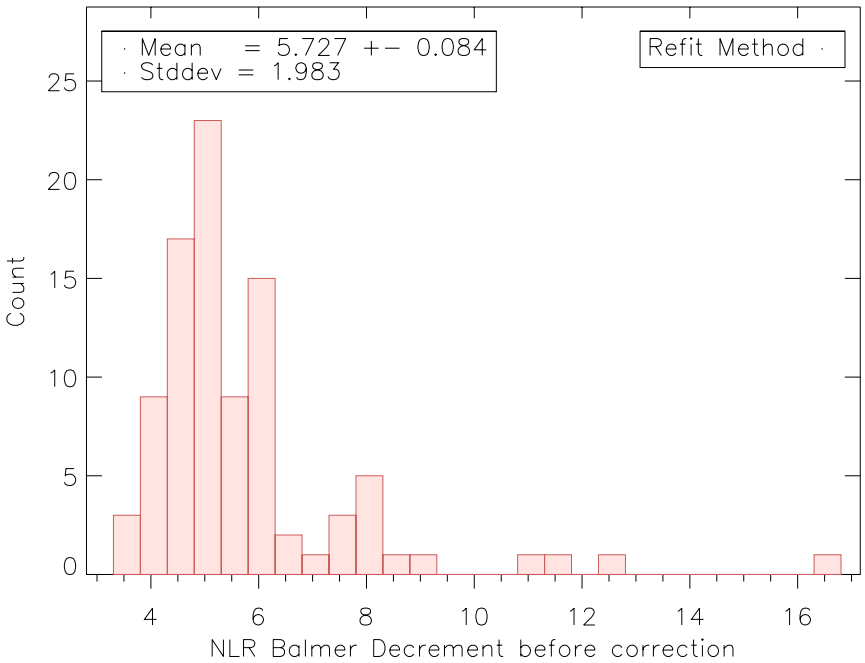

Figure 16: Same as figure 14, but using the refit method (§4.2).

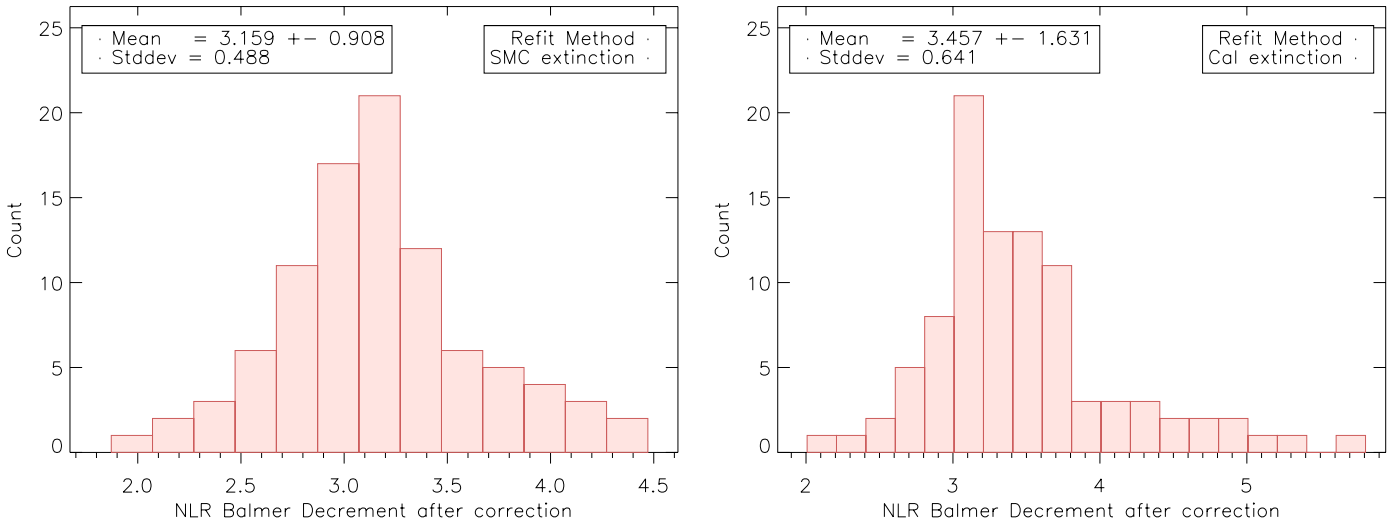

Figure 17: Same as figure 15, but using the refit method (§4.2).

The distribution of A(V) for the test sample using the isolation method is presented in figure 18 for both extinction curves. Figure 19 shows the distribution of A(V) for the test sample using the refit method, again for both extinction curves. For both methods, the mean A(V) based on the Calzetti extinction curve is significantly higher than the mean A(V) based on the SMC extinction curve. For the main sample, the distribution of A(V) is shown in figure 20. Some A(V) values in the main sample are negative. It does not make sense physically to have a negative extinction. By construction, E(B-V) and A(V) becomes negative for observed NLR Balmer decrements below the value of 3.1 (see eqn

(5)). Such low observed Balmer decrements could be the results of imprecise measurements. However, it could also be the case that the density of the NLR is not as high as expected, and that it would be more correct to use a Balmer decrement of 2.85 for the calculations. The value of 3.1 quoted for the intrinsic NLR Balmer decrement is an observed mean value (Osterbrock & Ferland, 2006). This means that individual measurements could be lower than 3.1. For the objects in the test sample, I do not get any negative values of A(V) with either the isolation method or the refit method. This indicates that these measurements are more robust than those of the main sample.

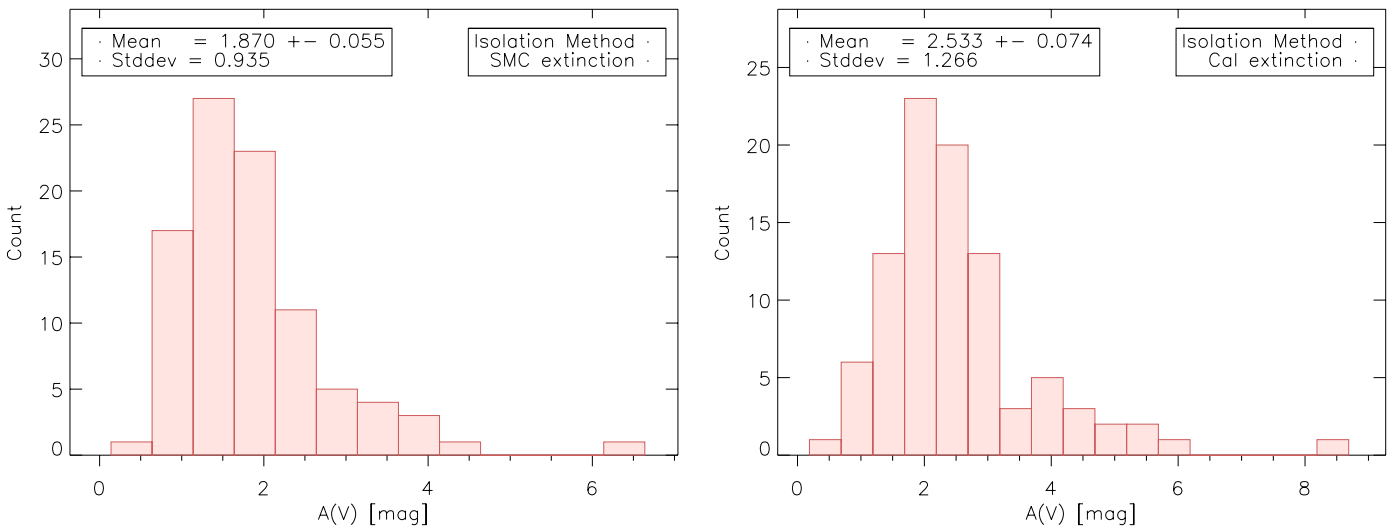

Figure 18: Distribution of A(V) for the test sample using the isolation method (§4.1). Left panel: Using the SMC extinction curve. Right panel: Using the Calzetti extinction curve.

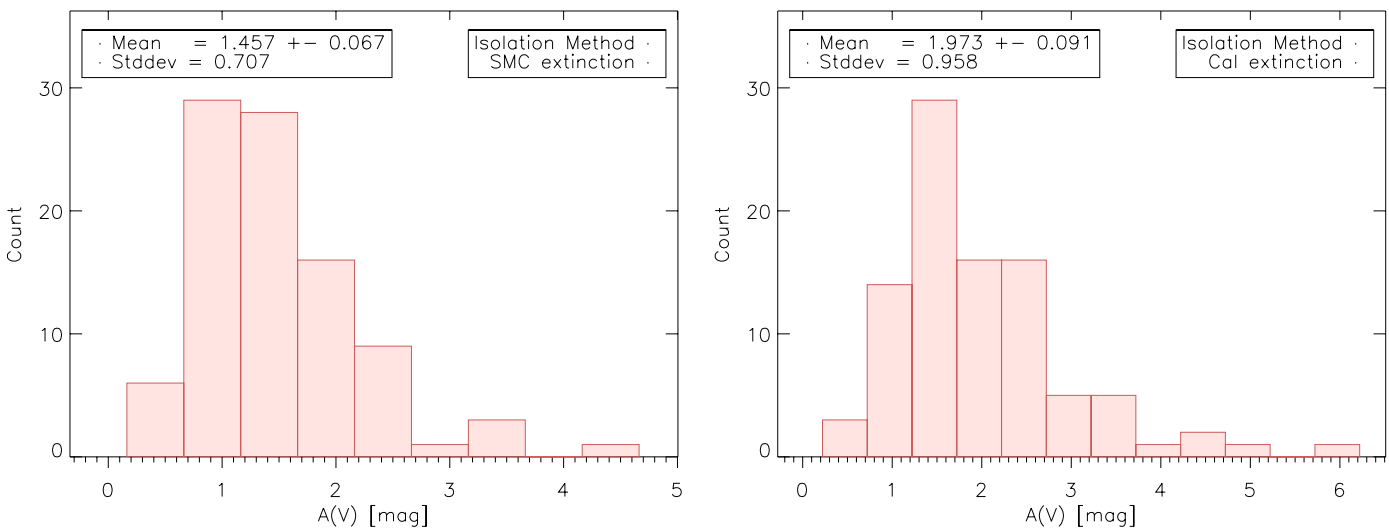

Figure 19: Same as figure 18, but using the refit method (§4.2)

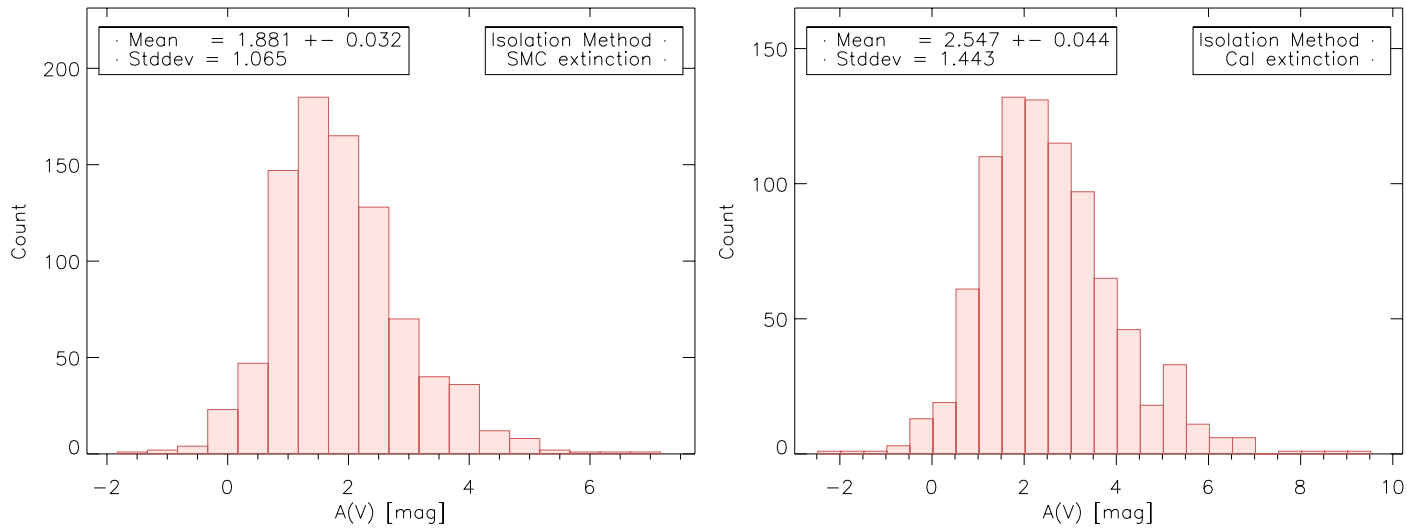

Figure 20: Same as figure 18, but for the main sample.

5.3 BLR Balmer Decrements Before and After Correction

To calculate the BLR Balmer decrements, I again used both the isolation method and the refit method for the test sample objects to be able to compare the results of the two methods. For the main sample, I only used the isolation method. Table 3 summarizes the mean, median and standard deviation of the distribution of NLR Balmer decrements before and after correction for the effects of dust for both samples.

Comparing the BLR Balmer decrements before correction for dust effects from the two methods of calculation used with the test sample (figure 21 and figure 23) shows that the mean of the distribution is slightly higher when using the refit method than when using the isolation method. This result could indicate that the refit method slightly underestimates the broad Hβ emission line flux, thereby making the Balmer decrements higher. Of course, it could also mean that the broad Hα emission line flux is overestimated, but as the Hβ line generally is weaker than the Hα line, the Hβ line typically is harder to model. Both distributions are quite wide, showing a large variation of BLR Balmer decrements in the test sample. However, the spread of the distribution of BLR Balmer decrements for the main sample before correction for the effects of dust, which is shown in figure 25, is significantly broader, with a long tail toward the high end. The maximum value in this distribution is 12.59, but this result is flagged because the broad Hβ line flux is below 3σ. Excluding this result, the maximum value of the BLR Balmer decrment before correction is 11.43, which is still quite high. However, BLR Balmer decrements as high as 10 have been observed (Dong et al., 2008).

After correction for dust effects, the distibution of BLR Balmer decrements for the test sample and the isolation method is shown in figure 22 for both extinction curves. For the test sample and the refit method, the distribution after correction is shown in figure 24. For the main sample, the distribution after correction is shown in figure 26. The mean of all three distributions is much lower than the value of 3.1 for the intrinsic NLR Balmer decrement and are not consistent with this value within the uncertainties. In §6.3, I discuss the implications of this.

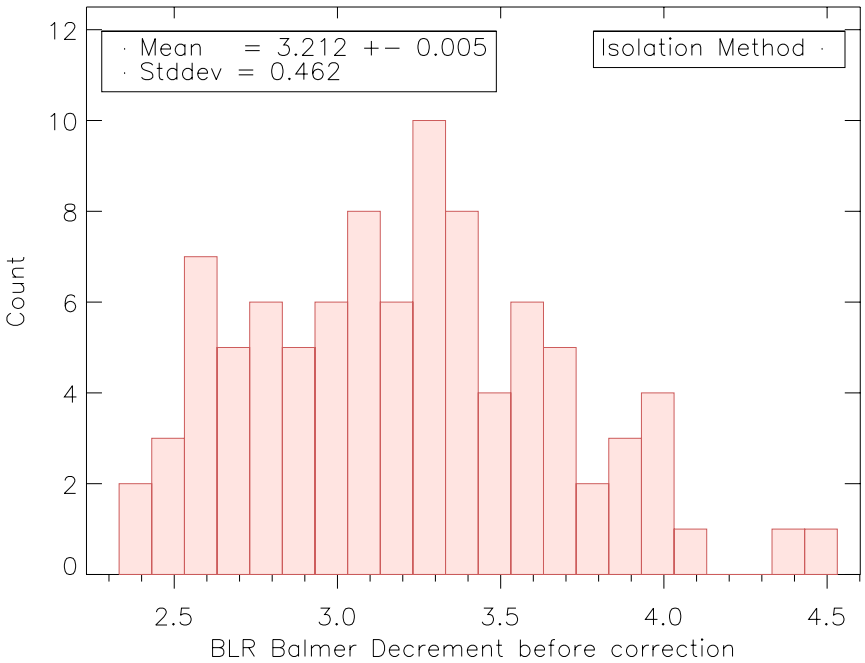

Figure 21: Distribution of BLR Balmer decrements for the test sample objects before correction for the effects of dust. These decrements are found using the isolation method.

For the main sample, the distributions after correction for dust effects are still wide due to a few high-value outliers. Without these outliers, the spread of the distributions would be comparable to those of test sample.

In figure 27, I present the BLR Balmer decrements vs redshift for the main sample. The test sample objects are marked with a blue diamond around the red dots. The left panel displays the distribution before correction for dust effects, and the right panel that after correction for dust effects. I show only the results using the SMC extinction curve, as the results using the two extinction curves are statistically the same. The theoretical value of the intrinsic Balmer decrement for the NLR of AGN is marked with a horizonal dashed line at 3.10. Another line marks 2.85, which is the theoretical value for a typcial low density HII region. The mean of the distribution after correction for dust effects is 1.785 ± 0.005, which lower than both of these theoretical values by more than 200σ.

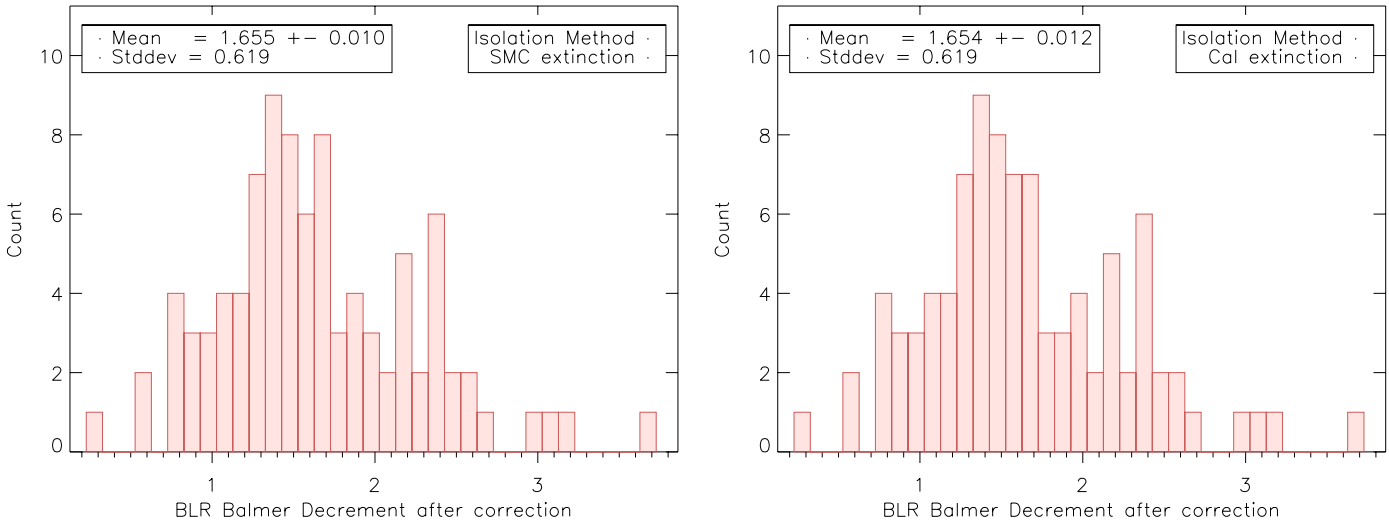

Figure 22: Distribution of BLR Balmer decrements for the test sample objects after correction for the effects of dust using both the SMC and the Calzetti extinction curves.

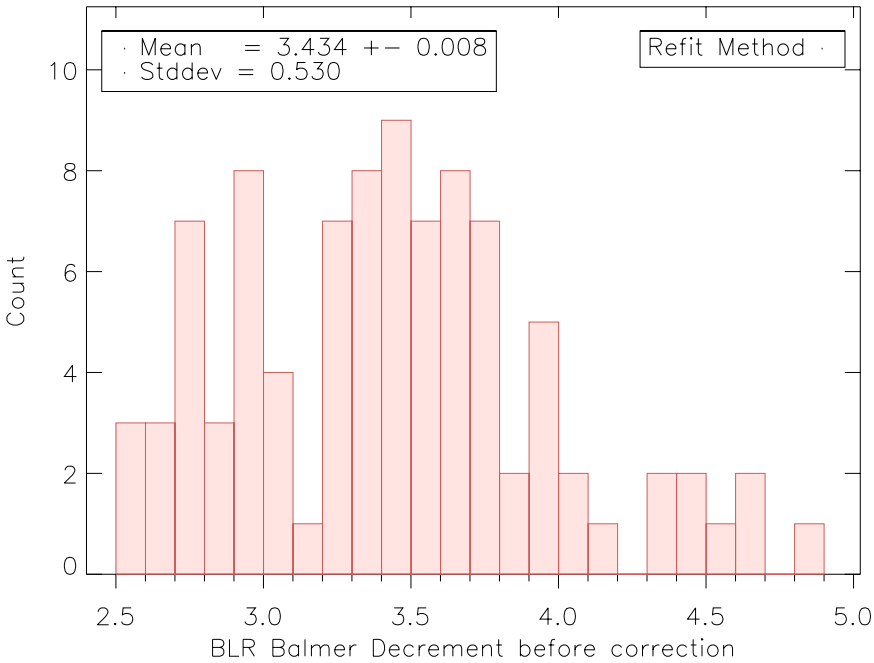

Figure 23: Same as figure 21, but using the refit method.

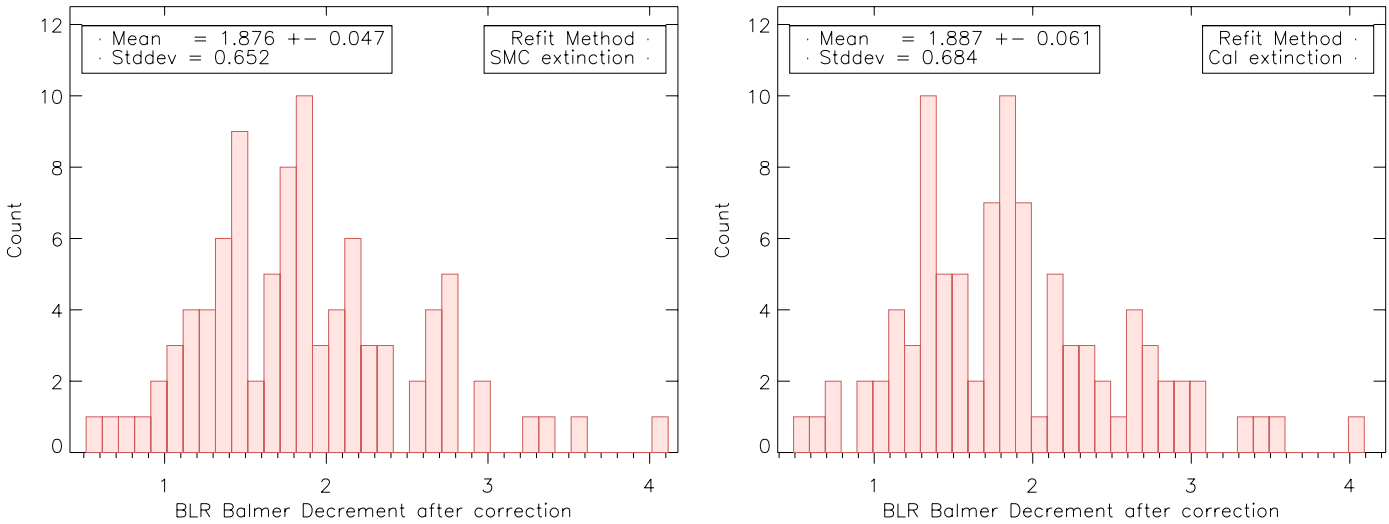

Figure 24: Same as figure 22 but using the refit method.

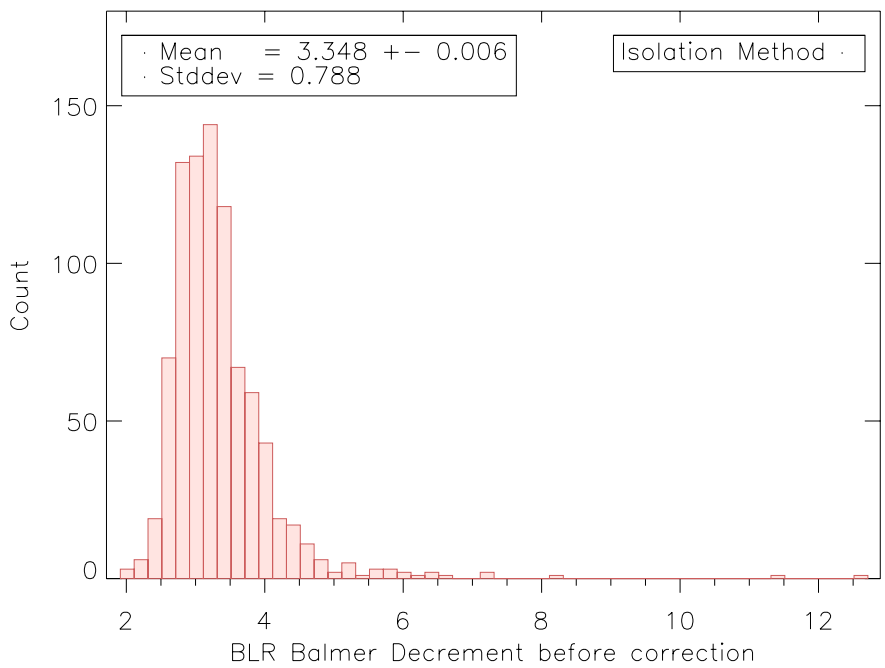

Figure 25: Same as figure 21 but for the main sample.

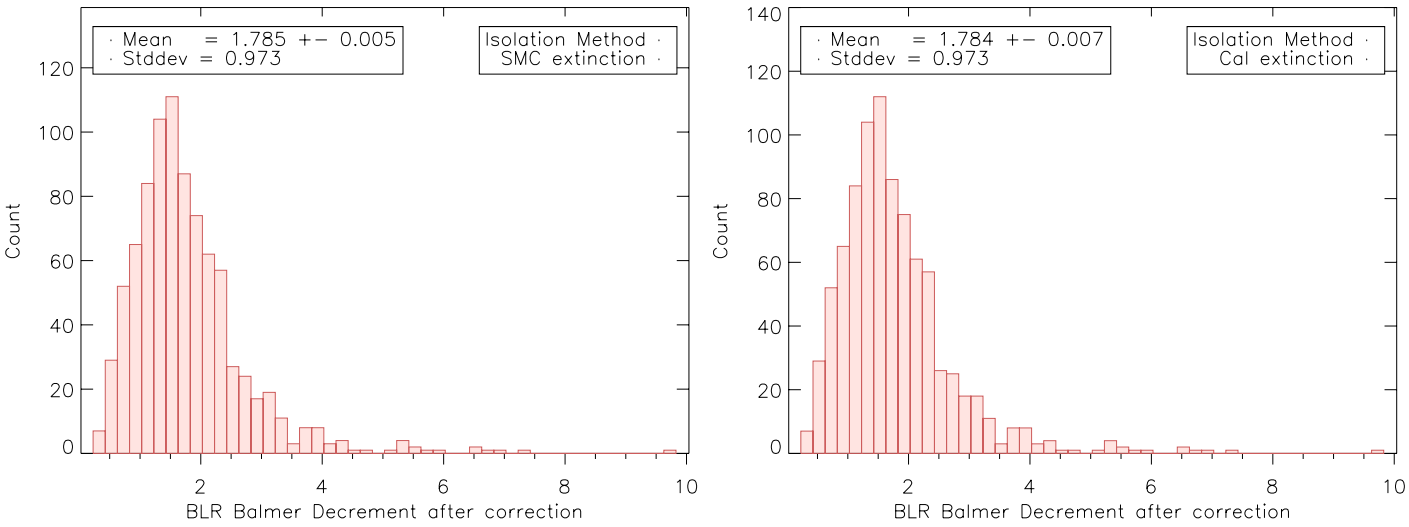

Figure 26: Same as figure 22, but for the main sample.

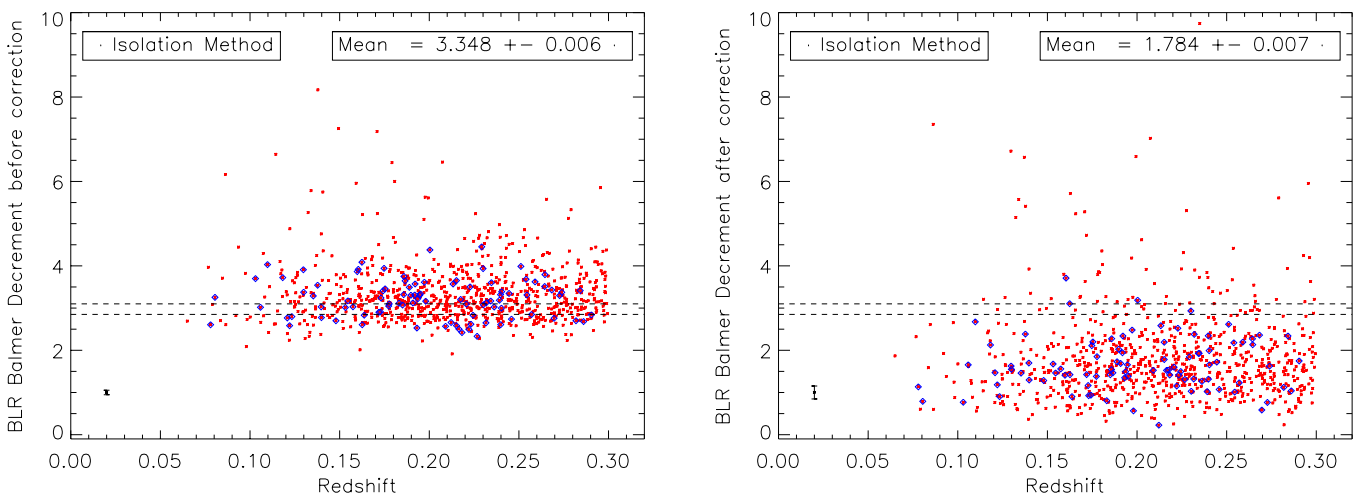

Figure 27: BLR Balmer decrements vs redshift for the main sample objects before correction for the effects of dust (left panel) and after correction for the effects of dust (right panel) using the isolation method and the SMC extinction curve. Test sample objects are marked with blue diamonds around the red dots. A typical error bar is shown in the lower left corner. Horizontal dashed lines mark 3.10 (the theoretical value of the intrinsic Balmer decrement for the NLR of AGN), and 2.85 (the theoretical value of the intrinsic Balmer decrement for a typical low density HII region). The mean of the distribution after correction for the effects of dust is 1.785 ± 0.005, which is significantly lower than both theoretical values.

6 Discussion

6.1 Comparing the Two Methods

When using the isolation method (for both samples), the results obtained for the NLR Balmer decrements are consistent within 1σ with the expected value of 3.1 after correction for the effects of dust. The refit method results are statistically the same but with larger errors. The uncertainties are higher when using the refit method than when using the isolation method. This is as expected and is due to the difficulty in measuring the line fluxes precisely when using line fitting even for a sample of high S/N spectre. The fact that the isolation method gives NLR Balmer decrements which so precisely recover the intrinsic value of 3.1 after correction for the effects of dust shows that the results obtained with this method are quite robust.

For the BLR Balmer decrements, the results using the two methods vary more. Comparing the results obtained for the test sample with the two methods shows that the refit method gives a mean BLR Balmer decrement which is higher than that obtained with the isolation method. For example, the mean BLR BD for the isolation method with the SMC extinction curve gives a mean BLR BD of 1.655 ± 0.010. With the refit method and the SMC extinction curve, the result is 1.876 ± 0.047. These results differ by $\sim 22\sigma$.

AGN are generally hard to model. I tried simpler models to fit the continuum (e.g. without a host galaxy component) and did not get good results. This is a challenge when using both the refit method and the isolation method, as both rely on fitting and removing the continuum. While I could not avoid modeling altogether when using the isolation method, I was able to obtain results which were consistent with the expected values within 1σ by not putting strong emphasis on the modeling of the narrow Balmer lines and just relying on the models of the broad lines, which are easier to model. This I consider an advantage of the isolation method.

After correcting the spectra for the effects of dust, it is quite difficult to model the continuum. Even with a NLR Balmer decrement of just 5 or 6, the spectra become very steep, and I had to cut the spectra off at 4600 Å to be able to obtain a reasonable continuum fit. This is definitely a challenge when using the refit method.

One of my main challenges has been to determine the line flux of the narrow Hβ line. The line is often very weak, and in some spectra, it simply is not possible to model well with the refit method. With the isolation method, it is still possible to determine the narrow line flux, as long as the broad line model can be trusted. When using the isolation method, it is however very important to compare the line flux found by integrating over the isolated narrow line spectrum to the error in the wavelength range of the line. This is to make sure that you are not just integrating over noise or a too weak signal.

Using data with higher spectral resolution, e.g. from X-shooter, would make it easier to properly separate the broad and narrow line components of the Hα and Hβ emission lines. This would be an advantage when using both methods.

6.2 The Extinction Curves

I computed the Balmer decrements using both the SMC and Calzetti extinction curves. For both samples and both methods, the results after correction for the effects of dust using the two different extinction curves are statistically the same. This applies to both the NLR and BLR Balmer decrements.

With the isolation method, the results for the NLR Balmer decrements are identical down to the third decimal (3.100±0.088 (SMC), 3.100±0.113 (Calzetti)). When using the refit method, the results using the Calzetti extinction curve are higher (3.46 ± 1.63) than those using the SMC extinction curve (3.16 ± 0.91), and the uncertainties are higher. The two results differ by less than 0.3 σ and both are consistent within 1σ with the expected value of 3.1.

As seen in figure 5, the two extinction curves are very close to the same value at the wavelength position of the Hα and Hβ emission lines, and my results are therefore not surprising. When working with a larger wavelength range where the extinction curves vary significantly, the choice of curve would have a greater impact on the results. When calculating the (Hα/Hβ) Balmer decrement after correcting the spectra, I find no significant difference, and I therefore conclude that the choice of ectinction curve is not of great importance when calculating the NLR and BLR Balmer decrements.

6.3 The BLR Balmer decrements and the Broad Line Region

The intrinsic value generally quoted for the NLR Balmer decrement is 3.1 (Osterbrock & Ferland, 2006; Dong et al., 2008), but it is an open question whether it is applicable to the BLR as well. The electron density of the NLR is in the order of $\sim 10^3$ cm^{-3}. The density of the BLR is higher to within an order of magnitude of $10^8 - 10^{10}$, and because of this high density, other factors than dust extinction affect the BLR Balmer decrement. These include collisional, optical-depth and radiative-transfer effects. It is therefore thought that the BLR Balmer decrement is not a good indicator of reddening in the BLR (Osterbrock & Ferland, 2006).

Theoretical calculations of the Balmer decrement in a high density environment (N_e of $10^9 - 10^{16}$ cm^{-3}) show that the intrinsic value of the Hα/Hβ decrement is strongly dependent on electron density (Adams & Petrosian, 1974). These calculations include the effect of inelastic electron-atom collisions. Their figure 3, here shown in figure 28, shows the Balmer decrement as function of electron density at 20000 K, 10000 K and 6000 K for Case B recombination, which is generally assumed for AGN.

After correction for dust effects, the mean BLR Balmer decrements of both my samples are lower than 2. Within the uncertainties, they are around 1.7-1.8. To explain these low intrinsic BLR Balmer decrements, the temperature would have to be between 6000 K and 10000 K and the electron density $\sim 10^{13}$ cm^{-3}.

The different emission lines are most efficiently emitted under very specific conditions. Detailed photoionization calculations of the broad emission line clouds in AGN specify these conditions (Korista et al., 1997). Their figure 3g is shown here in figure 29. The figure shows logarithmic contour plots of line strength as a function of hydrogen gas density (n(H)) and incident photon flux (ϕ(H)) for six different emission lines, including Hα and Hβ. The triangle indicates the conditions which most

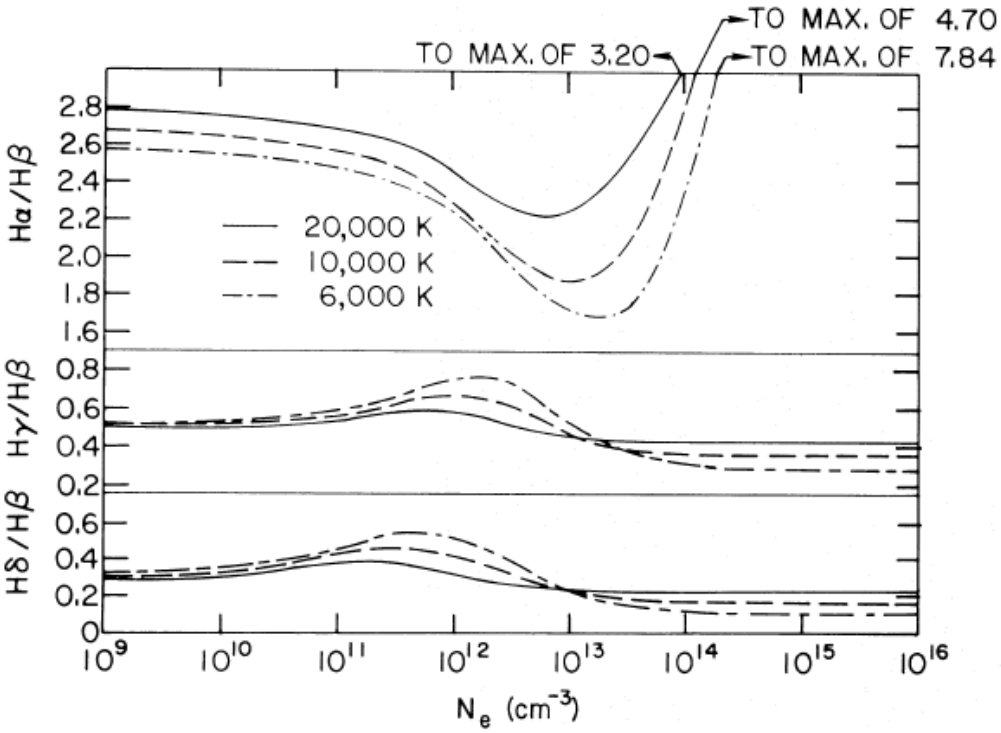

Figure 28: Case B Balmer decrements vs electron density for high electron densities. The theoretical decrements for 20000 K, 10000 K and 6000 K are shown. The top panel displays the Hα/Hβ decrements, which is what I am investigating. Source: (Adams & Petrosian, 1974).

efficiently give rise to the emission lines. As is seen, both Hα and Hβ are in fact strongly emitted at such high densities as $\sim 10^{13}$ cm^{-3} as long as the incident photon flux is not too high ($>$ 20dex). According to the LOC (Locally Optimally Emitting Clouds) model (Baldwin et al., 1995), each emission line is emitted from the part of the BLR where they are most efficiently emitted. Figure 29 shows that Hα and Hβ are clearly efficiently emitted at these very high densities of $10^{13} - 10^{14}$ cm^{-3}. As a consequence, such low BLR Balmer decrements as I find appear to be expected.

6.4 What Could Affect the Measurements?

Circumnuclear star formation: Hα and Hβ lines are emitted from ionisation nebulae, which are HII regions in star forming areas. If star formation does take place in some of the AGN in the sample, emission due to star formation would contribute to the measured narrow line emission. It would not be possible to separate this emission from that of the NLR gas because of the spectral resolution. The SDSS spectrographs use 3″ optical fibers which are placed on the center of the AGN. If any circumnuclear star formation is taking place, it could give a small contribution, but I assume that this contribution is negligible.

The gas density in the NLR: There are some indications that the NLR gas density varies with distance from the central black hole. It has recently been shown (Peterson et al., 2013) that the narrow [OIII] λ4959, [OIII]λ5007 emission lines vary over a 20 year period in NGC5548. This could indicate that the intrinsic NLR Balmer decrement is not exactly 3.1 for all AGN.

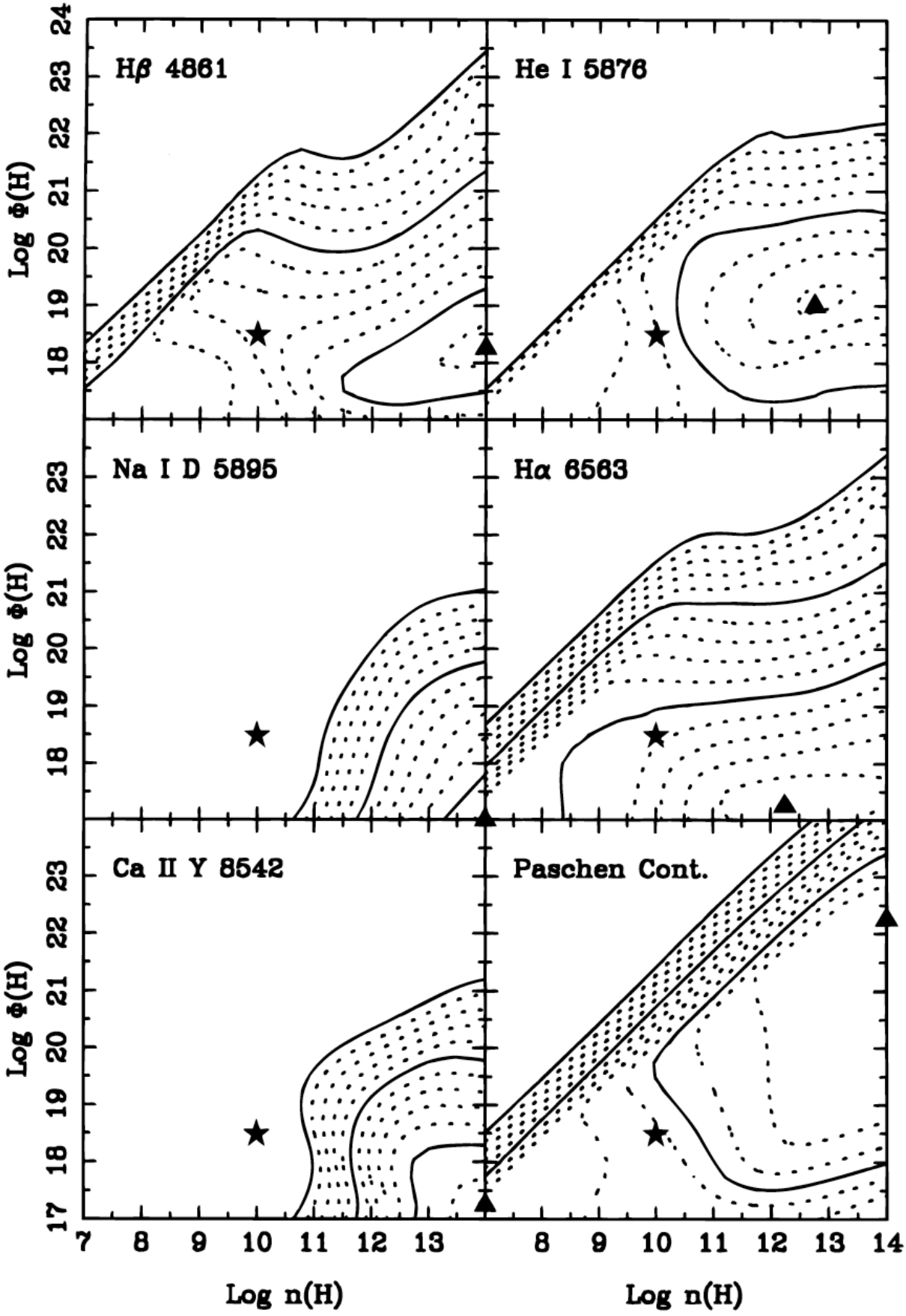

Figure 29: Source: (Korista et al., 1997).

6.5 Other Studies

Dong et al (Dong et al., 2008) examined the BLR Balmer decrements for a sample of 446 AGN from the SDSS Fourth Data Release. These objects were selected for having a steep continuum slope in the rest-wavelength range of 4000-5600 Å. Because of this steep continuum slope, they assumed the extinction due to dust of the objects to be negligible. They did not do any correction of their spectra to account for dust in the NLR. They did in fact fit the narrow component of the Hα and Hβ lines, but they did not use the ratio of these lines to check if it was consistent with no or very little dust in the NLR of their objects. For their distribution of BLR Balmer decrements, they found an average of 3.06 with a standard deviation of 0.03 dex. These results are comparable to my results for the mean BLR Balmer decrements before correction for the effcts of dust in both my samples.

Througout my analysis, I have assumed that dust is located only in the NLR of the AGN. However, this is contrary to the results presented recently by Heard & Gaskell (Heard & Gaskell, 2016). They used the results of other studies - such as those of (Dong et al., 2008) - to calculate and compare the NLR and BLR Balmer decrements of several samples of AGN. Through this analysis, they find that most of the examined objects have a higher reddening of the BLR than the NLR, and from this, they conclude that most of the dust which reddens the BLR is located between the NLR and the BLR. They use only observed Balmer decrements, not correcting for the effects of dust, and do not give much detail on the data processing and analysis. It is therefore hard for me to comment on these results or compare my results with theirs.

7 Conclusion

I have investigated two methods of calculating the BLR Balmer decrement (the ratio of the broad Hα and Hβ emission line fluxes) for a sample of 873 AGN from the SDSS DR7 Quasar Catalog. With the refit method, I used the emission line fluxes which I found by line fitting to calculate the BLR and the NLR Balmer decrements. With the isolation method, I integrated over the observed flux spectrum after isolating the narrow and broad components of the Balmer lines to obtain the emission line fluxes, and these fluxes I used to calculate the BLR and NLR Balmer decrements. Under the assumption that dust is only located in the NLR, not in the BLR, I used the NLR Balmer decrement to determine the amount of extinction due to dust in the objects and correct the spectra for this extinction. My results indicate between 1.5 and 2.5 magnitudes of dust on average in the NLR of the sample objects.

After correcting the spectra for the effects of dust, I calculated the intrinsic NLR and BLR Balmer decrements, and I used this intrinsic BLR Balmer decrement to investigate the density of the gas in the BLR. For my sample, I find a mean BLR Balmer decrement after correction for the effects of dust of $\sim 1.7 - 1.8$, depending on the method used for the calculation. This is significantly lower than 3.1, which is the value of the intrinsic NLR Balmer decrement often quoted. This result indicates an electron density in the BLR as high as 10^{13} cm^{-3}.

Comparing the results obtained using the isolation method and the refit method, I find that the isolation method gives more robust results than the refit method. Additionally, the isolation method is less time consuming than the refit method.

References

Adams, W. M., & Petrosian, V. (1974, August). Effect of Inelastic Electron-Atom Collisions on the Balmer Decrement. ApJ, *192*, 199-205. doi: 10.1086/153051

Baldwin, J., Ferland, G., Korista, K., & Verner, D. (1995, December). Locally Optimally Emitting Clouds and the Origin of Quasar Emission Lines. ApJ, *455*, L119. doi: 10.1086/309827

Boroson, T. A., & Green, R. F. (1992, May). The emission-line properties of low-redshift quasi-stellar objects. ApJS, *80*, 109-135. doi: 10.1086/191661

Calzetti, D., Kinney, A. L., & Storchi-Bergmann, T. (1994, July). Dust extinction of the stellar continua in starburst galaxies: The ultraviolet and optical extinction law. ApJ, *429*, 582-601. doi: 10.1086/174346

Dietrich, M., Hamann, F., Shields, J. C., Constantin, A., Heidt, J., Jäger, K., ... Wagner, S. J. (2003, June). Quasar Elemental Abundances at High Redshifts. ApJ, *589*, 722-732. doi: 10.1086/374662

Dong, X., Wang, T., Wang, J., Yuan, W., Zhou, H., Dai, H., & Zhang, K. (2008, January). Broad-line Balmer decrements in blue active galactic nuclei. MNRAS, *383*, 581-592. doi: 10.1111/j.1365-2966.2007.12560.x

Gordon, K. D., Clayton, G. C., Misselt, K. A., Landolt, A. U., & Wolff, M. J. (2003, September). A Quantitative Comparison of the Small Magellanic Cloud, Large Magellanic Cloud, and Milky Way Ultraviolet to Near-Infrared Extinction Curves. ApJ, *594*, 279-293. doi: 10.1086/376774

Heard, C. Z. P., & Gaskell, C. M. (2016, June). The location of the dust causing internal reddening of active galactic nuclei. *ArXiv e-prints*.

Hewett, P. C., & Wild, V. (2010, July). Improved redshifts for SDSS quasar spectra. MNRAS, *405*, 2302-2316. doi: 10.1111/j.1365-2966.2010.16648.x

Hopkins, P. F., Strauss, M. A., Hall, P. B., Richards, G. T., Cooper, A. S., Schneider, D. P., ... Szokoly, G. P. (2004, September). Dust Reddening in Sloan Digital Sky Survey Quasars. AJ, *128*, 1112-1123. doi: 10.1086/423291

Kauffmann, G., Heckman, T. M., Tremonti, C., Brinchmann, J., Charlot, S., White, S. D. M., ... Schneider, D. P. (2003, December). The host galaxies of active galactic nuclei. MNRAS, *346*, 1055-1077. doi: 10.1111/j.1365-2966.2003.07154.x

Korista, K., Baldwin, J., Ferland, G., & Verner, D. (1997). An Atlas of Computed Equivalent Widths of Quasar Broad Emission Lines. ApJS, *108*, 401-415. doi: 10.1086/312966

MacAlpine, G. M. (1985). Dust in active galactic nuclei and quasars. In J. S. Miller (Ed.), *Astrophysics of active galaxies and quasi-stellar objects* (p. 259-288).

Momcheva, I. G., Lee, J. C., Ly, C., Salim, S., Dale, D. A., Ouchi, M., ... Ono, Y. (2013, February). Nebular Attenuation in Hα-selected Star-forming Galaxies at z = 0.8 from the NewHα Survey. AJ, *145*, 47. doi: 10.1088/0004-6256/145/2/47

Netzer, H., & Laor, A. (1993, February). Dust in the narrow-line region of active galactic nuclei. ApJ, *404*, L51-L54. doi: 10.1086/186741

O'Donnell, J. E. (1994, February). R_{nu}-dependent optical and near-ultraviolet extinction. ApJ, *422*, 158-163. doi: 10.1086/173713

Osterbrock, D. E., & Ferland, G. J. (2006). *Astrophysics of gaseous nebulae and active galactic nuclei.*

Peterson, B. M. (1997). *An Introduction to Active Galactic Nuclei.*

Peterson, B. M., Denney, K. D., De Rosa, G., Grier, C. J., Pogge, R. W., Bentz, M. C., ... Ciroi, S. (2013, December). The Size of the Narrow-line-emitting Region in the Seyfert 1 Galaxy NGC 5548 from Emission-line Variability. ApJ, *779*, 109. doi: 10.1088/0004-637X/779/2/109

Schlegel, D. J., Finkbeiner, D. P., & Davis, M. (1998, June). Maps of Dust Infrared Emission for Use in Estimation of Reddening and Cosmic Microwave Background Radiation Foregrounds. ApJ, *500*, 525-553. doi: 10.1086/305772

Schneider, D. P., Richards, G. T., Hall, P. B., Strauss, M. A., Anderson, S. F., Boroson, T. A., ... Weinberg, D. H. (2010, June). The Sloan Digital Sky Survey Quasar Catalog. V. Seventh Data Release. AJ, *139*, 2360. doi: 10.1088/0004-6256/139/6/2360

Selsing, J., Fynbo, J. P. U., Christensen, L., & Krogager, J.-K. (2016, January). An X-Shooter composite of bright $1 \ll z \ll 2$ quasars from UV to infrared. A&A, *585*, A87. doi: 10.1051/0004-6361/201527096

Shen, Y., Richards, G. T., Strauss, M. A., Hall, P. B., Schneider, D. P., Snedden, S., ... Simmons, A. (2011, June). A Catalog of Quasar Properties from Sloan Digital Sky Survey Data Release 7. ApJS, *194*, 45. doi: 10.1088/0067-0049/194/2/45

Urry, C. M., & Padovani, P. (1995, September). Unified Schemes for Radio-Loud Active Galactic Nuclei. PASP, *107*, 803. doi: 10.1086/133630

Vanden Berk, D. E., Richards, G. T., Bauer, A., Strauss, M. A., Schneider, D. P., Heckman, T. M., ... Zheng, W. (2001, August). Composite Quasar Spectra from the Sloan Digital Sky Survey. AJ, *122*, 549-564. doi: 10.1086/321167

Véron-Cetty, M.-P., Joly, M., & Véron, P. (2004, April). The unusual emission line spectrum of I Zw 1. A&A, *417*, 515-525. doi: 10.1051/0004-6361:20035714

A Extra Plots:

A.1 Continuum and Line Fits

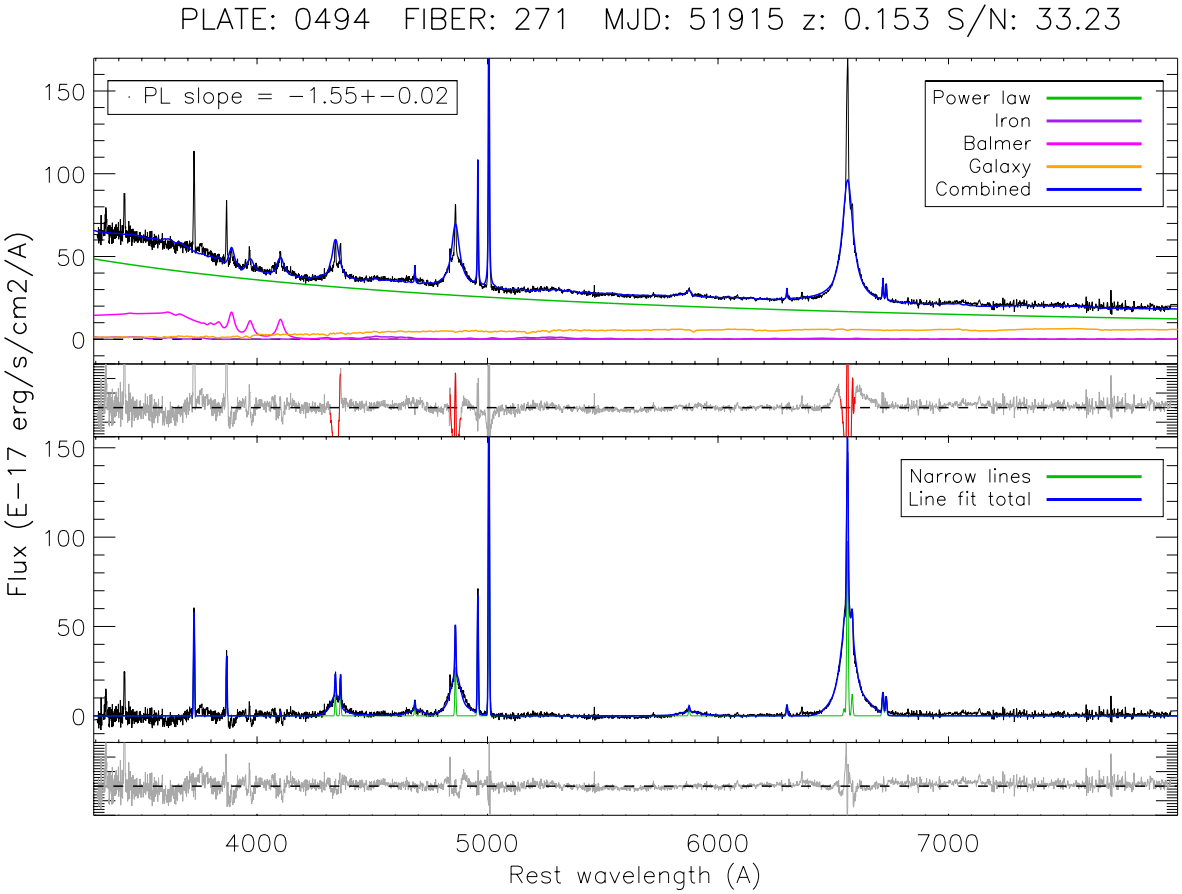

Figure 30: Representative example of spectrum showing the results of fitting of uncorrected spectra. Refer to figure 7 caption for further plot details. Expanded view of linefit shown in figure 33.

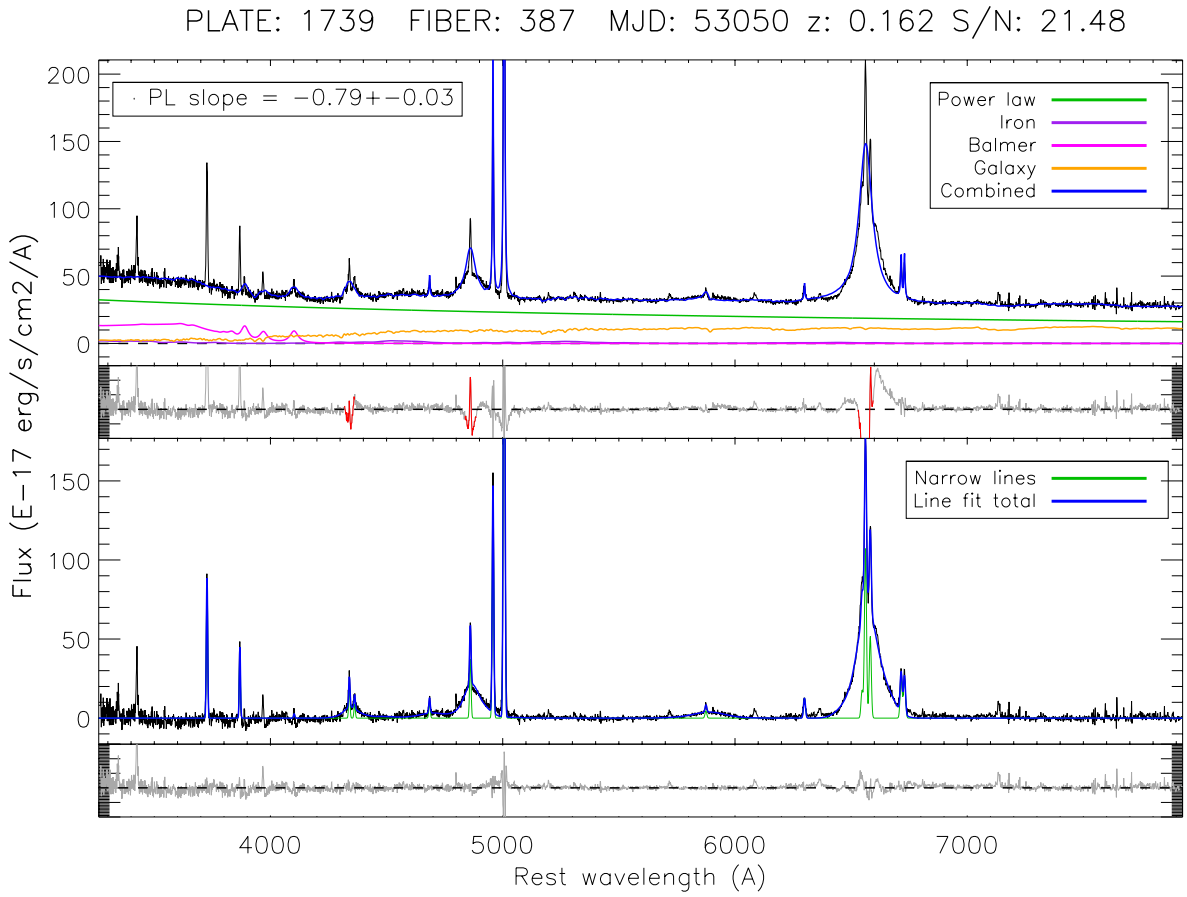

Figure 31: Representative example of spectrum showing the results of fitting of uncorrected spectra. Refer to figure 7 caption for further plot details. Expanded view of on linefit shown in figure 34.

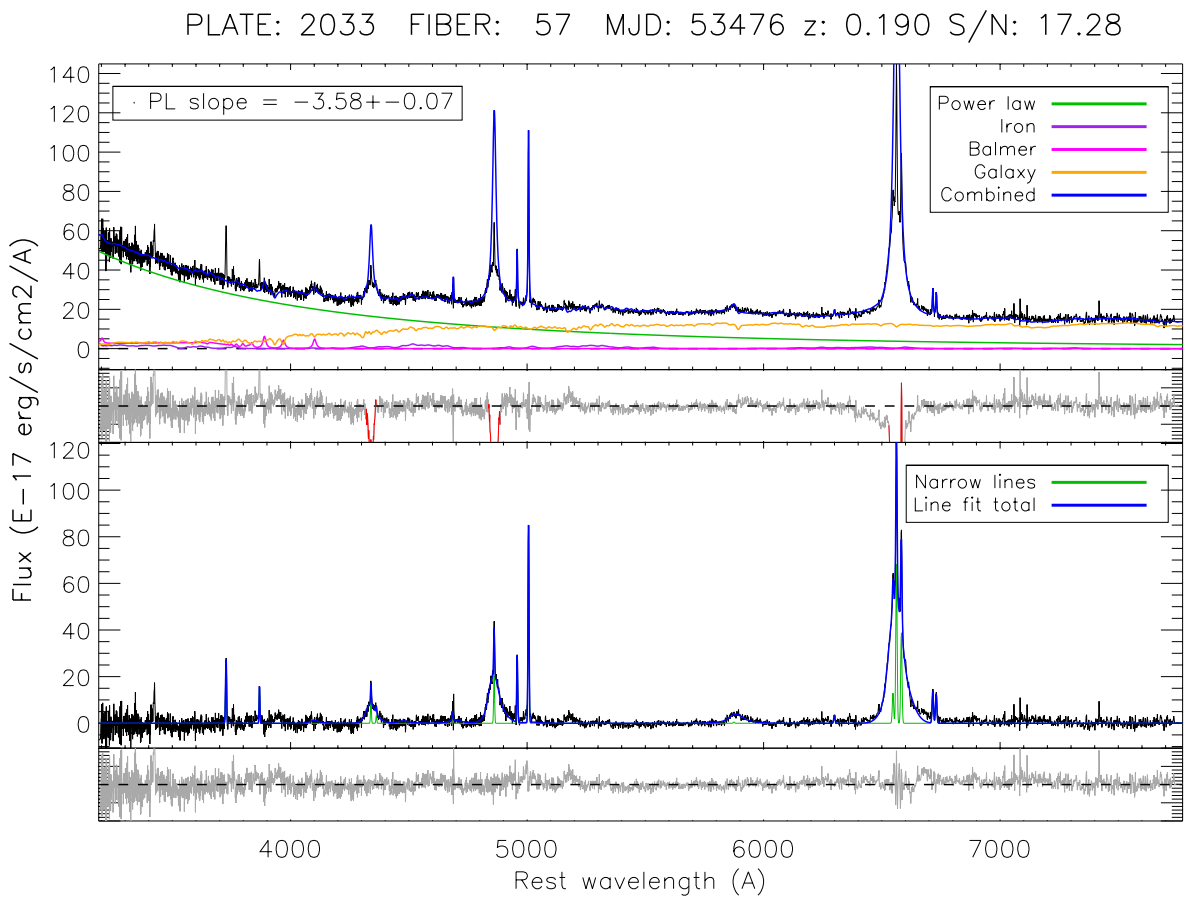

Figure 32: Representative example of spectrum showing the results of fitting of uncorrected spectra. Refer to figure 7 caption for further plot details. Expanded view of on linefit shown in figure 35.

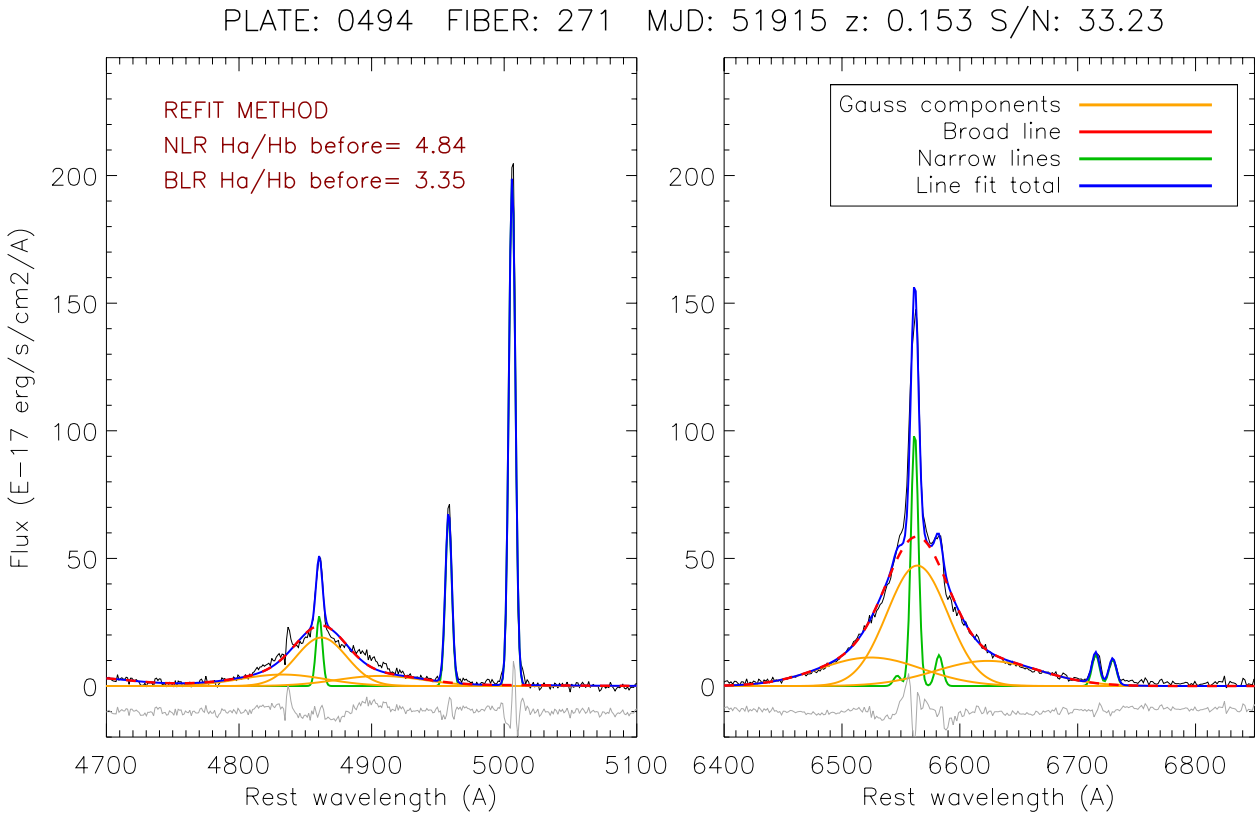

Figure 33: Expanded view of line fits for object shown in figure 30. Refer to figure 8 caption for further plot details.

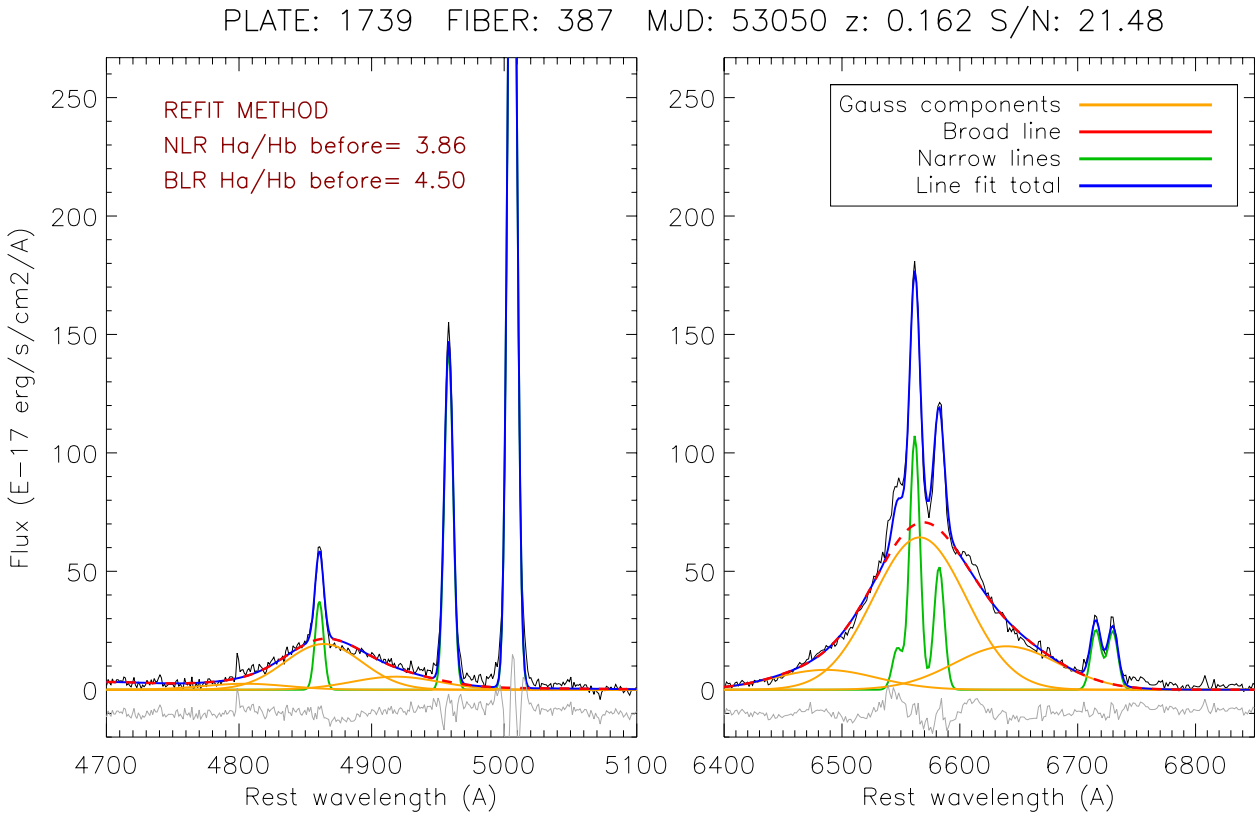

Figure 34: Expanded view of line fits for object shown in figure 31. Refer to figure 8 caption for further plot details.

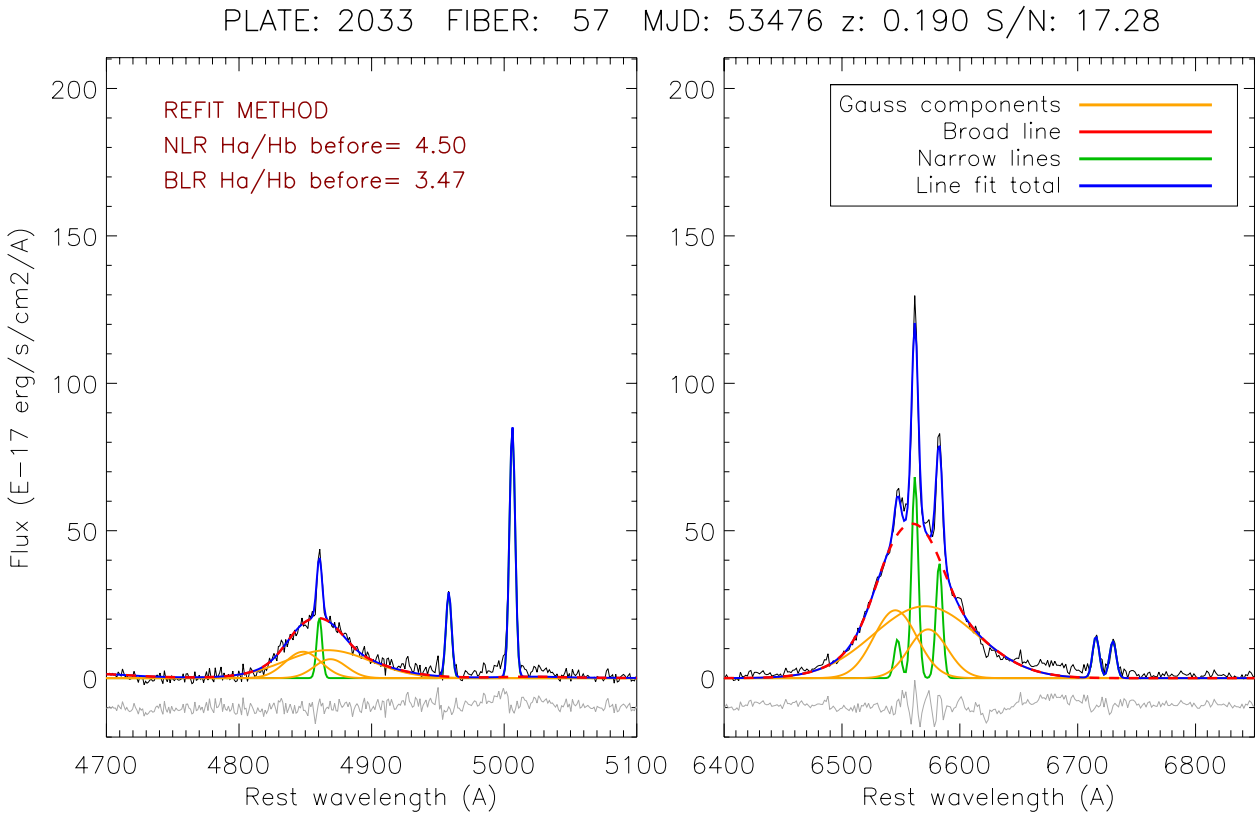

Figure 35: Expanded view of line fits for object shown in figure 32. Refer to figure 8 caption for further plot details.

A.2 Isolated Narrow and Broad Line Spectra

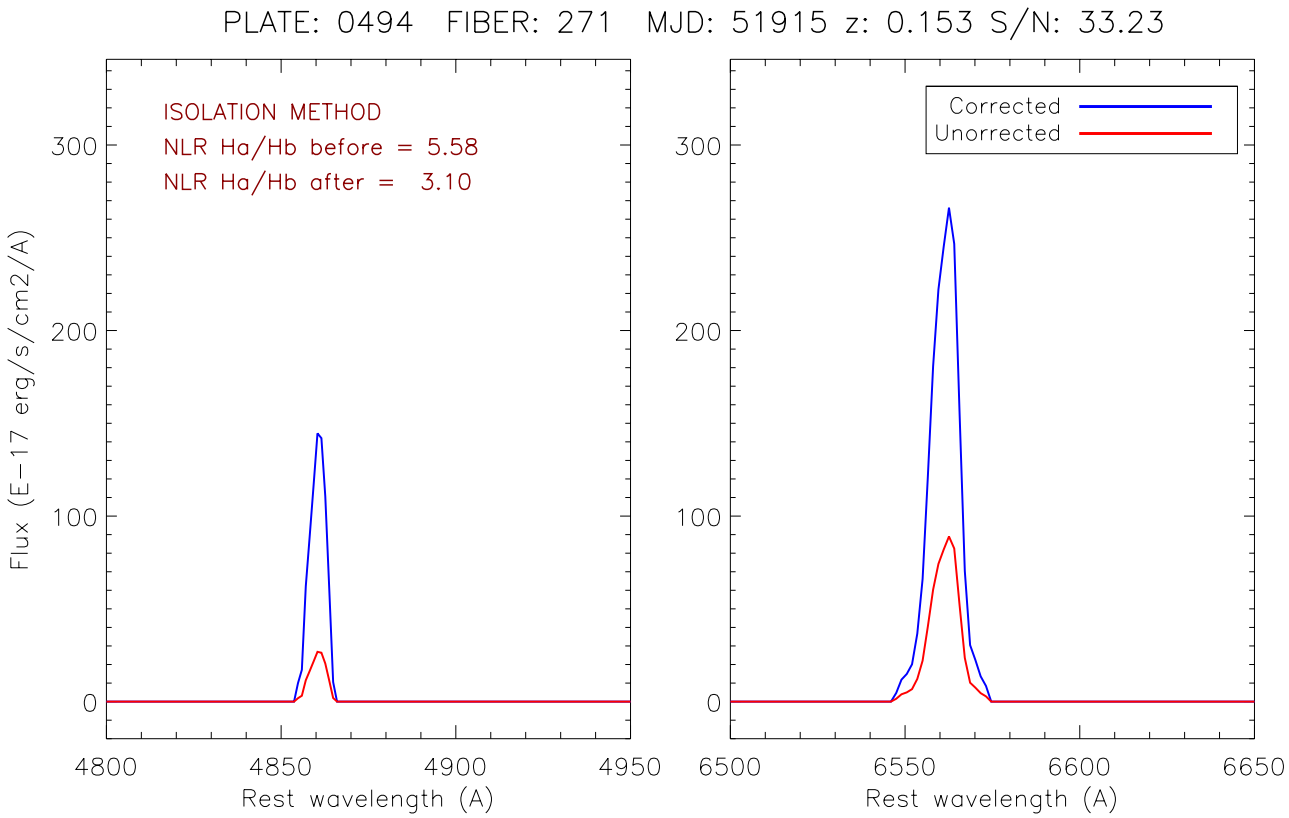

Figure 36: Same as figure 9, but for the object shown in figure 30, figure 33 and figure 39.

[h!]

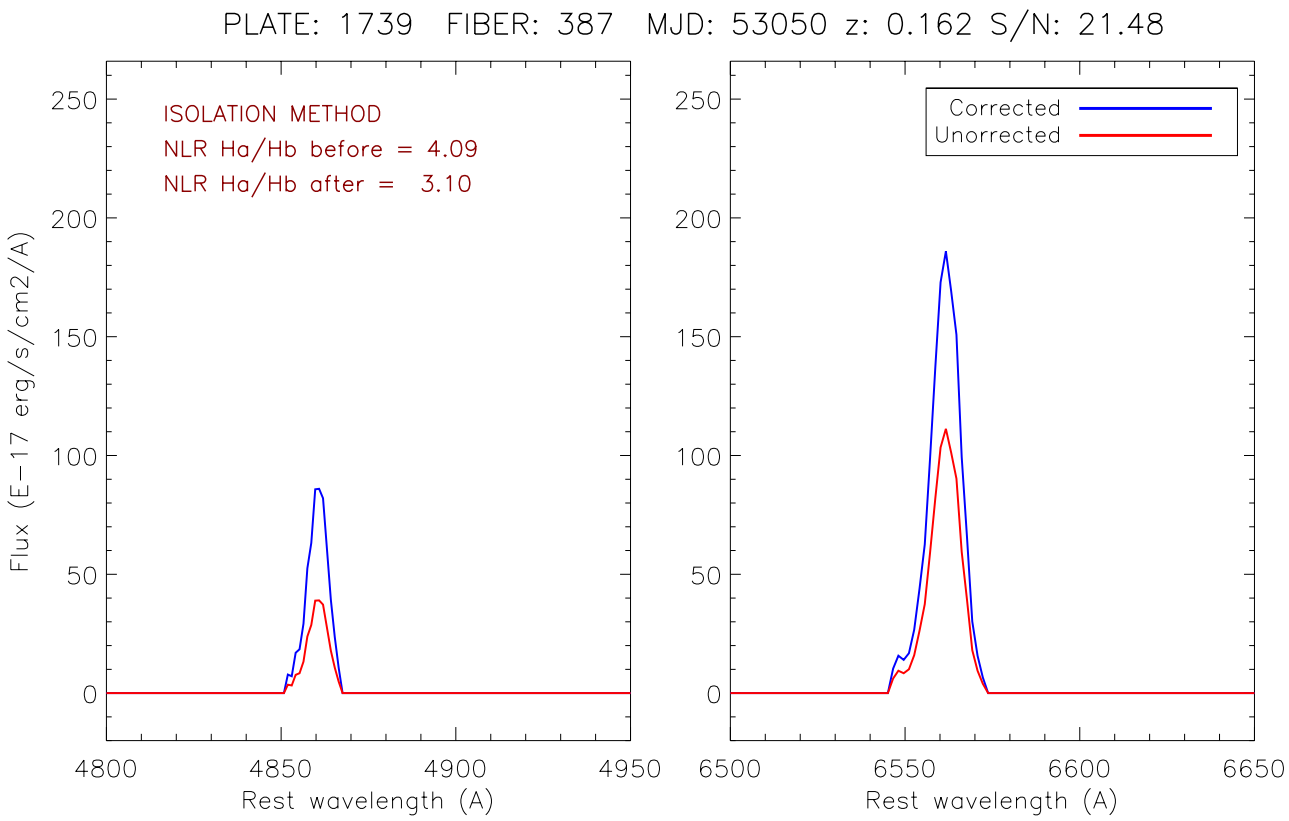

Figure 37: Same as figure 9, but for the object shown in figure 31 and figure 34 and figure 40.

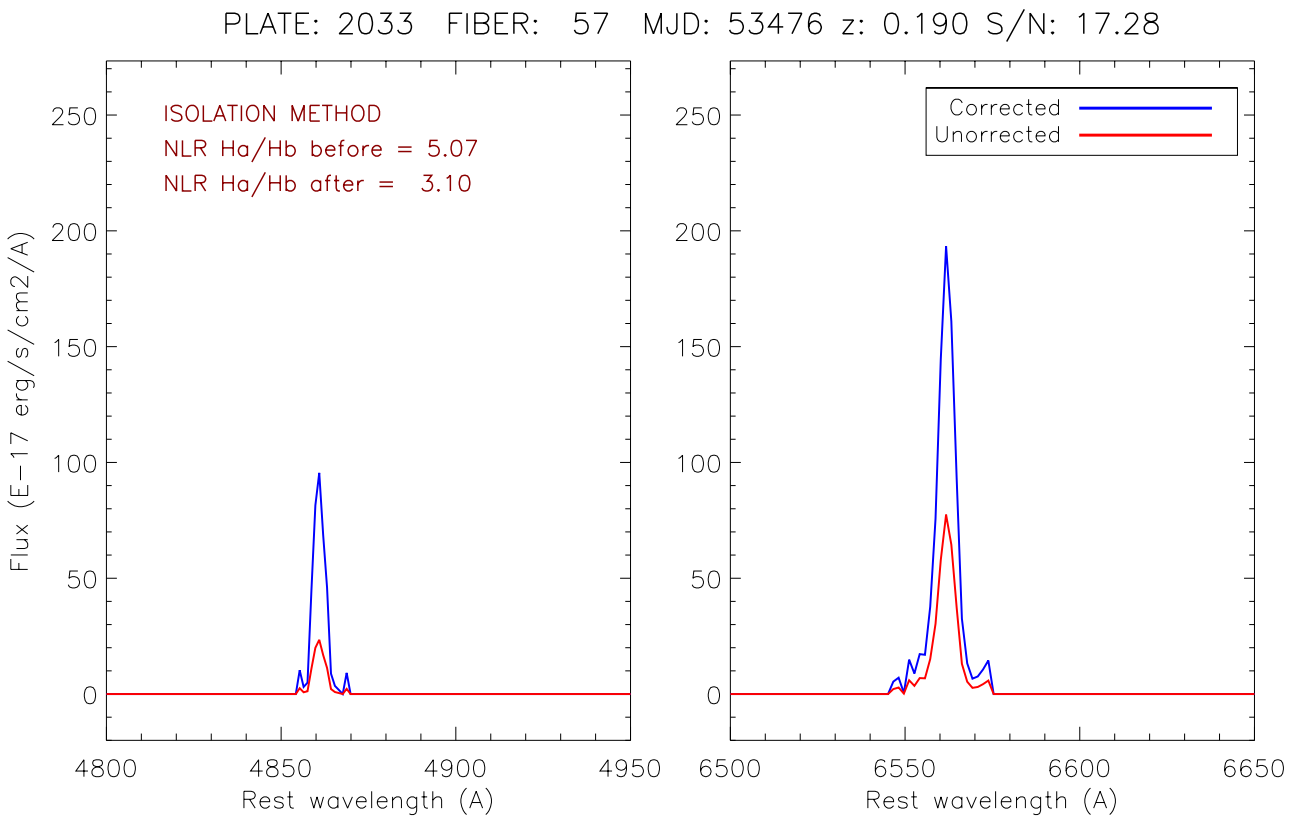

Figure 38: Same as figure 9, but for the object shown in figure 32, figure 35 and figure **??**

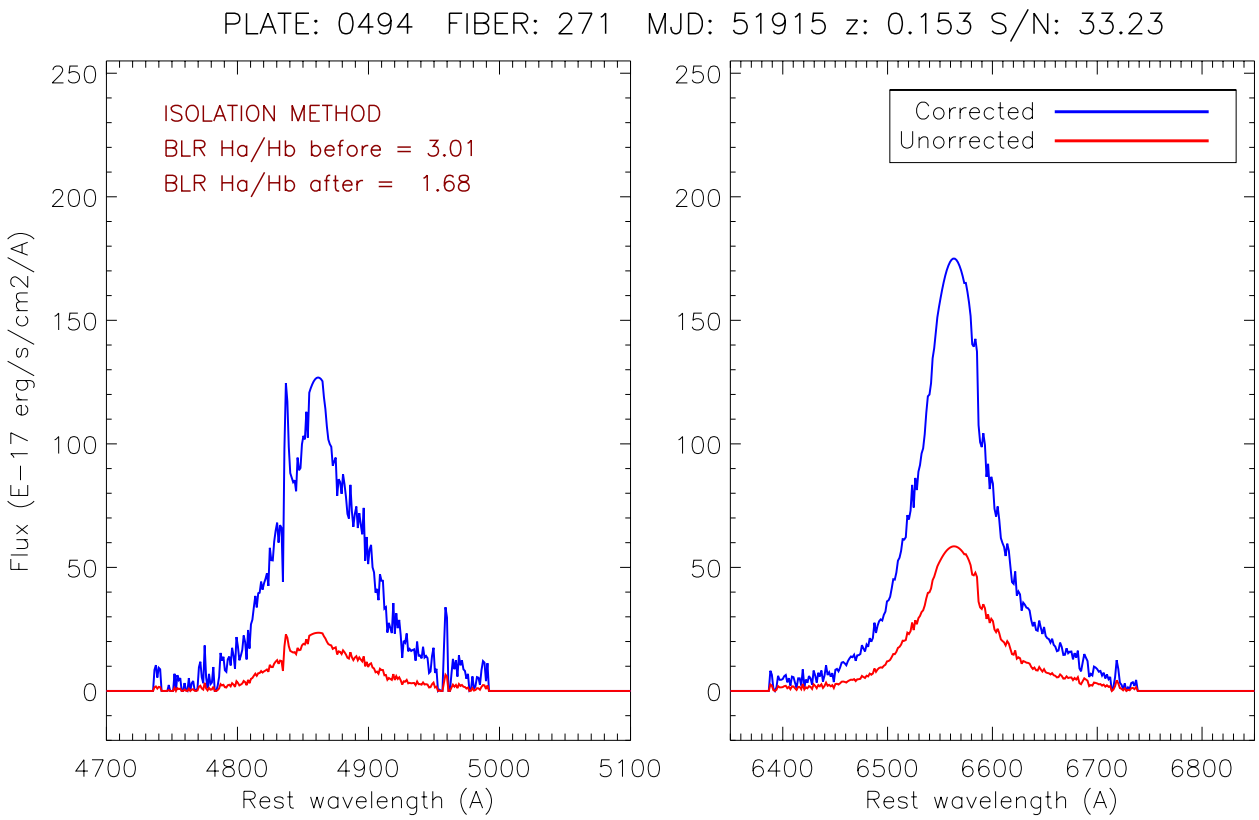

Figure 39: Same as figure 10, but for the object shown in figure 30 and figure 33.

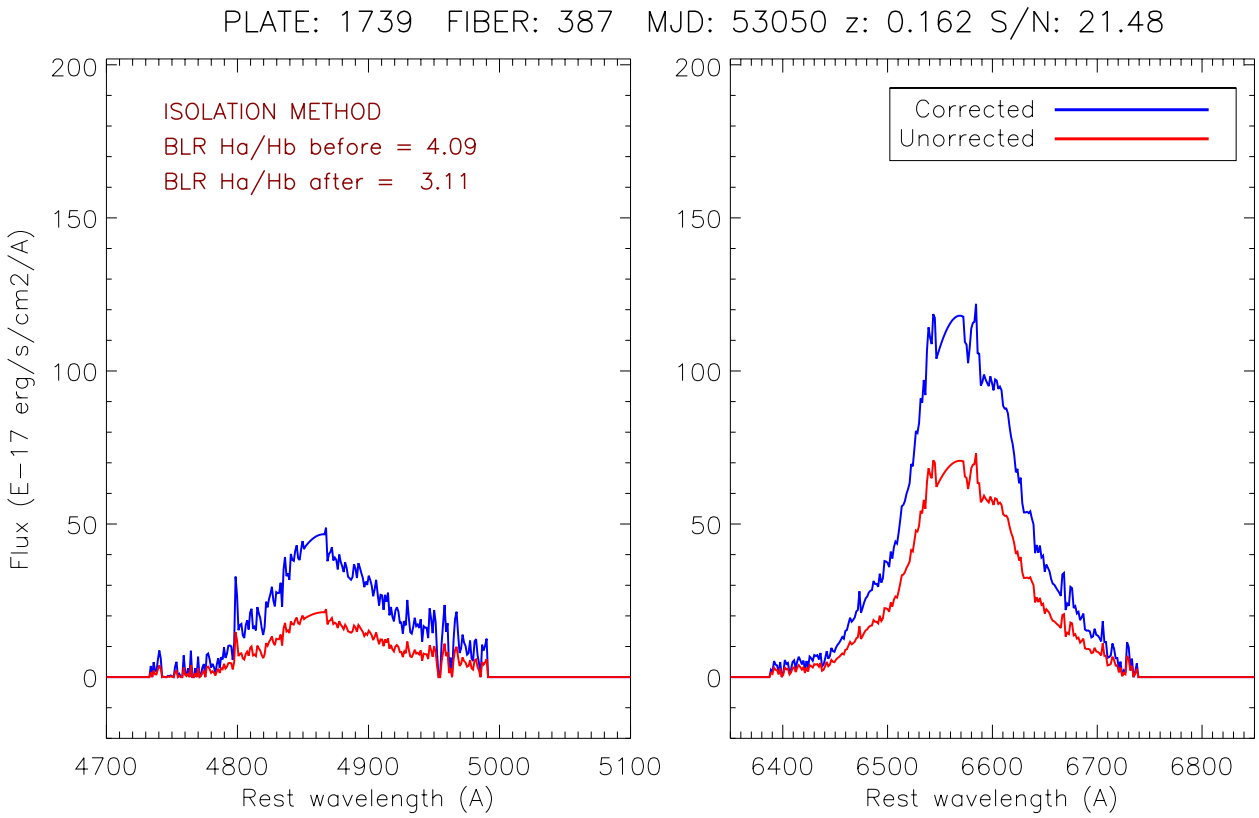

Figure 40: Same as figure 10, but for the object shown in figure 31 and figure 34.

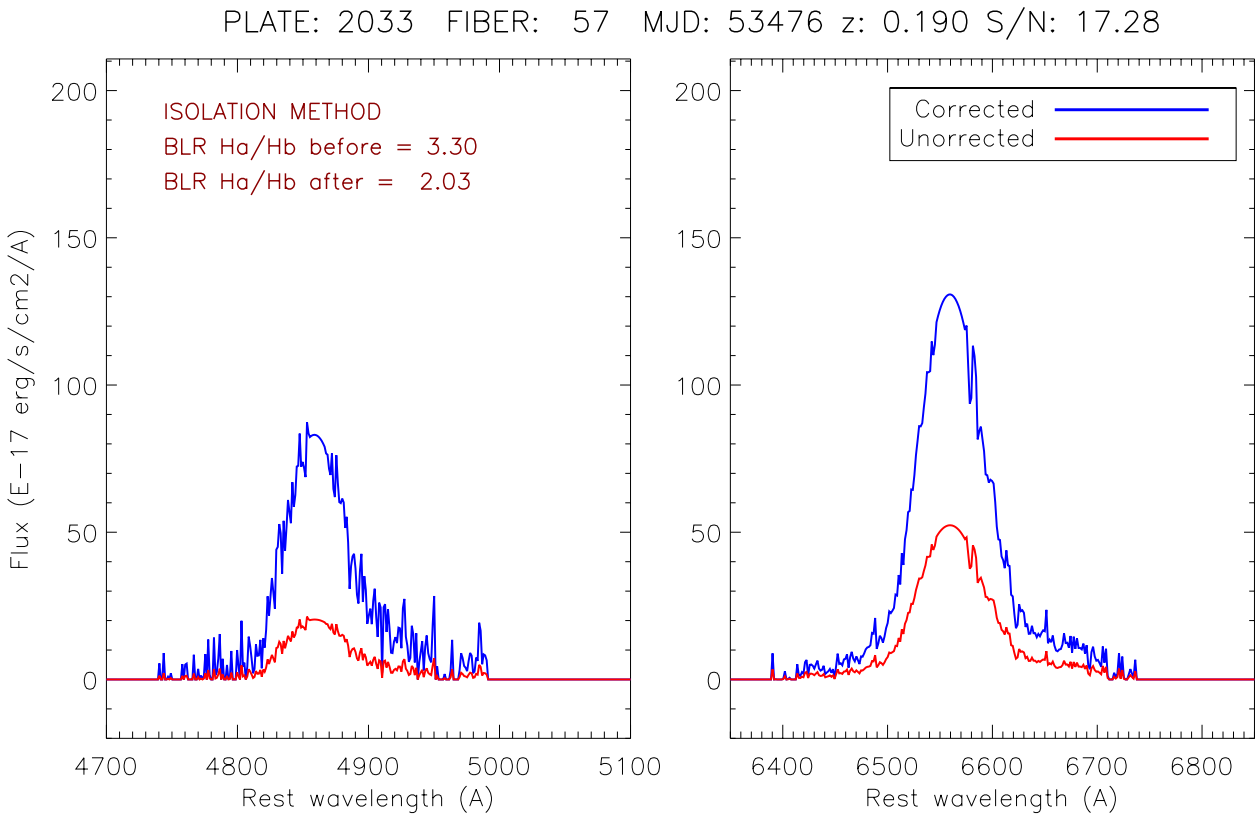

Figure 41: Same as figure 10, but for the object shown in figure 38, figure 32 and figure 35.

A.3 Spectra Before and After Correction

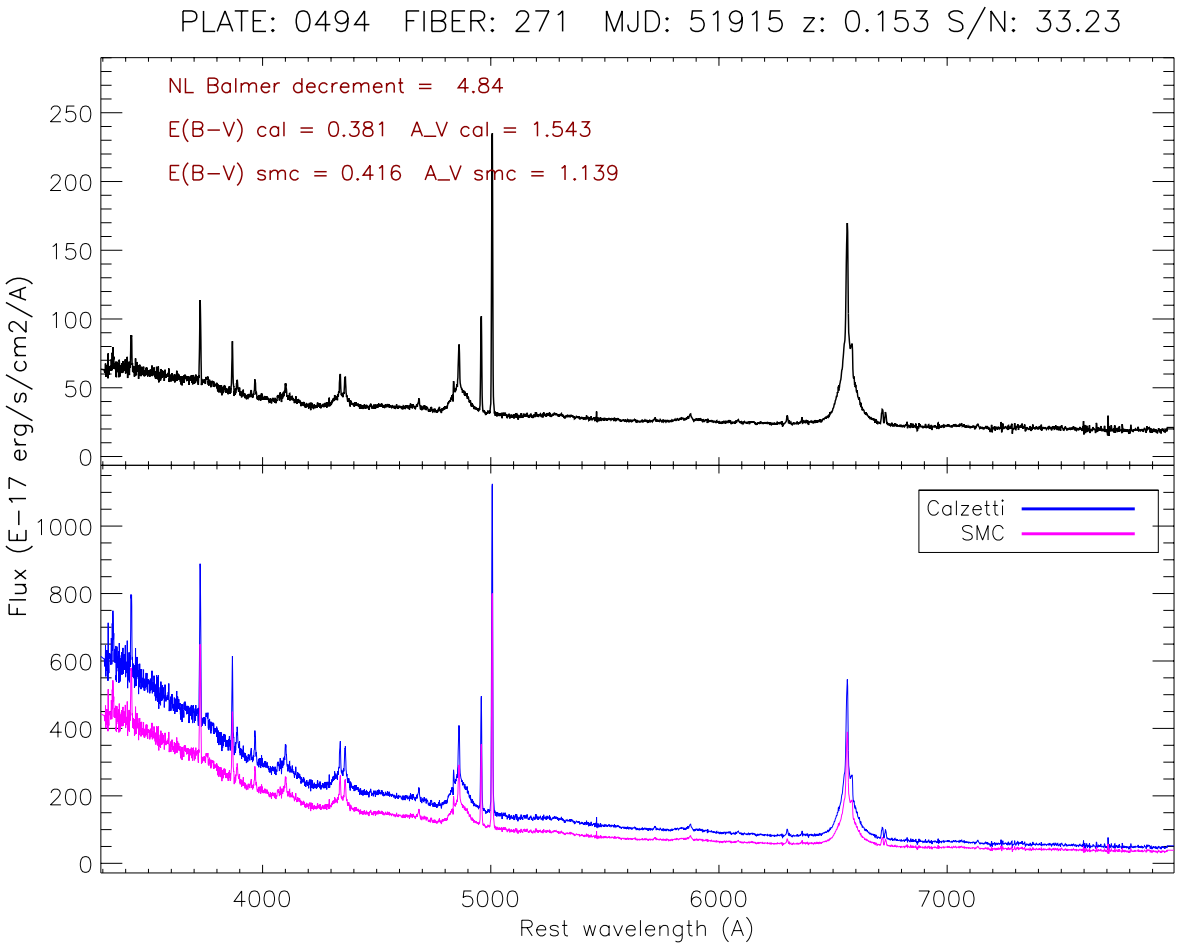

Figure 42: Same as figure 11, but for object shown in figure 30.

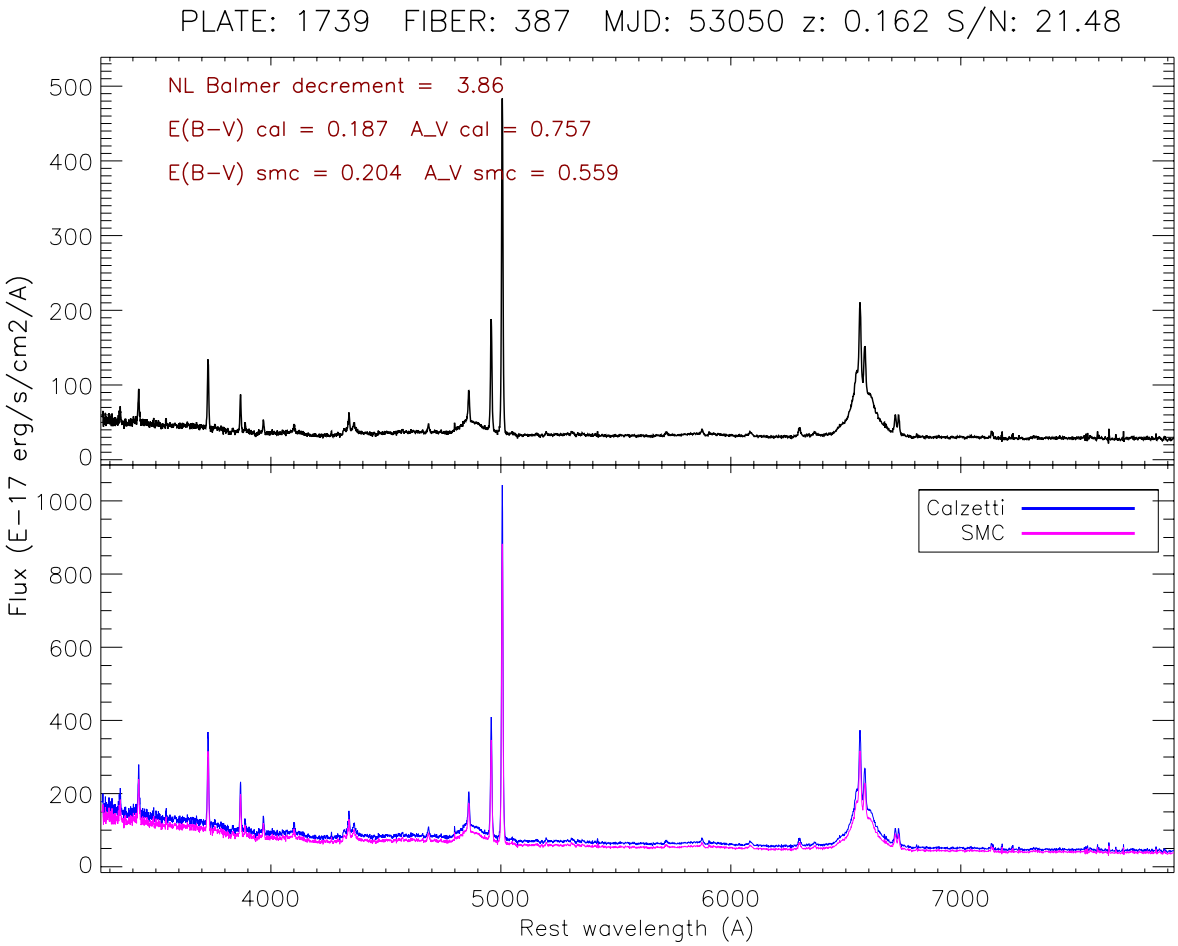

Figure 43: Same as figure 11, but for object shown in figure 31.

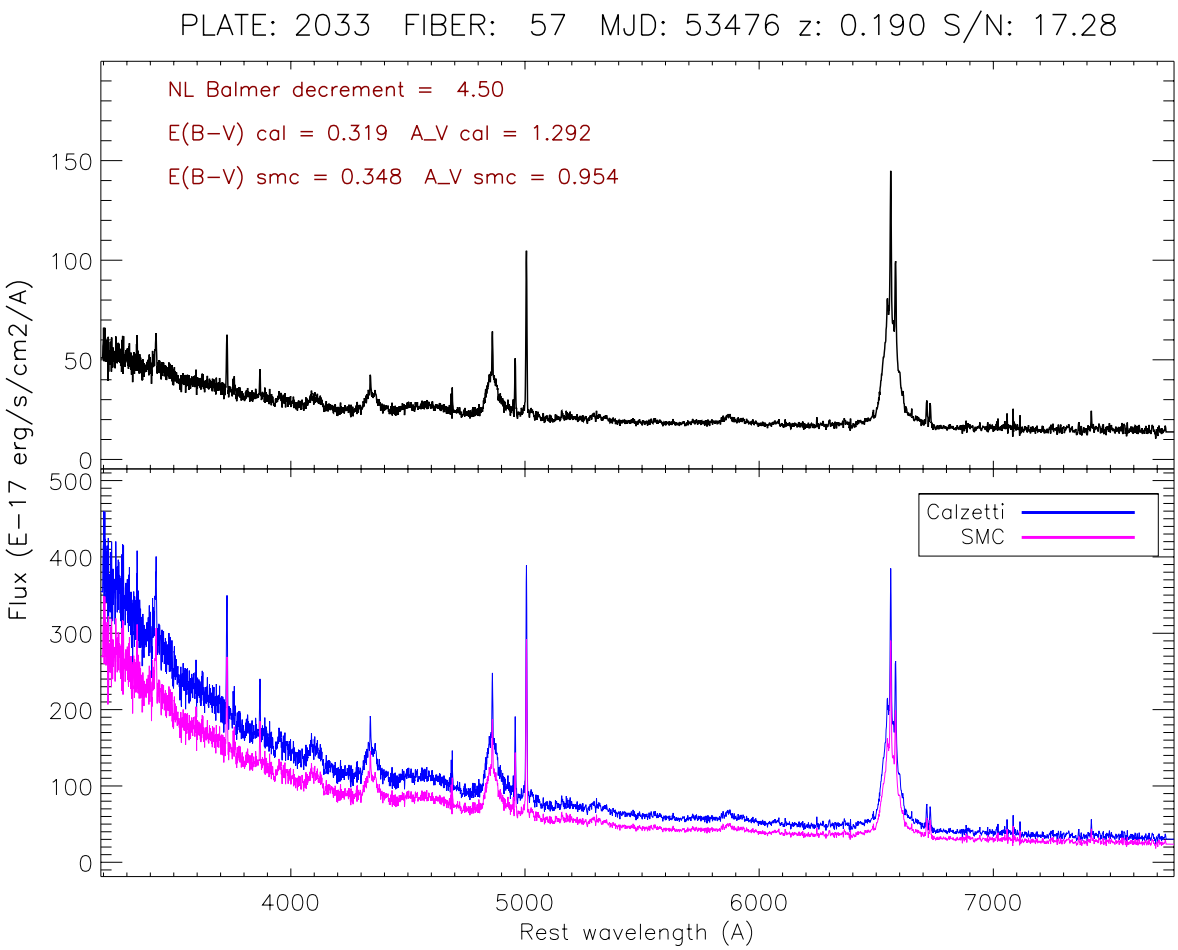

Figure 44: figure 11, but for object shown in figure 32.

A.4 Refitting of Corrected Spectra

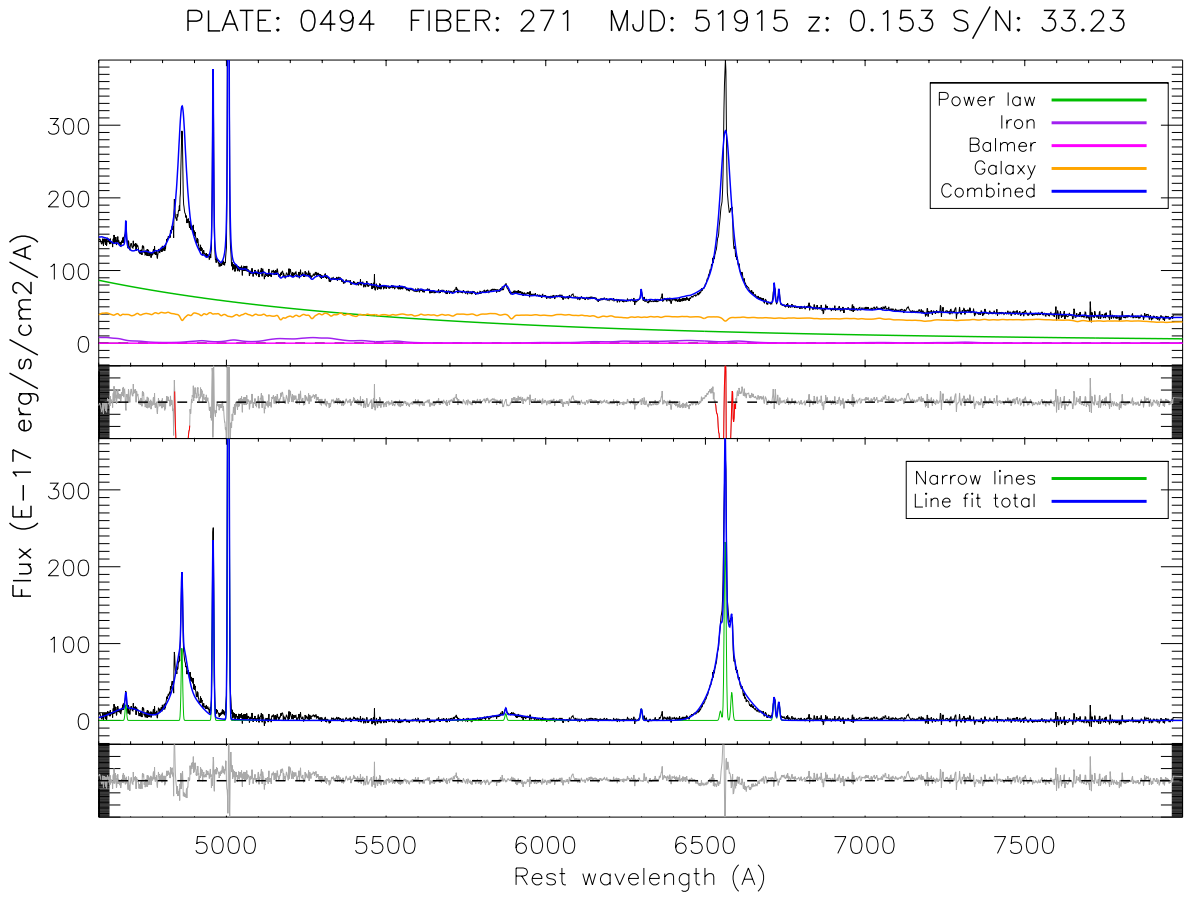

Figure 45: The results of fitting the spectra corrected for dust extinction for the same object as shown in figure 30. Refer to figure 7 caption for further plot details. Expanded view of linefit after correction for the effects of dust is displayed in figure 48.

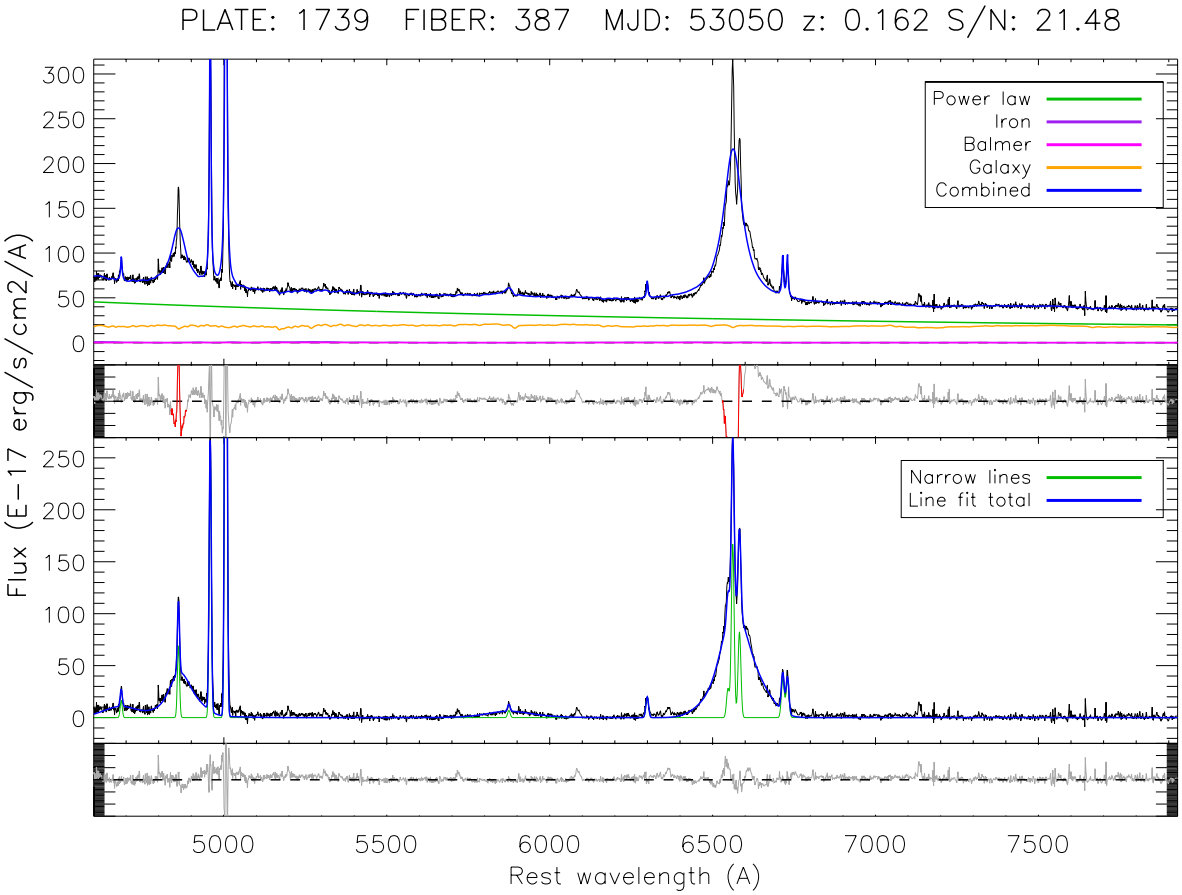

Figure 46: The results of fitting the spectra corrected for dust extinction for the same object as shown in figure 31. Refer to figure 7 caption for further plot details. Expanded view of linefit after correction for the effects of dust is displayed in figure 49.

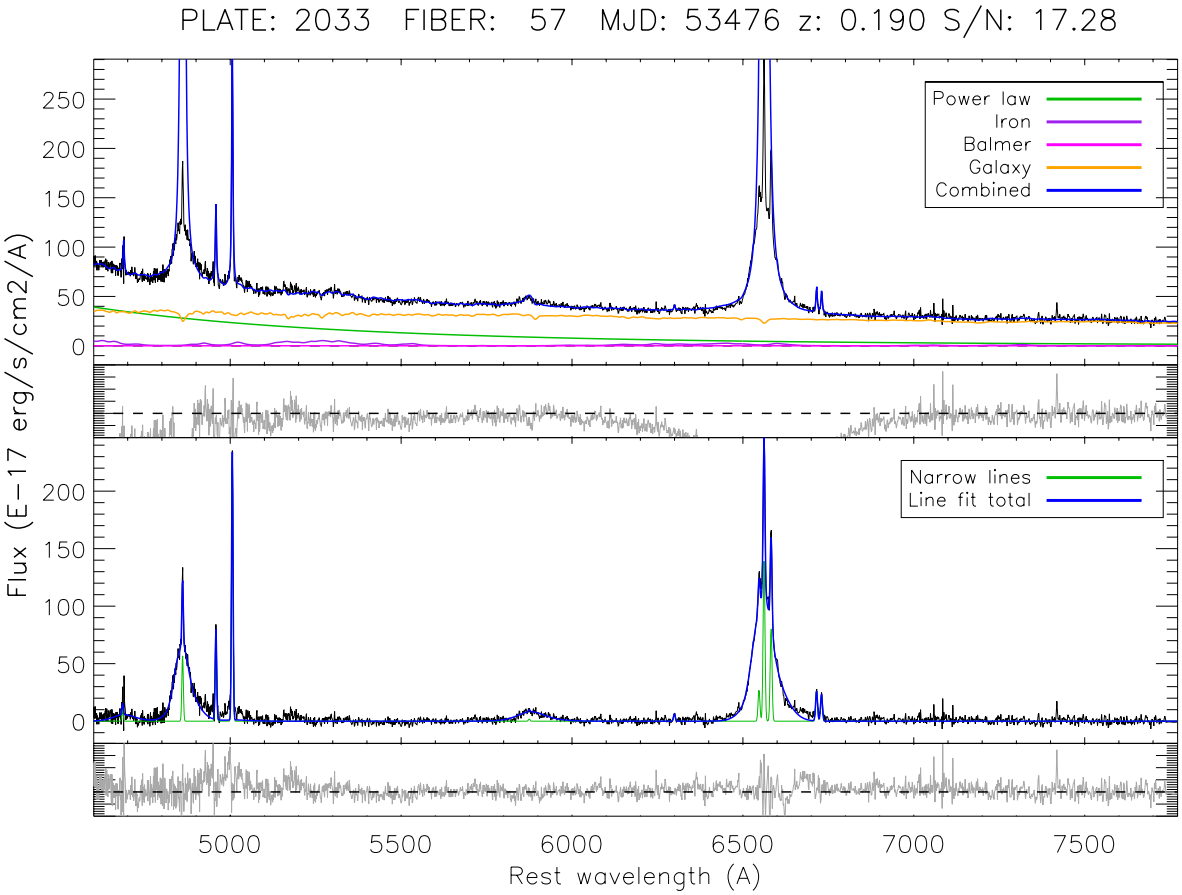

Figure 47: The results of fitting the spectra corrected for dust extinction for the same object as shown in figure 32. Refer to figure 7 caption for further plot details. Expanded view of linefit after correction for the effects of dust is displayed in figure 50.

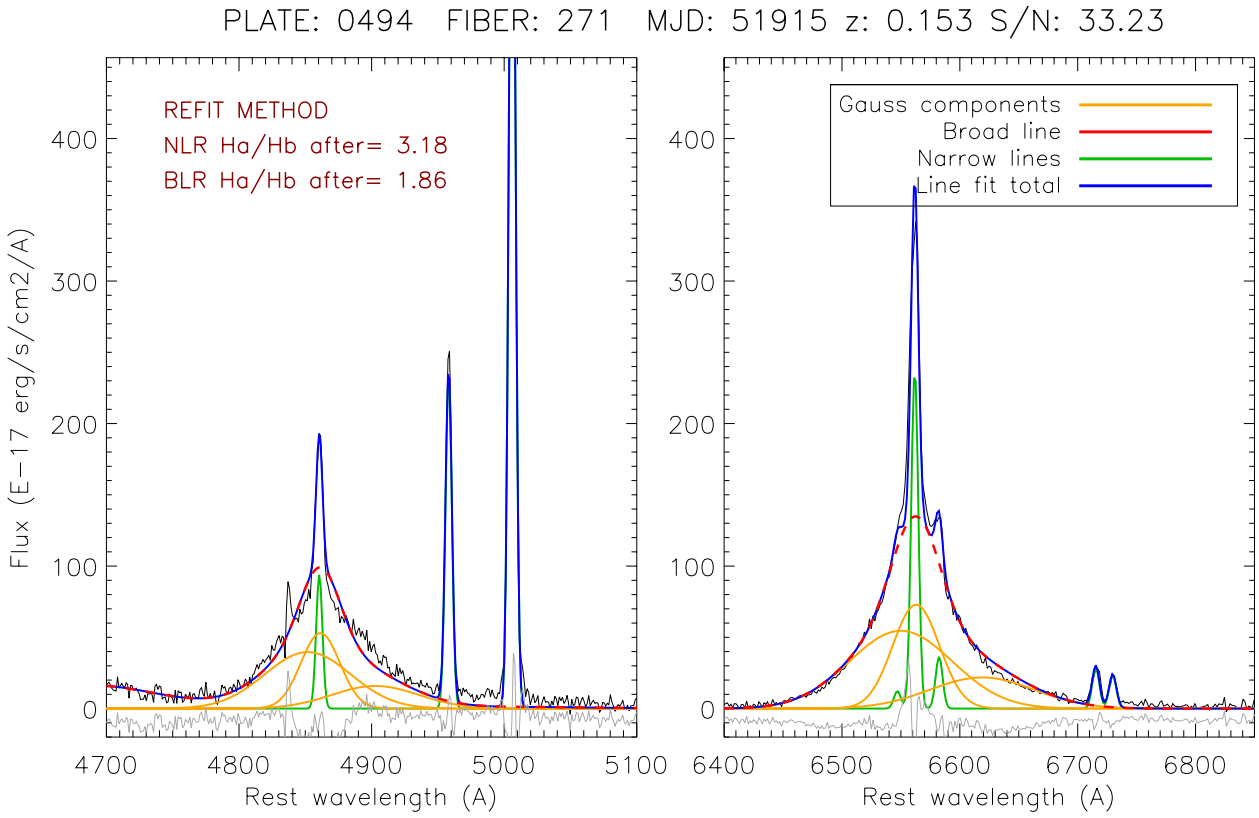

Figure 48: Expanded view of line fits for object shown in figure 45. Refer to figure 13 caption for further plot details.

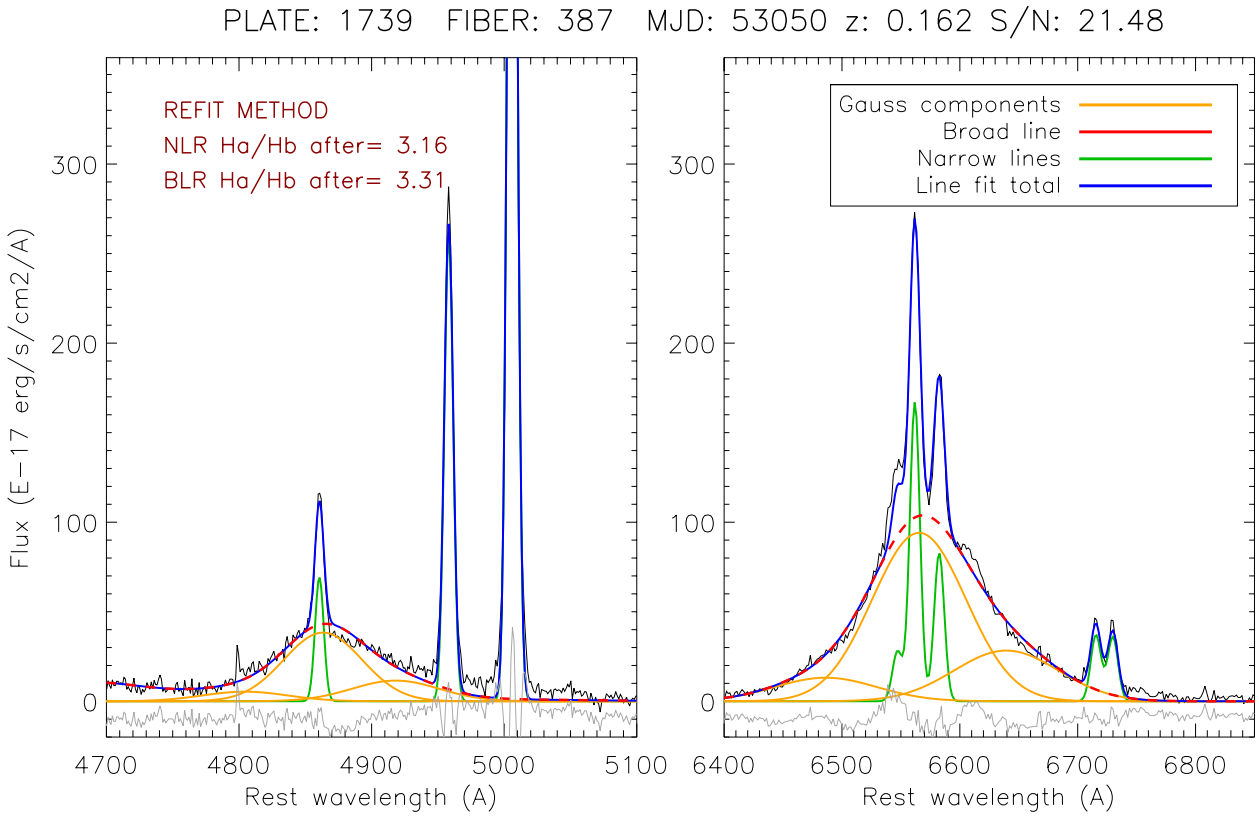

Figure 49: Expanded view of line fits for object shown in figure 46. Refer to figure 8 caption for further plot details.

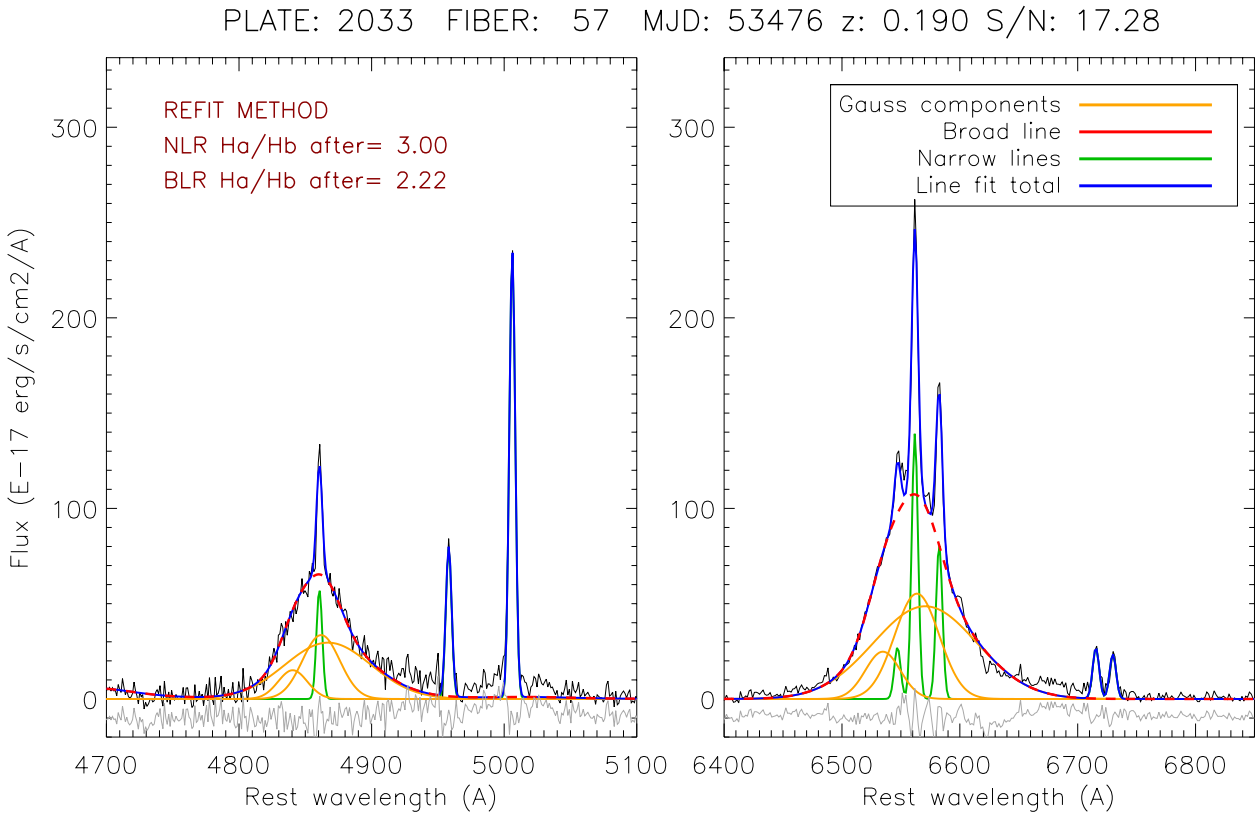

Figure 50: Expanded view of line fits for object shown in figure 47. Refer to figure 8 caption for further plot details.

A.5 NLR Balmer Decrements for the Main Sample

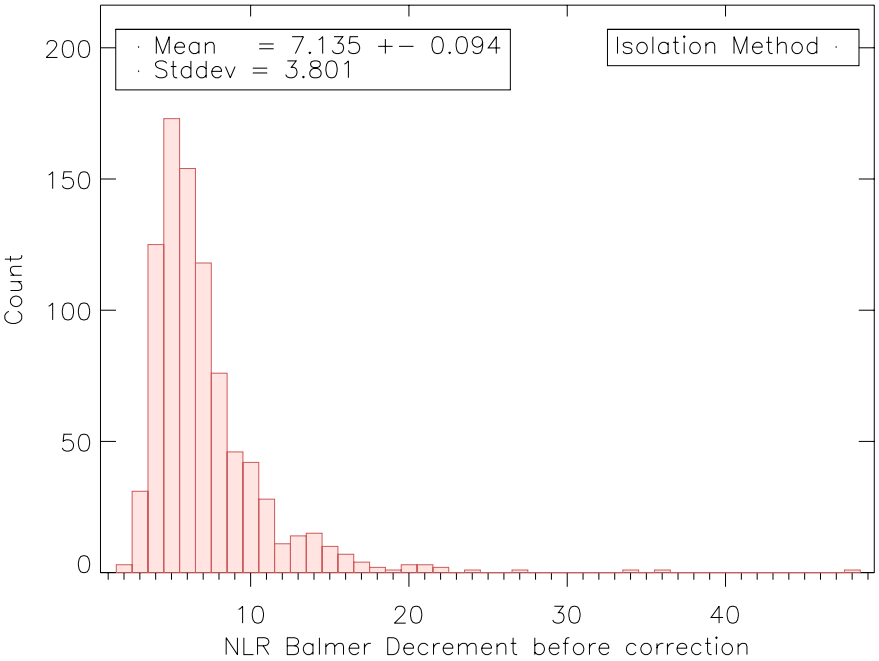

Figure 51: Distribution of NLR Balmer decrements before correction for the effects of dust for the main sample objects. The decrements are found using the isolation method (§4.1) and are used to calculate the color excess and correct the spectra for extinction due to dust.

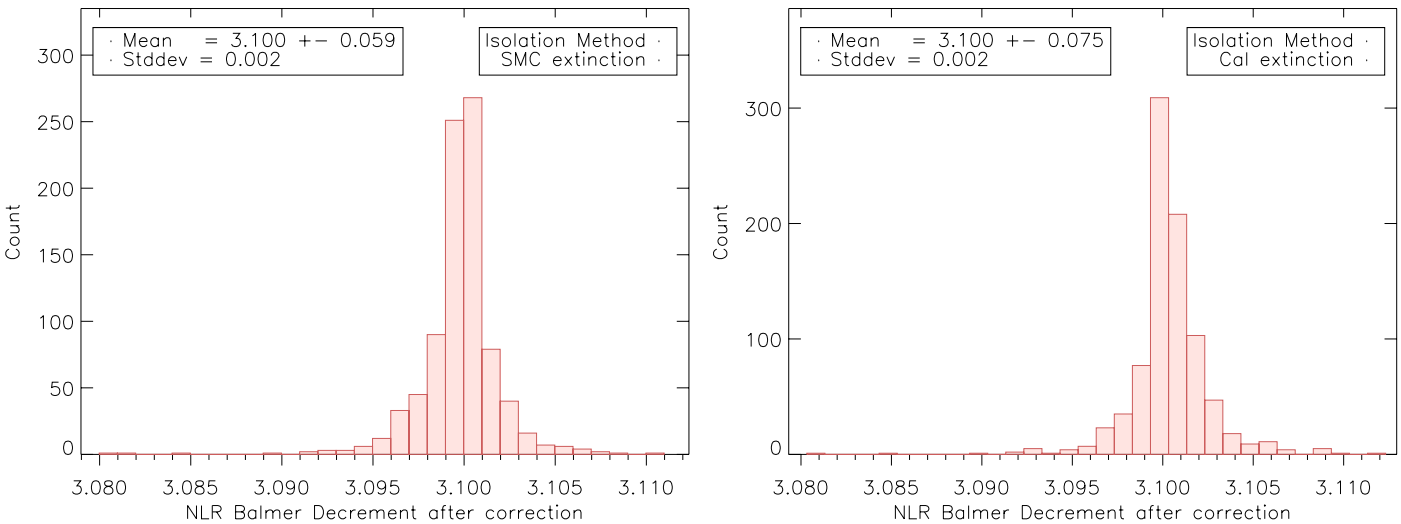

Figure 52: Distribution of NLR Balmer decrements for the main sample objects after correction for the effects of dsut using the isolation method. Left panel: Using the SMC extinction curve. Right panel: Using the Calzetti extinction curve. The mean of the distribution is consistent within 1 σ of the expected value of 3.1 for the intrinsic NLR Balmer decrement.